

Half-integer quantum Hall effect of disordered Dirac fermions at a topological insulator surfaceE. J. König,^{1,2} P. M. Ostrovsky,^{3,4} I. V. Protopopov,^{1,5,4} I. V. Gornyi,^{5,6} I. S. Burmistrov,^{4,7} and A. D. Mirlin^{5,1,2,8}¹*Institut für Theorie der kondensierten Materie, Karlsruhe Institute of Technology, 76128 Karlsruhe, Germany*²*DFG Center for Functional Nanostructures, Karlsruhe Institute of Technology, 76128 Karlsruhe, Germany*³*Max-Planck-Institute for Solid State Research, D-70569 Stuttgart, Germany*⁴*L. D. Landau Institute for Theoretical Physics, RAS, 119334 Moscow, Russia*⁵*Institut für Nanotechnologie, Karlsruhe Institute of Technology, 76021 Karlsruhe, Germany*⁶*A. F. Ioffe Physico-Technical Institute, 194021 St. Petersburg, Russia*⁷*Moscow Institute of Physics and Technology, 141700 Moscow, Russia*⁸*Petersburg Nuclear Physics Institute, 188300 St. Petersburg, Russia*

(Received 20 June 2014; revised manuscript received 18 September 2014; published 28 October 2014)

The unconventional (half-integer) quantum Hall effect for a single species of Dirac fermions is analyzed. We discuss possible experimental measurements of the half-integer Hall conductance g_{xy} of topological insulator surface states and explain how to reconcile Laughlin's flux insertion argument with half-integer g_{xy} . Using a vortex state representation of Landau level wave functions, we calculate current density beyond linear response, which is in particular relevant to the topological image monopole effect. As a major result, the field theory describing the localization physics of the quantum Hall effect of a single species of Dirac fermions is derived. In this connection, the issue of (absent) parity anomaly is revisited. The renormalization group (RG) flow and the resulting phase diagram are extensively discussed. Starting values of the RG flow are given by the semiclassical conductivity tensor which is obtained from the Boltzmann transport theory of the anomalous Hall effect.

DOI: [10.1103/PhysRevB.90.165435](https://doi.org/10.1103/PhysRevB.90.165435)

PACS number(s): 73.23.-b, 73.43.Nq, 73.20.Fz

I. INTRODUCTION

Topological states of matter constitute a vibrant field of current research. On the one hand, promising future applications—in particular, in the fields of spintronics and quantum computation—are expected. On the other hand, topological phases of matter provide fascinating realizations of fundamental concepts of field theory, mathematical physics, and geometry.

Topological phases considered in the present work are fermionic topological insulators (TIs) [1–4]: materials with a band gap in their bulk that are equipped with a “twist” in the structure of Bloch states. This leads to a nontrivial topological index, and, by the bulk-boundary correspondence [5] and Callias' theorem [6,7], to protected gapless states at the interface of two topologically distinct insulators.

The earliest example of a TI was the quantum Hall (QH) state [8]. The Landau levels (LLs) provide the bulk band gap, which is accompanied by the topological Thouless–Kohmoto–Nightingale–den Nijs (TKNN) index [9] and the protected chiral edge state. More recently, time-reversal (TR) invariant two- and three-dimensional (2D and 3D) TIs were discovered [10–16]. In contrast to the TKNN integer, their topological index takes only values in \mathbb{Z}_2 . The boundary states of a 3D TI represent a single species of 2D Dirac fermions.

Alternative descriptions of TIs are topological field theories. These include, first, the theory of electromagnetic (EM) gauge potentials, and, second, the diffusive nonlinear sigma model (NL σ M). In contrast to the Bloch-band description, these theories capture the general interacting problem with quenched disorder. In the case of the integer quantum Hall effect (QHE), the effective bulk EM theory contains a Chern-Simons (CS) term [17,18], whereas the field theory describing the localization physics in the bulk is the NL σ M supplemented with a theta term [19–21]. At this point, it is worth reminding

the reader that one of key ingredients of the QH physics is the disorder-induced Anderson localization of bulk states [22–25]. Both theories (EM and diffusive) can be unified within the framework of the $U(1)$ -gauged NL σ M [26].

In the language of topological EM field theory, the bulk of TR-invariant 3D TIs is characterized by the $\mathbf{E} \cdot \mathbf{B}$ term [2,27–29] with theta angle $\vartheta = \pi \pmod{2\pi}$. Terminating this bulk theory at the 3D TI boundary, one could therefore naively expect a CS surface theory. However, this would imply a surface Hall conductance $\sigma_{xy} \stackrel{?}{=} (\frac{1}{2} \pmod{1}) \frac{e^2}{h}$ and thus would be unphysical for two reasons: (i) the Hall conductance should be unambiguously defined, and (ii) its value should be zero in the presence of TR invariance. The absence of a CS term in the surface theory of TR-invariant 3D TI was shown employing BF theory [30], by straightforward integration of fermions including the bulk states [31], by means of the general conjecture of cancellation of anomalies [32], and by investigating the $U(1)$ -gauged diffusive NL σ M, i.e., the unified topological field theory of gauge potentials and diffusive soft modes [33].

In this paper we use the $U(1)$ -gauged NL σ M to explore the situation when TR symmetry is broken locally [34] on the surface of a 3D TI, or more generally, the QHE of a single Dirac fermion [35]. The QHE of Dirac fermions in the context of graphene [36–42] and 3D TI surface states [43–58] has been studied both theoretically and experimentally. The QH state is characterized by vanishing longitudinal conductance $\sigma_{xx} = 0$ and quantized transverse conductance taking values

$$\sigma_{xy} = g_D \left(v + \frac{1}{2} \right) \frac{e^2}{h}, \quad v \in \mathbb{Z}. \quad (1)$$

Here g_D denotes the number of degenerate Dirac cones, i.e., $g_D = 4$ for graphene and $g_D = 2$ for thin 3D TI slabs. In

particular the $\sigma_{xy} = \pm g_D e^2/2h$ states turn out to be extremely robust [59]; they can be observed up to room temperature [60] and can also be induced by pure exchange coupling (quantum anomalous Hall effect [61–67]).

Notwithstanding the immense general interest towards the subject, the single Dirac fermion QHE [$g_D = 1$ in Eq. (1)] did not enjoy the deserved and required attention. The following important questions were not or only partly answered to present date:

(i) How can half-integer $g_{xy} \equiv h\sigma_{xy}/e^2$ be measured experimentally?

(ii) Does not Laughlin’s flux insertion argument [68,69] forbid $\sigma_{xy} = (\nu + \frac{1}{2})\frac{e^2}{h}$?

(iii) What is the field theory describing the localization physics of the single-species Dirac-fermion QHE?

In this work we present a comprehensive analysis of these questions and detailed answers to them.

While our primary consideration leading to the answers on the posed questions is very general and is based on topology and gauge invariance, important physical insight can be gained by a microscopic analysis of simple models. Thus, we supplement our analysis by two complementary semiclassical calculations of the conductivity tensor of Dirac fermions in magnetic field. The first one is based on the vortex-state representation of LL wave functions [70–72] and addresses the situation of potential disorder which is smooth on the scale of the magnetic length. In particular, this calculation is also applicable beyond linear response. The second one is based on the Boltzmann transport theory of the anomalous Hall effect (AHE) [73,74] and, as usual, applies when the kinetic energy of charge carriers exceeds the scattering rate. The semiclassical (Boltzmann) conductivity tensor provides starting values for the RG dictated by the field theory discussed in the context of question (iii).

The paper is structured as follows. In Sec. II, which concerns question (i), we review and clarify the physics of the topological magnetoelectric effect (TME). In Sec. III we answer question (ii) regarding Laughlin’s argument. Section IV contains the first semiclassical calculation of current density (vortex states). In Sec. V we derive the unified field theory treating both diffusive matter fields and EM gauge potentials [question (iii)]. Subsequently, in Sec. VI, we present the second semiclassical (Boltzmann) calculation of the conductivity tensor for gapped Dirac fermions in magnetic field and examine the phase diagram of the problem. The renormalization group fixed points of the field theory bring us back to the TME and question (i), motivating a discussion of experimental conditions in Sec. VII. We close the article with a summary of obtained results and an outlook, Sec. VIII.

II. (HALF-)INTEGER QHE AND TOPOLOGICAL MAGNETOELECTRIC EFFECT

This section and Sec. VII are devoted to question (i) posed in the introduction. To make the paper self-contained, we begin by briefly reviewing and clarifying the current state of the literature.

A. The QHE of a single Dirac cone in condensed matter reality: 3D TI

The appearance of the single Dirac fermion on the 3D TI surface crucially relies on TR symmetry. Therefore, two questions arise concerning the realization of the single Dirac fermion QHE on the 3D TI surface:

(a) Up to which magnetic field strength do surface states exist?

(b) If surface states are present, does the half-integer quantization of g_{xy} immediately follow?

Regarding question (a), we recall that a 3D TI is characterized by the inverted structure of the energy bands which can be captured by the \vec{k} -dependent mass term $\mathcal{M}(\vec{k})$ in its effective 3D Dirac-like bulk Hamiltonian

$$\mathcal{M}(\vec{k}) = M - B_1 k_z^2 - B_2 \mathbf{k}^2. \quad (2)$$

Here we follow the notation of Eq. (31) in Ref. [2], assume positive M , B_1 , and B_2 , and denote (2D) vectors by bold italic symbols.

The 2D interface (which we assume for concreteness to occupy the $z = 0$ plane) between a 3D TI and a topologically trivial insulator (e.g., vacuum) can be modeled by spatially dependent Dirac mass $M = M(z)$ which interpolates between positive (topological phase) and negative (trivial phase) values changing its sign at $z = 0$. As a consequence of the band inversion in the topological insulator the interface supports massless Dirac fermions in the vicinity of $\mathbf{k} = 0$ [6,7,75].

The magnetic field $\mathbf{B} = (0, 0, B)$ applied to the interface cannot destroy the surface states provided the bulk gap is sufficiently large. More precisely, for

$$M|_{z=\infty} > B_2/l_B^2 \quad (3)$$

the massless surface excitations give rise to a zero-energy Landau level (LL) localized at the interface $M(z) - B_2/l_B^2 = 0$. Here $l_B = \sqrt{\hbar/(|e|B)} \approx 26 \text{ nm}/\sqrt{B [\text{T}]}$ is the magnetic length. In the exemplary case of Bi_2Se_3 , we can estimate [2] $B_2/l_B^2 \sim 0.6 \text{ meV} \times B [\text{T}]$, while $M \sim 0.3 \text{ eV}$.

In the rest of the paper (and consistently with the previous works) we will use the term “local breaking of TR symmetry on the 3D TI surface” if the magnetic field does not destroy the surface states. As we have just explained, this does not necessarily require spatially inhomogeneous magnetic field configurations.

Let us now turn to question (b). To avoid confusion, we stress that the physics of the half-integer QHE, which we discuss in this work, can be described in a single-particle picture and has no direct relation to the physics of the fractional QHE (in the sense of Störmer’s and Tsui’s discovery) which is a many-body phenomenon.

The half-integer QHE can be expected as soon as surface states are present. We emphasize that it does not rely on a precise dispersion but rather on the low-energy spin texture and on the fact that there is an odd number of Dirac fermions on the surface. More precisely, the half-integer QHE is a manifestation of fermion-number fractionalization in the sense of Jackiw and Rebbi [76,77]. The 3D TI surface states are topologically protected fermionic zero modes associated with a spatial kink in a background bosonic field (the mass “field” in the present context). Generally, the fermion number in

the presence of a bosonic kink is shifted by one-half as compared to the situation without a kink. Specifically, if the zero mode is filled (empty), the fermion number is $1/2$ ($-1/2$). In the presence of the magnetic field, the zero-energy state has additional LL degeneracy $\frac{BA}{\Phi_0}$, where A is the area penetrated by the flux and $\Phi_0 = h/e$ is the flux quantum. Consequently, the fermion density at chemical potential $\mu = 0^+$ is $n = N/A = \frac{B}{2\Phi_0}$. In view of the relationship between fermion density and (the quantum part of) the transverse conductivity [78], this unveils the fundamental topological reason for the half-integer QHE. The result of argument remains unchanged even in the presence of finite but small Zeeman energy $E_Z \ll M$ (gapped 3D TI surface states).

B. Can one measure a half-integer g_{xy} in a transport experiment?

Typical transport experiments are carried out on 3D TI slabs, which have two major surfaces (called “top” and “bottom” in what follows) with a single Dirac fermion each. In most experimental situations, contacts are attached at or near the side walls of the probes, and thus both major surfaces are probed simultaneously. Therefore, quantum Hall data [43] of 3D TIs display the odd-integer series described by Eq. (1) for $g_D = 2$.

One could expect that it is sufficient to attach all measuring contacts on a single surface of the 3D TI slab to measure the QHE of a single Dirac fermion [53]. If the contacts are sufficiently far away from the sample boundaries, one might then hope to measure a half-integer Hall response. To be specific, let us assume that a bias voltage is applied between two electrodes attached to a TI surface, as depicted in Fig. 1. One measures the Hall current passing through an amperemeter connecting two perpendicular probing contacts and hopes to extract a half-integer σ_{xy}^{top} from $I_{\text{Hall}}/V_{\text{bias}}$. However, this attempt will fail. Indeed, let us assume that the surface is characterized by a half-integer-quantized Hall conductivity and zero longitudinal conductivity. In order to

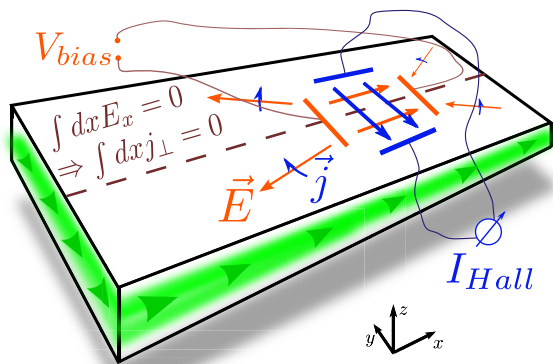


FIG. 1. (Color online) Failure of transport measurement of half-integer Hall response. A thin 3D TI slab in a QH state $\sigma_{xy}^{\text{top}} = \sigma_{xy}^{\text{bottom}} = \frac{e^2}{2h}$ (one shared green edge channel) is probed by a local four-contact measurement consisting of two opposite bias gates (orange) and, perpendicularly, two probing gates connected by an amperemeter (blue). For further explanation, see main text.

find the total current between the current probes one should take into account not only the current flowing in the part of the TI surface between the contacts but also the current distribution in the rest of the surface. The total current can be found by integrating the transverse current density $\int d\mathbf{l} \times \mathbf{j}$ along a contour shown by the dashed line in Fig. 1. This integral is, however, proportional to $\int d\mathbf{l} \cdot \mathbf{E}$ and is equal to zero, since the surface is terminated by a metallic edge which represents an equipotential line. Thus, such an experiment would yield $I_{\text{Hall}} = 0$.

The above discussion assumed applying bias voltage and measuring current. One can equally analyze the reverse situation when a current is injected and the Hall voltage is probed. To this end, two metallic contacts are supposed to be attached in the central region of the TI surface. They serve as source and drain for the current. However, as in the $\sigma_{xx} = 0$ limit current always flows along equipotential lines, it is actually not possible to inject current in the middle of a QH system. Instead, “edge states” circulating around the contact will be formed. Therefore, this measurement will yield a null result as well.

Thus, an attempt to measure a half-integer-quantized g_{xy} in a transport experiment fails. The reason for this is as follows. To measure directly a half-integer g_{xy} , one should explore local characteristics of a single TI surface. As is clear from the above analysis, transport experiments do not satisfy this requirement. One can, however, devise an alternative approach by measuring an electromagnetic response of the system to a local perturbation. As discussed below, this kind of measurement does probe local properties of the system and, therefore, is able to yield directly a half-integer Hall conductivity. The case of transport experiments in nonideal situations ($\sigma_{xx} \neq 0$) and with a more complex arrangement of contacts is left for future investigation.

C. Topological electromagnetic field theory and TR-invariant 3D TI

In a series of papers [79–81], S.-C. Zhang and coworkers proposed to characterize 3D TIs by associated electromagnetic field theories. In particular, they argued that the corresponding bulk EM theory contains the $\mathbf{E} \cdot \mathbf{B}$ term (second Chern character):

$$S_{\vartheta} = \frac{\vartheta}{2\pi} \frac{\alpha}{16\pi} \int d^3x dt \epsilon^{\mu\nu\rho\tau} F_{\mu\nu} F_{\rho\tau} \quad (4a)$$

$$= \frac{\vartheta}{2\pi} \frac{\alpha}{2\pi} \int d^3x dt \mathbf{E} \cdot \mathbf{B} \quad (4b)$$

$$= \frac{\vartheta}{2\pi} \frac{\alpha}{4\pi} \int d^3x dt \epsilon^{\mu\nu\rho\tau} \partial_{\mu}(A_{\nu} \partial_{\rho} A_{\tau}). \quad (4c)$$

Here $\alpha = e^2/c\hbar$ denotes the fine-structure constant of QED. If not specified otherwise, we set the speed of light and Planck’s constant to unity $c = \hbar = 1$ in the entire paper. Greek indices label space-time coordinates. Since this term leads to nontrivial constituent equations, the authors of Ref. [79] coined the term “topological magnetoelectric effect” (see also Sec. VII, below). As can be seen from Eq. (4c), the $\mathbf{E} \cdot \mathbf{B}$ term

(1) is proportional to a quantized (topological) integral: $S_\vartheta = \vartheta n$ (where $n \in \mathbb{Z}$) if the base manifold has no boundary; then, TR invariance restricts ϑ to values 0 or $\pi \pmod{2\pi}$ [82];

(2) is intimately related to the CS term on a possible boundary and thus to the QHE.

From the viewpoint of topological EM field theory, a TR invariant 3D TI is defined by the presence of S_ϑ with $\vartheta = \pi \pmod{2\pi}$ in the bulk.

Let us now consider the interface between a 3D TI and an ordinary insulator with $\vartheta = 0$. In the presence of such a boundary (for definiteness, we here consider a 3D TI in the half space $z < 0$) the evaluation of Eq. (4c) yields $S_\vartheta = S_{CS}$ on the surface $z = 0$, where

$$S_{CS} = \frac{\vartheta}{2\pi} \frac{\alpha}{4\pi} \int d^2x dt \epsilon^{\nu\rho\tau} A_\nu \partial_\rho A_\tau. \quad (5)$$

The value $\vartheta = \pi \pmod{2\pi}$ corresponds to the surface Hall conductivity $\sigma_{xy} = (\frac{1}{2} \pmod{1})e^2/h$, with uncertainty in an integer multiple of e^2/h . Here the following questions arise. First, the Hall conductivity is a measurable quantity and should be defined unambiguously. Second, any nonzero Hall conductivity is in conflict with time-reversal invariance of the system.

Recall that time-reversal symmetry in the case $\vartheta = \pi \pmod{2\pi}$ is ensured by the quantized integral in Eq. (4) for the system without boundary. In contrast, for a finite system, the fermionic surface modes should be included. Being gapless (and nonlocalizable), the latter are important even at longest length scales. This is why they must be treated differently from bulk degrees of freedom.

In a number of recent works [31–33] it was shown that the CS term is in fact absent on the surface of a TR-invariant 3D TI unless the TR symmetry is explicitly broken on the surface. We will return to this issue and the closely related question of parity anomaly [83–86] in Sec. V A.

D. Local TR breaking: Topological magnetoelectric effect

While the EM theory describing a surface of a TR-invariant 3D TI does not contain a CS term, an elegant TME description is recovered once TR invariance is locally broken. Let us emphasize that a TME response associated with the $\mathbf{E} \cdot \mathbf{B}$ term is a general property of QH systems. The special feature of 3D TI surfaces (with locally broken TR invariance) is in a half-integer value of the associated Hall conductance.

The most prominent physical manifestations of TME include topological Faraday and Kerr rotations [79,87,88] and the image magnetic monopole effect [80,88–90] (see also Sec. VII). In this work we concentrate on the latter. The essence of the effect is that an electric charge Q placed above a QH system (posed in the plane $z = 0$) induces an inhomogeneous magnetic field configuration which can be described by a mirror magnetic monopole.

To obtain the electromagnetic field developed in the system in response to the charge Q we introduce the electric and magnetic field strengths \mathbf{E}_a and \mathbf{H}_a together with electric and magnetic inductions \mathbf{D}_a and \mathbf{B}_a . The index $a = 1$ ($a = 2$) refers to the half space $z > 0$ ($z < 0$) separated by the QH system. They satisfy the standard boundary conditions at the

$z = 0$ plane

$$\begin{aligned} (\mathbf{D}_1 - \mathbf{D}_2)_z &= 4\pi J_0, & \epsilon_{ij} (\mathbf{E}_2 - \mathbf{E}_1)_j &= 0, \\ (\mathbf{B}_1 - \mathbf{B}_2)_z &= 0, & \epsilon_{ij} (\mathbf{H}_2 - \mathbf{H}_1)_j &= 4\pi J_i. \end{aligned} \quad (6)$$

Here and throughout the paper i, j denote spatial indices x and y , and ϵ_{ij} is the antisymmetric tensor of rank two defined by $\epsilon_{xy} = 1$. Further, J_0 and \mathbf{J} in Eq. (6) represent the charge density $\rho_{3D} = J_0 \delta(z)$ and current density $\mathbf{J}_{3D} = \mathbf{J} \delta(z)$ in the QH system.

The image magnetic monopole effect can be understood from two equivalent perspectives. One approach (which we call the “orthodox” theory) utilizes the linear response theory [51] of the QH state, while the other views the QH plane as a domain wall of the $\mathbf{E} \cdot \mathbf{B}$ term. We review both these approaches below.

1. Orthodox description of TME: Surface currents

In the “orthodox” approach the inductions \mathbf{D}_a and \mathbf{B}_a are related to \mathbf{E}_a and \mathbf{H}_a via the permittivity ϵ_a and permeability μ_a of the media surrounding the QH plane in half spaces $a = 1, 2$:

$$\mathbf{D}_a = \epsilon_a \mathbf{E}_a, \quad \mathbf{H}_a = \frac{\mathbf{B}_a}{\mu_a}. \quad (7)$$

On the other hand the linear response theory of the QH state gives

$$J_0 = \sigma_{xy} B_z, \quad (8a)$$

$$J_i = \sigma_{xy} \epsilon_{ij} E_j. \quad (8b)$$

Since B_z and E_i are continuous, it does not matter whether we associate the terms proportional to σ_{xy} to fields stemming from region $z > 0$ or $z < 0$.

The nontrivial continuity conditions can now be presented as follows:

$$[\mathbf{D}_1 - (\mathbf{D}_2 + 4\pi \sigma_{xy} \mathbf{B})]_z = 0, \quad (9a)$$

$$\epsilon_{ij} (\mathbf{H}_2 - 4\pi \sigma_{xy} \mathbf{E} - \mathbf{H}_1)_j = 0. \quad (9b)$$

As we are going to discuss, these conditions imply formation of image electric and magnetic charges whose values are controlled by the Hall conductivity of the QH system.

2. Theory with $\mathbf{E} \cdot \mathbf{B}$ term

Instead of considering currents J_μ , we can include a QH system into the electromagnetic theory as a domain wall [89] of $\mathbf{E} \cdot \mathbf{B}$ terms with theta angles sufficing $\vartheta_2 - \vartheta_1 = \vartheta = -(2\pi)^2 \sigma_{xy} / \alpha$. In the bulk regions $a = 1, 2$ we obtain the relations [80,88]

$$\mathbf{D}_a = \epsilon_a \mathbf{E}_a - \frac{\vartheta_a}{2\pi} 2\alpha \mathbf{B}_a, \quad \mathbf{H}_a = \frac{\mathbf{B}_a}{\mu_a} + \frac{\vartheta_a}{2\pi} 2\alpha \mathbf{E}_a, \quad (10)$$

leading to the same continuity conditions as Eqs. (9).

As was first discovered in the 1980s [89], these continuity conditions imply the mirror magnetic monopole effect. Assuming for simplicity $\epsilon_1 = \epsilon_2$ and $\mu_1 = \mu_2$, one finds the

magnetic (g) and electric (q) mirror charges

$$g = Q \frac{\left(\frac{\partial \alpha}{2\pi}\right)}{1 + \left(\frac{\partial \alpha}{2\pi}\right)^2}, \quad q = -Q \frac{\left(\frac{\partial \alpha}{2\pi}\right)^2}{1 + \left(\frac{\partial \alpha}{2\pi}\right)^2}. \quad (11)$$

Physically, the inhomogeneous magnetic field is created by the nonuniform, circular QH currents [80] emerging in response to the radial electric field in the QH system. This \mathbf{B} field induces locally varying charge density [see Eq. (8a)] which again leads to a radial electric field. Summing up the corresponding geometric series one finds both g (starting from linear order in ϑ) and q (starting from quadratic order in ϑ).

Contrary to transport experiments (see Sec. II B), the image charge experiment does probe directly the local value of g_{xy} . Therefore, the image magnetic monopole can be used to measure a half-integer g_{xy} , as was first proposed in Ref. [80]. Clearly, the monopole character of the magnetic field persists only in the 2D “bulk” of the QH system; in finite systems the magnetic field lines always close [80,91]. In Sec. VII we will return to the image monopole effect: we there further generalize the problem to a double layer of QH systems, e.g., a thin 3D TI slab.

III. LAUGHLIN ARGUMENT

A. Phenomenology

This section is devoted to question (ii) of the introduction: Is the half-integer Hall conductance of a single Dirac fermion compatible with Laughlin’s flux-insertion argument, according to which the integer QH conductance is a direct consequence of gauge invariance [68,69]?

In its conventional form [69], the argument assumes a QH film in an annular geometry and a time-dependent flux threading the ring’s hole. However, as a consequence of the Nielsen-Ninomiya theorem [92], a film of a single Dirac fermion cannot be realized in a condensed matter system. Therefore, it is inevitable to modify the setup of the gedanken experiment. The simplest and most direct modification is a doughnut-shaped 3D TI [45,50]; see Fig. 2. The unavoidable change of the setup constitutes the crucial difference to the original argument.

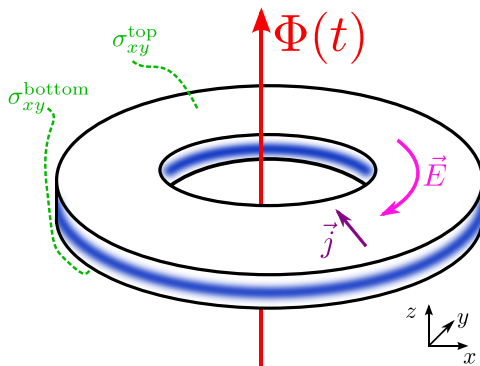


FIG. 2. (Color online) Since the surface of a 3D TI is itself boundaryless, the modified setup for the flux insertion argument involves a torus of 3D TI surface states. (Here, \vec{j} is shown for the exemplary case of $\sigma_{xy}^{\text{top}} > 0$.)

The setup in Fig. 2 depicts the 3D TI in a QH state determined by σ_{xy}^{top} and $\sigma_{xy}^{\text{bottom}}$. If $\sigma_{xy}^{\text{top}} + \sigma_{xy}^{\text{bottom}} \neq 0$ [93], chiral boundary modes appear at inner and outer perimeters of the slab annulus (blurred blue lines). Most naturally, this occurs if the QH state is created by an orbital magnetic field in the z direction. (The 3D TI surface Dirac fermions are not gapped on the side walls.)

In the process of the gedanken experiment the flux passing through the hole is slowly ramped up by one flux quantum in the period T ; e.g., $\Phi(t) = \frac{2\pi t}{T} \frac{\hbar}{e}$. An azimuthal electric field and corresponding electromotive force $\mathcal{E} = -\frac{d\Phi}{dt}$ are created inducing a radial current $I = \sigma_{xy}\mathcal{E}$. Over the period T an overall charge $\Delta Q = (\sigma_{xy}^{\text{top}} + \sigma_{xy}^{\text{bottom}}) \frac{\hbar}{e}$ is transferred between the two perimeters.

The 2D gauge potential associated with the flux piercing the hole is $A_i = -\frac{\Phi(t)}{2\pi} \partial_i \phi$ (ϕ is the azimuthal angle in 2D polar coordinates). At $t = T$ this is a pure gauge and can be removed by a (large) gauge transformation [94]. Thus, the electronic states at $t = 0$ and at $t = T$ are actually the states of the same system (with $\Phi = 0$) and the charge ΔQ is the charge of its edge excitation. In a noninteracting system, all states have integer charge and thus $\Delta Q = \text{integer} \times e$. As a consequence, $(\sigma_{xy}^{\text{top}} + \sigma_{xy}^{\text{bottom}})$ is restricted to integer multiples of e^2/h , in full accordance with the half-integer QHE on a 3D TI surface.

B. Edge states, spectral flow, and microscopies

In Sec. III A we discussed the adiabatic flux insertion from the macroscopic point of view and came to the conclusion that the sum $(g_{xy}^{\text{top}} + g_{xy}^{\text{bottom}})$ is quantized to integer values. We now turn to refinements, by means of which we can understand half-integer quantization of g_{xy}^{top} and g_{xy}^{bottom} .

To this end, it is necessary to specify the actual nature of the edge states (blurred blue regions in Fig. 2), between which the charge ΔQ is transferred. We remind the reader that, due to the Klein tunneling phenomenon, Dirac electrons cannot be confined by application of scalar potential. A physical way to model a finite 3D TI slab is shown schematically in Fig. 3: In the vicinity of the perimeters of the torus ($r \approx R_{i,e}$), the 3D TI slab gradually becomes thinner and top and bottom surfaces are strongly hybridized in the region $|r - R_{i,e}| \ll l_t$. This motivates introducing the Hamiltonian as a 4×4 matrix in the space of top/bottom and (pseudo)spin space:

$$H = H_0^{\text{tot}} + H_{\text{dis}}^{\text{tot}}, \quad (12)$$

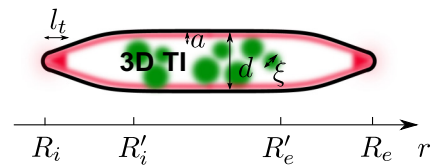


FIG. 3. (Color online) Cross section of the 3D TI torus depicted in Fig. 2 in a plane perpendicular to the azimuthal unit vector. Here $r = \sqrt{x^2 + y^2}$. For the discussion of length scales and boundary conditions, see main text.

with

$$H_0^{\text{tot}} = \begin{pmatrix} H_0^{\text{top}} & T(r) \\ T(r)^\dagger & H_0^{\text{bottom}} \end{pmatrix}. \quad (13)$$

In the 2D “bulk,” we assume well-defined gapless surface states with negligible penetration depth $a \ll d$ (here d is the slab thickness) and thus the intersurface hopping falls off exponentially. In contrast, at the boundary $T(r)$ is expected to be the dominant energy scale, which is of the order of the bulk band gap M :

$$T(r) \sim M e^{-\frac{|r-R_{i,e}|}{l_t}}. \quad (14)$$

Microscopically, the tunneling matrix element $T(r)$ can be determined integrating out the sidewall states of the 3D TI. For simplicity, we assume real, scalar $T(r) \propto \mathbf{1}_\sigma$; this is not essential for conclusions of our analysis.

Following Halperin [69], we assume the disorder ($H_{\text{dis}}^{\text{tot}}$, represented by green, blurry dots in Fig. 3) to be confined to the inner part of the sample $R'_i < r < R'_e$. In Fig. 3 and subsequent Secs. IV–VI, for simplicity we assume the disorder potential to be uncorrelated between the surfaces ($\xi \ll d$). Qualitatively, all results of this paper are independent of this assumption; in particular it is completely immaterial for the modified Halperin argument discussed in the present section.

The clean Hamiltonian is determined by $H_0^{\text{top}} = -H_0^{\text{bottom}} = H_0$ with

$$H_0 = v_0(\Pi_x \sigma_y - \Pi_y \sigma_x). \quad (15)$$

The symbols $\Pi_i = -i\partial_i - e\mathcal{A}_i(\mathbf{x})$ denote long derivatives; $e = -|e|$ is the electron charge. We assume for definiteness that the magnetic field $B = \epsilon_{ij}\partial_i\mathcal{A}_j > 0$.

The eigenstates of the clean Hamiltonian (15) are given by LLs [95,96] (see also Appendix A)

$$|n,k\rangle_D = \frac{1}{\sqrt{1+\eta_n^2}} \begin{pmatrix} -\eta_n |n-1,k\rangle \\ |n,k\rangle \end{pmatrix}, \quad (16)$$

with quantum numbers $n \in \mathbb{Z}$ associated with energies

$$E_n = \Omega_c \eta_n \sqrt{|n|}, \quad \Omega_c = \sqrt{2|e|B}v_0^2. \quad (17)$$

Here $\eta_n = \text{sgn}(n)$ for $n \neq 0$ and $\eta_0 = 0$, Ω_c is the (quantum) cyclotron frequency, v_0 is the velocity of the Dirac electrons, and $k = 1, 2, \dots, \frac{\Phi_{\text{tot}}}{\Phi_0}$ accounts for degeneracy. The states $|n,k\rangle$ describe the LLs of usual electrons with parabolic dispersion. In this section we choose to work in symmetric gauge and the quantum number k determines the radius r_k around which the LL wave functions are peaked [69,97].

The length scale l_t of hybridization at the edges is assumed to fulfill

$$l_B \ll l_t \ll (R'_{i,e} - R_{i,e}). \quad (18)$$

To lowest order in small parameter l_B/l_t we can neglect the mixing of Landau levels and approximate the Hamiltonian H_0^{tot} , Eq. (13), by its diagonal (in LL space) blocks

$$H_{0,n}^{\text{tot}} = \begin{pmatrix} E_n & T(r) \\ T(r) & -E_n \end{pmatrix}. \quad (19)$$

Each Hamiltonian $H_{0,n}^{\text{tot}}$ acts in the LL specific surface space spanned by $(|n,k\rangle_D, 0)^T$ and $(0, |n,k\rangle_D)^T$. The Hamiltonian

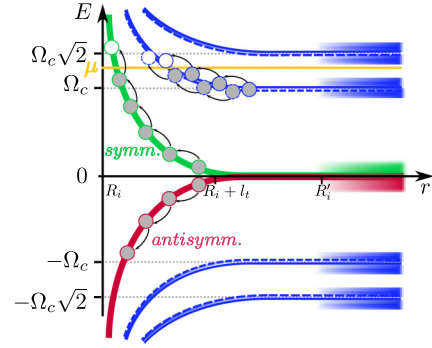


FIG. 4. (Color online) Schematic representation of the spectrum at the inner boundary of the TI torus shown in Figs. 2 and 3.

$H_{0,n}^{\text{tot}}$ has eigenstates

$$|n,k,\pm\rangle = \frac{1}{\sqrt{2\mathcal{E}_{n,\pm}(\mathcal{E}_{n,\pm} + E_n)}} \begin{pmatrix} (E_n + \mathcal{E}_{n,\pm})|n,k\rangle_D \\ T(r)|n,k\rangle_D \end{pmatrix} \quad (20)$$

with energies $\mathcal{E}_{n,\pm} = \pm\sqrt{E_n^2 + T(r)^2}$.

Faraway from the edge ($|r - R_{i,e}| \gg l_t$), $|n,k,+ \rangle$ is a state living on solely the top (bottom) surface if $E_n > 0$ ($E_n < 0$), while $|n,k,- \rangle$ has its weight on the opposite bottom (top) surface. It is a crucial observation that in contrast to the $n \neq 0$ case, the zeroth LL wave functions $|0,k,\pm\rangle$ are symmetric and antisymmetric combinations of top and bottom states without any r -dependent envelop. Note that $T(r)$ drops out of Eq. (20) for $n = 0$.

Figure 4 gives a schematic representation of the LL bending around the inner perimeter of the sample $r = R_i$. In the 2D bulk region $r \ll l_t + R_i$ states with $n \neq 0$ live on the top (solid lines) or bottom surface (dashed lines). They become hybridized (fat lines) close to the boundary. In contrast, states of the zeroth LL always mix top and bottom surfaces.

The intersections of the bended LLs with the line of chemical potential define the edge states. For the case of Fig. 4 there are three of them: two originating from the filled first LL in the two surfaces and another from the surface-symmetrized combination of the zeroth LL. When the flux threading the hole is increased by one flux quantum, the LL states contract and states right above (below) the chemical potential get filled (emptied) at the internal (external) perimeter (“spectral flow”) [69]. In the present case (Fig. 4) the states $|1,k_i,\pm\rangle$ and $|0,k_i,+ \rangle$ (with $r_{k_i} \approx R_i$) were filled. Similarly, the states $|1,k_e,\pm\rangle$ and $|0,k_e,+ \rangle$ were emptied at the outer edge. As a consequence of energy conservation, we conclude that during the process of flux insertion, two electrons with energy $E = \Omega_c$ are injected into (ejected from) the disordered region of the top surface at $r = R'_e$ ($r = R'_i$). In addition, a third electron with $E = 0$ enters (exists) the disordered region in a symmetric superposition of top states and bottom states at the same radial positions. By consequence, the associated current is driven through the upper and lower surface with equal weight [98]. Altogether, we conclude that $\sigma_{xy}^{\text{top}} = 3e^2/2h$ and $\sigma_{xy}^{\text{bottom}} = 3e^2/2h$.

The above analysis can be extended to a generic situation with the chemical potential μ located in the mobility gaps of

the two surfaces. In particular one finds half-integer values $\sigma_{xy}^{\text{top}} = (n + 1/2)e^2/h$ for μ located between the n th and the $(n + 1)$ th bulk delocalized state of the top surface and an analogous expression for the bottom surface [99].

IV. SEMICLASSICAL CALCULATION OF CURRENT DENSITY

In the previous sections we came to the conclusion that the Dirac fermions on the surface of a 3D TI give rise to a half-integer-quantized g_{xy} provided that the time-reversal invariance is locally broken. Our argumentation was very general, as it relied only on gauge invariance and topology. It is instructive, however, to have a model for which an explicit controllable calculation of half-integer g_{xy} is possible. In this section we present and analyze such a model consisting of a single species of 2D Dirac fermion in the presence of orbital coupling to a magnetic field and arbitrarily strong but sufficiently smooth potential landscape $V(\mathbf{x})$. Apart from an externally applied electrostatic potential (caused, e.g., by a test charge in the image magnetic monopole experiment), the potential $V(\mathbf{x})$ can include smooth disorder. The externally applied potential is not required to be weak (in comparison with the cyclotron frequency), so that our findings are valid beyond the linear response. While the model we consider in this section is sufficiently general, it is amenable to an analytical treatment due to semiclassical nature of the potential. Specifically, we will calculate the Hall conductivity in this model by using the vortex state representation of LLs [70–72]. The results of this section shed light on the deep field-theoretical origin of the half-integer shift of Hall conductance.

Our fermionic Hamiltonian reads

$$H = H_0 + V(\mathbf{x}). \quad (21)$$

Here H_0 is the clean fermionic Hamiltonian introduced in Eq. (15). In this section we will use symmetric gauge and the overcomplete vortex state representation of LLs [70–72]. In this representation the discrete degeneracy quantum number k is replaced by the continuous guiding center position $\mathbf{R} \in \mathbb{R}^2$. The wave function for the n th Landau level is then given by

$$\langle \mathbf{r} | n, \mathbf{R} \rangle = \frac{e^{in \arg(\mathbf{r}-\mathbf{R})}}{\sqrt{2\pi n!} l_B} \left| \frac{\mathbf{r}-\mathbf{R}}{\sqrt{2} l_B} \right|^n e^{-\frac{(\mathbf{r}-\mathbf{R})^2 - 2iz(\mathbf{r} \times \mathbf{R})}{4l_B^2}}. \quad (22)$$

The vortex states are “semiorthogonal,”

$$\langle n, \mathbf{R} | n', \mathbf{R}' \rangle = \delta_{nn'} e^{-\frac{(\mathbf{R}-\mathbf{R}')^2 - 2iz(\mathbf{R} \times \mathbf{R}')}{4l_B^2}}, \quad (23)$$

and produce the resolution of identity [100]

$$\int \frac{d^2 R}{2\pi l_B^2} \sum_{n=0}^{\infty} |n, \mathbf{R}\rangle \langle n, \mathbf{R}| = \mathbf{1}. \quad (24)$$

On the other hand, for fixed n and n'

$$\int d^2 R \langle \mathbf{r} | n, \mathbf{R} \rangle \langle n', \mathbf{R} | \mathbf{r}' \rangle = \langle n, \mathbf{r} | n' \mathbf{r}' \rangle, \quad (25)$$

as follows from the identity $\langle \mathbf{r} | n, \mathbf{R} \rangle = \langle n, \mathbf{r} | \mathbf{R} \rangle$. The vortex states $|n, \mathbf{R}\rangle_D$ for the Dirac Hamiltonian are the spinors constructed out of states (22) analogously to Eq. (16).

We are interested in the current density which couples to the macroscopic probing gauge potentials A_μ via local coupling

Lagrangian

$$\mathcal{L}_{\text{coupling}} = \sum_{i=x,y} J_i A_i \quad (26)$$

and enters subsequently the Maxwell equations for A_μ .

We concentrate on stationary current distributions. Our semiclassical calculation relies on the following assumptions:

(1) The scalar potential $V(\mathbf{x})$ is smooth on the scale of the magnetic length.

(2) The macroscopic gauge potential $A(\mathbf{x})$ is smooth on the scale of the magnetic length.

(3) Local thermodynamic equilibrium is maintained on the typical length scale of $V(\mathbf{x})$.

Requirement (2) is the defining distinction between the gauge potential \mathcal{A}_i creating the magnetic field responsible for QHE and the probing gauge potential A . It guarantees that the electron position and the vortex (guiding center) position are indistinguishable for A .

It is convenient to combine the current densities $J_{x,y}$ into complex combinations $J_\pm = J_x \pm iJ_y$ given by

$$J_\pm(\mathbf{x}) = \lim_{\mathbf{x}' \rightarrow \mathbf{x}} \langle \psi^\dagger(t, \mathbf{x}) j_\pm \psi(t, \mathbf{x}') \rangle. \quad (27)$$

The first quantized current operators $j_\pm = j_x \pm ij_y$, defined by $\mathbf{j} = ie[H_0, \mathbf{r}]$ in the Hamiltonian formalism, are

$$j_+ = -2iev_0 \begin{pmatrix} 0 & 1 \\ 0 & 0 \end{pmatrix}, \quad (28a)$$

$$j_- = 2iev_0 \begin{pmatrix} 0 & 0 \\ 1 & 0 \end{pmatrix}. \quad (28b)$$

The operators $\psi^\dagger(t, \mathbf{x})$ and $\psi(t, \mathbf{x})$ entering Eq. (27) are fermionic field operators with two spinor components. Thus, J_\pm are proportional to the off-diagonal elements of the fermionic Green's function $G_{\sigma\sigma'}(t, \mathbf{x}; t, \mathbf{x})$ at equal point and time. Since we expect ultraviolet divergences [unbounded spectrum of Hamiltonian (15)], we regularize $J_\pm(\mathbf{x})$ via point splitting. Strictly speaking, to make this procedure $\mathbf{U}(1)$ gauge invariant, a Wilson line $e^{ie \int_{\mathbf{x}'}^{\mathbf{x}} (A+A)d\mathbf{y}}$ should be inserted in the end of Eqs. (27), (29), and (30). However, it drops out in the limit $\mathbf{x} \rightarrow \mathbf{x}'$ and is thus omitted for simplicity. The physical reason is that at small splitting $|\mathbf{x} - \mathbf{x}'| \ll l_B$, the right-hand side of Eq. (27) is invariant under the “macroscopic” (slow) local $\mathbf{U}(1)$ symmetry associated with potentials A even before taking the limit $\mathbf{x} \rightarrow \mathbf{x}'$.

Under the assumptions (1)–(3), we find (see Appendix A)

$$J_\pm(\mathbf{x}) \approx \frac{\pm i|e|}{2\pi} \lim_{\mathbf{x}' \rightarrow \mathbf{x}} \int d^2 R \sum_{|n|=0}^{\infty} \sum_{\eta_n} n_F[E_n + V(\mathbf{R})] \times_D \langle n, \mathbf{R} | \mathbf{x} \rangle \langle \mathbf{x}' | n, \mathbf{R} \rangle_D \partial_\pm V(\mathbf{R}). \quad (29)$$

This formula has the following simple physical interpretation. In order to find the local current density $J_\pm(\mathbf{x})$ as a response to the electric field $\partial_\pm V(\mathbf{R})$, one should sum over all locally filled Landau levels and perform a convolution with $|\langle \mathbf{x} | n, \mathbf{R} \rangle_D|^2$ representing the response of a single vortex state.

The integral in Eq. (29) diverges at $\mathbf{x} = \mathbf{x}'$. However, the point-splitting procedure, which implies the formal rule $\lim_{\mathbf{x}' \rightarrow \mathbf{x}} \delta(\mathbf{x} - \mathbf{x}') \equiv 0$, renders Eq. (29) finite. To make the regularization manifest, we add and subtract the

zero-temperature linear-response current to/from Eq. (29):

$$\begin{aligned} X_{\pm}(\mathbf{x}) &= J_{\pm}(\mathbf{x})|_{T=0} = \frac{\pm i|e|\partial_{\pm}V(\mathbf{x})}{2\pi} \\ &\times \lim_{\mathbf{x}' \rightarrow \mathbf{x}} \int d^2R \sum_{n \leq 0} \langle n, \mathbf{R} | \mathbf{x} \rangle \langle \mathbf{x}' | n, \mathbf{R} \rangle_D \\ &= \pm i|e|\partial_{\pm}V(\mathbf{x}) \left[\lim_{\mathbf{x}' \rightarrow \mathbf{x}} l_B^2 \delta(\mathbf{x} - \mathbf{x}') + \frac{1}{4\pi} \right]. \end{aligned} \quad (30)$$

The first term in the square brackets (delta function) comes from the resolution of identity of the usual (equidistant) LLs [see Eq. (24)] and vanishes after the point splitting. In contrast, the second term will turn out to be responsible for half-integer g_{xy} . Its appearance is a direct consequence of the definite chirality of the zeroth LL wave function (see Appendix A) and thus a manifestation of the Atiyah-Singer (AS) index theorem [101,102].

The integral determining the quantity $J_{\pm} - X_{\pm}$ is now regular, since the divergence has been shifted entirely into X_{\pm} and is cured by the formal point-splitting procedure: $X_{\pm} = \pm i|e|\partial_{\pm}V(\mathbf{x})/4\pi$. We can therefore take the $\mathbf{x}' \rightarrow \mathbf{x}$ limit, rearrange integrals and sums, and exploit once more the smoothness of $V(\mathbf{x})$ [assumption (1)] to obtain

$$\begin{aligned} J_{\pm}(\mathbf{x}) &= \frac{\pm i|e|}{2\pi} \partial_{\pm}V(\mathbf{x}) \left\{ \sum_{n>0} n_F(E_n + V(\mathbf{x})) \right. \\ &\quad \left. + \sum_{n \leq 0} [n_F(E_n + V(\mathbf{x})) - 1] + \frac{1}{2} \right\}. \end{aligned} \quad (31)$$

The local transverse conductivity is thus given by

$$\begin{aligned} \sigma_{yx}(\mathbf{x}) &= -\sigma_{xy}(\mathbf{x}) = \frac{e^2}{h} \frac{1}{2} + \frac{e^2}{h} \left\{ \sum_{n>0} n_F(E_n + V(\mathbf{x})) \right. \\ &\quad \left. + \sum_{n \leq 0} [n_F(E_n + V(\mathbf{x})) - 1] \right\}. \end{aligned} \quad (32)$$

The semiclassical, local current density, Eq. (31), for a continuum, single-species 2D Dirac theory has the following features: (i) The current density follows equipotential lines (i.e., it is perpendicular to the local electric field). (ii) The strength of the current density is determined by the local filling factor of LLs; see Eq. (32). (iii) The crucial difference between electrons with parabolic dispersion and Dirac fermions is the half-integer contribution by the filled-hole band, i.e., the last term in the curly brackets of Eq. (31). As explained, it is a consequence of the AS index theorem and fermion number fractionalization. (iv) Recall that, in view of global fermion doubling in a TI, there is always a second area which provides an additional half-integer contribution. In the simplest setup, see Figs. 1 and 2, the two additive contributions stem from the opposite major surfaces of a 3D TI slab. (v) Let us finally reiterate that, in contrast to usual linear response calculations, Eqs. (31) and (32) are also valid in the case of a strong static electric field. In particular, they can be applied to study the magnetic image monopole effect in the situation when the voltage between test charge Q and the QH system exceeds $\Omega_c/|e|$.

In summary, the semiclassical calculation of the conductivity tensor in a smooth disorder exposed in this section sheds light on the deep origin of the half-integer QHE. At the same time, the semiclassical calculation can explain the quantization of Hall conductance only when the Fermi level resides in the energy gaps between LLs. In order to understand the quantization in the generic situation, the field-theoretical formalism describing Anderson localization is derived in the following section.

V. FIELD THEORY OF LOCALIZATION

This section is devoted to the field theory describing the localization physics in the half-integer QH state. It should be emphasized that the QHE crucially depends on the presence of disorder. Specifically, it is the disorder-induced localization that provides mobility gaps with a finite density of states in the bulk of a 2D system, which in turn leads to plateaus with quantized values of σ_{xy} as a function of carrier density. Thus, the analysis of half-integer QHE should contain a discussion of Anderson localization as one of key ingredients.

On the basic level the 3D TI surface fermions are described by the Euclidean field theory

$$\mathcal{Z} = \int \mathcal{D}[\bar{\psi}, \psi] e^{-S[\bar{\psi}, \psi]} \quad (33)$$

with the Matsubara action

$$S[\bar{\psi}, \psi] = \int_{\tau, \mathbf{x}} \bar{\psi} [D_{\tau} + H_0 + V(\mathbf{x}) - \mu] \psi + S_{\text{int}}. \quad (34)$$

Throughout the paper we use the notation $\int_{\tau, \mathbf{x}} = \int d^2x \int_0^{\beta} d\tau$; as usual $\beta = 1/T$ is the inverse temperature (in our units, Boltzmann's constant is $k_B = 1$). We compactify the space, so that the base manifold of our field theory is $(\mathbb{R}^2 \cup \{\infty\}) \times \mathbb{S}^1$. The clean, free Hamiltonian H_0 was introduced in Eq. (15). The long derivatives $\Pi_i = -i\partial_i - e(\mathcal{A}_i + A_i)$ include both the vector potential \mathcal{A}_i responsible for the quantizing magnetic field B and a source field A_i . The long Matsubara derivative is $D_{\tau} = \partial_{\tau} - ie\Phi$; $V(\mathbf{x})$ and μ represent Gaussian δ -correlated disorder potential and chemical potential, respectively. The fermionic fields $\bar{\psi}(\mathbf{x}, \tau) = (\bar{\psi}^{\uparrow}, \bar{\psi}^{\downarrow})$ and $\psi(\mathbf{x}, \tau) = (\psi^{\uparrow}, \psi^{\downarrow})^T$ describe the spinful (\uparrow, \downarrow) surface excitations. The electron-electron interaction (S_{int}) can also be included in our treatment (see Refs. [26,33]). It can be strong ($r_s = e^2/\epsilon\hbar v_0 \sim 1$), with the only condition that it does not induce any spontaneous symmetry breaking.

Our aim in this section is to determine the effective low-energy theory of gauge potentials $A_{\mu} = (\Phi, A_i)$ in the 2D “bulk” of the general interacting, disordered system without resorting to QH edge states. Let us summarize shortly our strategy. We first note that there are two relevant energy scales in this problem: the elastic scattering rate $1/\tau$ and the (inelastic) phase breaking rate $1/\tau_{\phi}(T)$. At low temperatures, these scales form the hierarchy

$$\frac{1}{\tau_{\phi}(T)} \ll \frac{1}{\tau}. \quad (35)$$

Consequently, to get the desired theory for the gauge field, we integrate out matter fields in a stepwise fashion: since electrons with quantum numbers n, k (see Sec. III B) are good

excitations only above $1/\tau$, they are integrated out first. The resulting theory then involves gauge fields and diffusive soft modes (diffusive sigma model). To account for the interaction of the diffusive modes (also known as quantum interference effects) at energies lower than $1/\tau$ the renormalization group approach is employed. The renormalization group flow stops at the energy scale $1/\tau_\phi(T)$ where the phase breaking destroys quantum interference. The remaining modes of the matter field can then be integrated out in the saddle-point approximation resulting in the effective low-energy theory of the gauge potential, which was discussed on phenomenological grounds in Sec. II.

A. Parity anomaly

We will first review the concept of parity anomaly. The high-energy action (34) is invariant under transformations of the gauge group \mathbf{G} , and in our case $\mathbf{G} = \mathbf{U}(1)$. Later we will replicate the theory N_R times and \mathbf{G} will turn out to be $(\mathbf{U}(1))^{\otimes N_R}$. In addition, in the absence of a net magnetic field or Zeeman term and after disorder average it is also invariant under the parity transformation of (2+1)-dimensional spacetime:

$$(x, y, \tau) \rightarrow (-x, y, \tau), \tag{36a}$$

$$\psi \rightarrow \sigma_x \psi, \tag{36b}$$

$$\bar{\psi} \rightarrow \bar{\psi} \sigma_x. \tag{36c}$$

Clearly, to keep the fermionic action invariant, the vector potential should transform under $x \rightarrow -x$ as

$$(A_x, A_y, \Phi) \rightarrow (-A_x, A_y, \Phi). \tag{37}$$

For dynamic gauge fields we note that this transformation leaves the Maxwell term invariant. Contrarily, a fixed background B field does not respect this symmetry (B is a pseudoscalar).

The peculiar fact about (2+1)-dimensional gauge theories is that invariance under parity transformation does not always persist to the quantized theory [83–86]. Following Ref. [103] we will however distinguish between “parity anomaly” and “intrinsic parity anomaly” for our problem of QED₃ on a spacetime manifold $(\mathbf{x}, \tau) \in \mathbb{S}^2 \times \mathbb{S}^1$. Of course both effects are related.

The notion of parity anomaly follows Ref. [83] and arises often in the context of condensed matter physics. It boils down to calculating σ_{xy} for the problem of massive (2+1)-dimensional Dirac fermions in the absence of any other energy scale. The result is $\sigma_{xy} = -\frac{\text{sgn}(m)}{2} \frac{e^2}{h}$. As there is no other energy scale, the mass m breaks time reversal and parity symmetries on all scales and therefore $\sigma_{xy}(m)$ is discontinuous at $m = 0$. One concludes that upon integration of Dirac electrons and subsequent $m \rightarrow 0$ limit the effective gauge theory contains a CS term with prefactor $\vartheta = \pm\pi$. The notion of parity anomaly means that the Lagrangian of fermions coupled to gauge potentials preserves parity upon taking the massless limit, while the effective electrodynamic Lagrangian does not. Not surprisingly, this “anomaly” disappears as soon as another infrared energy scale is introduced, for example finite temperature [103], a finite disorder scattering rate [64], or

a finite bulk band gap M [31]. Then, $\sigma_{xy}(m)$ becomes a continuous function of m and $\sigma_{xy}(0) = 0$.

The notion of intrinsic parity anomaly is more subtle. According to the early works [84,85,104], which treat the case of strictly massless fermions, in the process of field quantization one has two options:

(i) One can choose a regularization scheme in a manner preserving parity. But then the partition function acquires a sign $(-)^k$ under large gauge transformations.

(ii) Alternatively, one can regularize the theory in a manner preserving gauge invariance. In this case, a CS term with angle $\vartheta = \pi \pmod{2\pi}$ appears after integration of fermions. The latter breaks parity.

A theory with anomalously broken gauge symmetry is inconsistent, therefore, whenever $(-)^k \neq 1$ option (ii) must be chosen for a purely (2+1)-dimensional theory. A common variant of these regularization schemes is to use regularization as in (i) and to add the CS 3-form by hand to the fermionic action [85] when the latter contributes an additional factor of $(-)^k$ under large gauge transformations.

To prove assertion (i) one needs to unwind the gauge potentials $eA_n(\mathbf{x}, \tau) = -iU_n^{-1}\nabla U_n$ associated with large gauge transformations $U_n \in \mathbf{G}$. A fourth dimension is introduced and it can be shown that k equals the analytical index $\nu_+ - \nu_-$ of the corresponding four-dimensional Dirac operator. For non-Abelian gauge groups with third homotopy group $\Pi_3(\mathbf{G}) = \mathbb{Z}$ the AS index theorem [101,102] immediately implies $k = n$ (n is the homotopy class of U_n) [84,85].

Contrarily, for the case of QED₃ on $\mathbb{S}^2 \times \mathbb{S}^1$ the topology is more complicated: as $\Pi_1(\mathbf{G}) = \mathbb{Z}$, large gauge transformations act in the imaginary time sector. Further, topologically distinct instanton (monopole) configurations in the spatial $\mathbb{S}^2 \simeq \mathbb{R}^2 \cup \{\infty\}$ sector (i.e., field configurations with different magnetic flux Φ through the \mathbb{R}^2 plane) have to be treated with care. (We recall that the gauge potential, which explicitly enters the CS term, cannot be defined on the whole manifold.) Nevertheless, k can still be associated with the topological index of extended gauge fields. Specifically, it turns out that $k = n\Phi/\Phi_0$, where n is the winding in time direction [104]. In the presence of time-reversal symmetry we have $\Phi = 0$ and hence $k = 0$. We thus conclude that for the 2D theory of time-reversal-invariant surface states of 3D TIs there is no reason for inclusion of an additional CS term that would violate the parity of the theory.

More generally, we can consider the Dirac fermions on the entire surface wrapping the 3D TI sample [105]. This field theory again lives on a manifold homotopical to $\mathbb{S}^2 \times \mathbb{S}^1$. Then, since there are no physical monopoles, the total flux through the spatial sector vanishes even in the case of broken time-reversal symmetry and hence the topological insulator surface states do not exhibit intrinsic parity anomaly. We conclude that additional CS terms never need to be included. Such terms will therefore not appear in the effective electromagnetic actions to be derived in the following sections.

Recently [31], similar topological arguments for 3D TIs avoiding the intrinsic parity anomaly were presented. While the topological peculiarities of $\mathbf{U}(1)$ gauge theories were disregarded by the authors of that work, their argument in favor of the absence of parity anomaly in the theory of 3D TI surface states is in agreement with our conclusion.

An alternative line of argumentation with the same outcome is based on the concept of cancellation of anomalies [32]. It relies on the Callan-Harvey mechanism [106], according to which the anomaly of the boundary modes of a TI is canceled up exactly by the anomaly of the bulk states. A famous example is the theory [107] of chiral edge states in QH systems.

B. Gauged NL σ M of integer QHE

Before turning to Dirac fermions, we briefly review the field-theoretic description of the conventional integer QHE. The $U(1)$ -gauged NL σ M [19,26] describing the interaction of diffusive modes and the gauge potential has the action

$$S = \frac{1}{8} \int_x \text{tr} \left[g_{xx} D_i Q D_i Q + \epsilon_{ij} \frac{\vartheta}{2\pi} Q D_i Q D_j Q \right] + S_{\eta+int+B^2}. \quad (38)$$

According to the double cutoff regularization of Matsubara frequencies [26], the diffusive $(2N'_M \times N_R) \times (2N'_M \times N_R)$ matrix fields $Q(x)$ carry both Matsubara and replica indices and are typically represented as $(Q_{lm}^{\alpha\beta} = (U^{-1} \Lambda U)_{lm}^{\alpha\beta})$ ($\alpha, \beta = 1, \dots, N_R$ denote replicas and $l, m \in \{-N'_M, \dots, N'_M - 1\}$ Matsubara indices). The unitary matrices U have nontrivial entries belonging to $U(2N_M \times N_R)$ in the central block $l, m \in \{-N_M, \dots, N_M - 1\}$ ($N_M \ll N'_M$) and are unity outside. Recall that the dimensionless conductances are denoted by $g_{ij} = \sigma_{ij} h / e^2$. The term $S_{\eta+int+B^2}$ is less important for the present discussion and we mention it here for completeness only. It contains frequency and interaction contributions, as well as a term quadratic in magnetic field which renormalizes the permeability. The kinetic term (proportional to g_{xx}) and the theta term (proportional to ϑ) contain long derivatives acting as

$$D_i Q = \partial_i Q - i e [\hat{A}_i, Q]. \quad (39)$$

Hatted objects are defined by $\hat{a} \equiv \sum_{m,\alpha} a_m^\alpha J_m^\alpha$. In the above, we have introduced the following $(2N'_M \times N_R) \times (2N'_M \times N_R)$ matrices:

$$\Lambda_{lm}^{\alpha\beta} = \text{sgn}(\epsilon_m) \delta^{\alpha\beta} \delta_{lm}, \quad (40a)$$

$$(I_{m_0}^{\alpha_0})_{lm}^{\alpha\beta} = \delta^{\alpha_0\alpha} \delta^{\alpha_0\beta} \delta_{l-m, m_0}. \quad (40b)$$

The limits $N_M \rightarrow \infty$, $N'_M \rightarrow \infty$ ($N'_M/N_M \rightarrow \infty$) as well as the final replica limit $N_R \rightarrow 0$ are implicitly assumed.

Differentiation of Eq. (38) with respect to the vector potential and evaluation of the functional integral in the saddle-point approximation leads to the identification of the NL σ M coupling constants g_{xx} and $\frac{\vartheta}{2\pi}$ with the bare longitudinal and transversal (Hall) conductivities of the QH system (in units of e^2/h) [26]. At the diffusive saddle point $Q = \Lambda$ the theta term becomes the CS term [26].

C. Gauged NL σ M of half-integer QHE

1. Gauged NL σ M of Dirac fermions at $B = 0$

We turn now to the localization physics of a single Dirac fermion. Let us assume that TR symmetry is present on average (i.e., there is no net magnetic field) but broken by a random magnetic field or random Zeeman coupling [108]. In this

case, the gauged NL σ M can be derived using the non-Abelian bosonization technique (see Ref. [33] and Appendix B 1)

$$S = \frac{1}{8} \int_x \text{tr} \left[g_{xx} D_i Q D_i Q + \epsilon_{ij} \frac{\theta}{2\pi} Q \partial_i Q \partial_j Q \right] + S_{\eta+int}, \quad (41)$$

where $\theta = \pi \pmod{2\pi}$. It is worth emphasizing that the derivatives in the theta term are *not* covariant derivatives. Yet, the action (41) is gauge invariant. Indeed, local $U(1)$ transformations of fermionic fields translate into the following operation on NL σ M matrices:

$$Q(x) \rightarrow e^{i\hat{\chi}(x)} Q(x) e^{-i\hat{\chi}(x)}. \quad (42)$$

The theta term in Eq. (41), being quantized, is unchanged under smooth gauge transformations.

Since the theta term does not include coupling to the electromagnetic field, the Hall conductance of the Dirac fermions is not related to θ . Instead, $g_{xy} = 0$, which is exactly what one should expect in the absence of a net B field.

2. Gauged NL σ M at $B \neq 0$

The gauged NL σ M describing both electromagnetic response and localization physics of a single Dirac fermion is

$$S = \frac{1}{8} \int_x \text{tr} \left[g_{xx} D_i Q D_i Q + \epsilon_{ij} \frac{\theta}{2\pi} Q \partial_i Q \partial_j Q + \epsilon_{ij} \frac{\vartheta}{2\pi} Q D_i Q D_j Q \right] + S_{\eta+int+B^2}. \quad (43)$$

The derivation of this action can be found in Appendix B 2. It is crucial to observe that only ϑ couples to electromagnetic gauge potentials. Thus the transverse conductivity σ_{xy} is determined by ϑ alone, while the localization physics is governed by the sum $\vartheta + \theta = \vartheta \pm \pi$. In the renormalization group flow this will lead to an overall shift of g_{xy} by $\pm 1/2$; see Eqs. (44) below. The Matsubara NL σ M description of the QHE allows for inclusion of electron-electron interactions [109,110]. The shift of the RG flow by half a conductance quantum equally applies to the interacting case.

D. RG analysis of the sigma model

1. RG flow and phase diagram

Up to the important shift of the theta angle, the action (43) corresponds to the standard Pruisken NL σ M for spinless fermions. Therefore its renormalization [19,21] is analogous to the conventional case. The only modification is a connection between the theta angle and the Hall conductivity. This implies the following RG equations [109–111]:

$$\frac{dg_{xx}}{dy} = -A - \frac{B}{g_{xx}} - C g_{xx}^2 e^{-2\pi g_{xx}} \cos \left[2\pi \left(g_{xy} \pm \frac{1}{2} \right) \right], \quad (44a)$$

$$\frac{dg_{xy}}{dy} = -C g_{xx}^2 e^{-2\pi g_{xx}} \sin \left[2\pi \left(g_{xy} \pm \frac{1}{2} \right) \right]. \quad (44b)$$

In these equations $y = \ln L/l$, where L is the running scale and l the UV reference scale (mean-free path). The equations are written with the two-loop perturbative accuracy

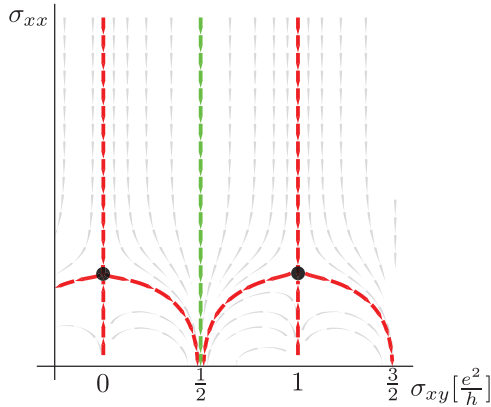


FIG. 5. (Color online) RG flow diagram for Dirac fermions, based on the scaling proposed by Khmelnitskii. As compared to the case of fermions with parabolic dispersion, the diagram is shifted by half a conductance quantum.

and contain in addition the leading nonperturbative (instanton) contributions. The prefactors A, B, C entering these RG equations are numerical constants. Below we give their values both for the case of noninteracting electrons [111] and for the Coulomb interaction [110]:

$$A = \begin{cases} 0 & \text{no interaction,} \\ \frac{2}{\pi} & \text{Coulomb interaction;} \end{cases} \quad (45a)$$

$$B = \begin{cases} 1/2\pi^2 & \text{no interaction,} \\ \approx 0.66 & \text{Coulomb interaction;} \end{cases} \quad (45b)$$

$$C = \begin{cases} 4\pi \exp(-1) & \text{no interaction,} \\ 4\pi \exp(1 - 4\gamma) & \text{Coulomb interaction.} \end{cases} \quad (45c)$$

Here $\gamma \simeq 0.577$ is the Euler-Mascheroni constant.

Equations (44) lead to the RG-flow diagram for the half-integer QHE of Dirac fermions [48,112,113]; see Fig. 5 [114]. The attractive fixed points are now $(g_{xx}^*, g_{xy}^*) = (0, (\nu + 1/2)e^2/h)$ while the delocalized critical state (black dot) appears at integer valued g_{xy} [115,116].

Starting values of the RG flow at the scale of the mean-free path l are given by the Drude expression of the conductivity tensor. We will discuss them in detail in Sec. VI below.

2. The $g_{xy} = 0$ transition

Generally, the universality class of the Dirac QH transition coincides with the QH transition in parabolic 2DEG [22,24,110,117]. However, if in the absence of magnetic impurities the QH transition from $\sigma_{xy} = -e^2/2h$ to $\sigma_{xy} = +e^2/2h$ is driven by the variation of the magnetic field from negative to positive, then additional soft modes, cooperons, modify the physics at length scales smaller than the magnetic length. This changes the nature of the transition and is represented in Fig. 6 by the blue upward arrows at $\sigma_{xy} \approx 0$ for the case without electron-electron interactions. At small length scales the system follows the RG of symplectic symmetry class (weak antilocalization). In the one-loop approximation the interference corrections can be understood as a renormalization of the elastic scattering rate, and the RG equations take

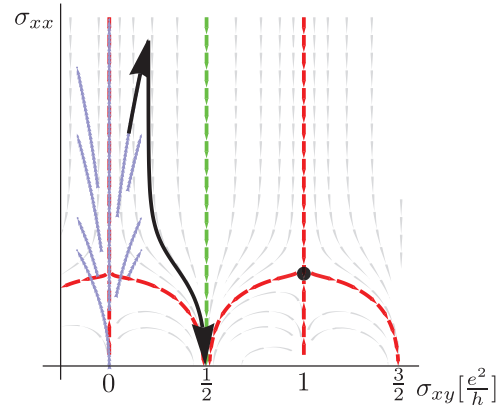


FIG. 6. (Color online) RG flow diagram for noninteracting Dirac fermions for the case when the magnetic field is the only source of time-reversal-symmetry breaking (i.e., assuming no magnetic impurities and no Zeeman coupling). The QH transition at $B = 0$ ($\sigma_{xy} = 0$) is qualitatively different from all others; see main text. The corresponding flow is depicted by black bold arrows. It follows the behavior of the symplectic class for $L < l_B$ and crosses over to the unitary class at $L \sim l_B$.

the form [118]

$$\frac{dg_{xx}}{dy} = \frac{1}{\pi}, \quad (46a)$$

$$\frac{dg_{xy}}{dy} = 2 \frac{g_{xy}}{g_{xx}} \times \frac{dg_{xx}}{dy} = \frac{2}{\pi} \frac{g_{xy}}{g_{xx}}. \quad (46b)$$

The crossover to the unitary class occurs when the running scale L hits l_B , and for larger length scales the flow follows Eqs. (44). Integrating the symplectic RG equations up to l_B we obtain

$$g_{xy}(l_B) \sim \frac{1}{(k_F l_B)^2} (k_F l + \ln l_B/l)^2 \ll 1. \quad (47)$$

Therefore, as long as the bare (Drude) value of the Hall conductivity is small, the renormalized value $g_{xy}(l_B)$ at the output of the symplectic stage of evolution remains small as well, and the system flows, in the infrared limit, into one of the lowest QH states $\sigma_{xy} = \pm e^2/2h$.

With the notation $t = 2/(\pi g_{xx})$ we rewrite the RG equations (46) as follows:

$$\frac{dt}{dy} = -\frac{1}{2}t^2, \quad (48a)$$

$$\frac{dg_{xy}}{dy} = g_{xy}t. \quad (48b)$$

The RG flow dictated by Eqs. (48) is shown in Fig. 7.

E. Effective electromagnetic theory

The RG stops at the scale of the infrared cutoff, e.g., the dephasing rate. To determine the effective electromagnetic theory at even lower energies, the diffusive modes should be integrated out at tree level. We here choose a gauge in which the scalar potential vanishes and restrict ourselves to the local

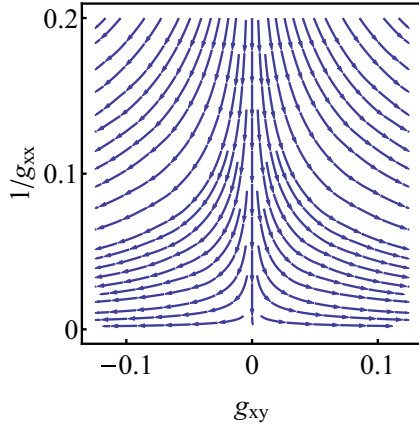


FIG. 7. (Color online) RG flow describing the $B = 0$ transition near the “supermetallic” fixed point $(1/g_{xx}^*, g_{xy}^*) = (0,0)$; see Eqs. (48).

part of the linear response functions. Then the effective action for the vector potential $A_{m,i}^\alpha$ becomes

$$S_{\text{eff}}[A] = \int_x \sum_{m>0, \alpha} e^2 m A_{-m,i}^\alpha A_{m,j}^\alpha (\delta_{ij} g_{xx} + \epsilon_{ij} g_{xy}), \quad (49)$$

where m is the Matsubara frequency, α the replica index and i, j denote spatial coordinates; see Sec. VB.

At the QH fixed points, Eq. (49) reproduces the CS theory. A more detailed discussion in the context of the integer quantum Hall effect can be found in Ref. [26].

VI. STARTING VALUES OF RG: LEVITATION SCENARIO AND PHASE DIAGRAM

The RG flow represented in Fig. 5 allows us to study the phase diagram of the Dirac QH effect [119,120] and discuss the levitation of extended states taking place at low magnetic field (or, equivalently, strong impurity scattering) [121].

A. Phase diagram

The phase diagram of the Dirac quantum Hall effect can be built by equating the Drude value of transverse conductance (which determines the electromagnetic response of our system at length scales of the order of the mean-free path and constitutes the initial conditions for the RG flow discussed in the previous section) to its values on the transition lines:

$$\sigma_{xy}^{(0)} = n \frac{e^2}{h}, \quad n \in \mathbb{Z}. \quad (50)$$

Figure 8 shows the resulting phase diagram of our system in terms of the Drude resistivities. The major quantitative difference to the situation of parabolic 2DEG [119] is the absence of any usual (the one with $\sigma_{xy} = 0$) insulating phase: the diagram is covered by QH states only. In addition, positions and radii of semicircular phase boundaries are modified.

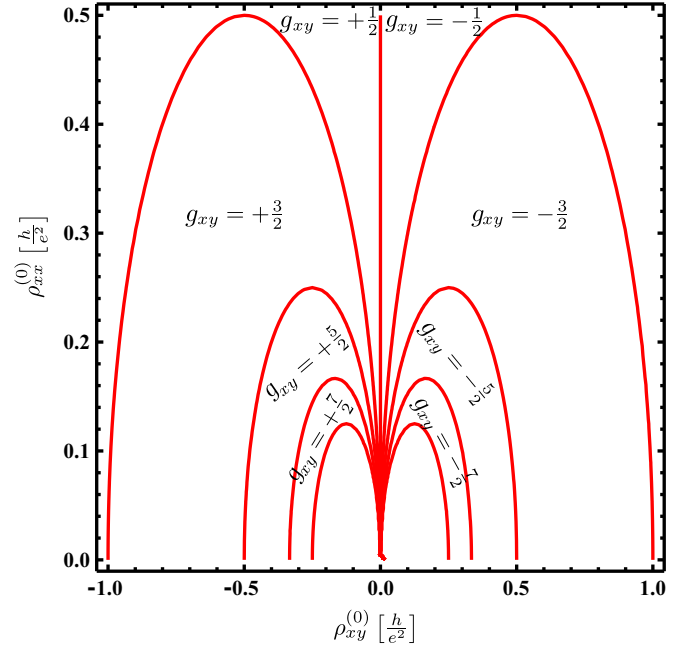


FIG. 8. (Color online) Phase diagram for the QHE of Dirac fermions in the plane of longitudinal and Hall resistivities.

B. Drude conductance

In order to build the phase diagram of the Dirac quantum Hall effect in terms of the magnetic field B and the chemical potential μ and to discuss the levitation scenario, we need to know the Drude conductivity tensor as a function of these parameters. In this section we present a semiclassical derivation of the Drude conductivity tensor based on the Boltzmann kinetic equation. We consider the general situation of Dirac fermions subject to orbital magnetic field B and Zeeman term $H_Z = E_Z \sigma_z$ ($E_Z \ll \mu$), thus allowing for the anomalous Hall effect. To the best of our knowledge, a comprehensive study of the Drude conductivity tensor in these settings has not been reported in the literature so far (see Refs. [122,123] for earlier work on the subject).

Our approach to the problem is justified provided that the quantum scattering time $\tau_q \gg 1/\mu$ (which is the usual condition of applicability of a semiclassical treatment). In the following we also assume that the classical cyclotron frequency $\Omega_c^{\text{cl}} = |eBv_0^2/\mu c| \ll 1/\tau_q$, which allows us to neglect the modification of the scattering integral by the orbital magnetic field. We note that for smooth disorder the transport scattering time $\tau_{tr} \gg \tau_q$, so that in this case both regimes of the classically strong ($1/\tau_{tr} \gg \Omega_c^{\text{cl}}$) and classically weak ($1/\tau_{tr} \ll \Omega_c^{\text{cl}}$) magnetic field can be studied. On the other hand, for short-range impurities $\tau_{tr} \sim \tau_q$, so that our approach does not apply to the limit of strong fields.

The relation between the Zeeman energy E_Z (which is assumed to be small compared to μ) and the quantum scattering time τ_q controls the importance of the coherence in the scattering between the Zeeman-split bands. In the case of weak scattering $E_Z \gg 1/\tau_q$ the interband coherence should be taken into account and leads to the anomalous Hall effect.

To the leading order in small parameters E_Z/μ and Ω_c^{cl}/μ the Drude conductivities are given by (we refer the reader to

Appendix C for detailed derivation)

$$\sigma_{xx} = \frac{\sigma_{xx}^{(B)}}{1 + (\Omega_c^{\text{cl}} \tau_{tr})^2} \left[1 + \frac{2\zeta \Omega_c^{\text{cl}} \tau_{tr}^2 / \tau_a}{1 + (\Omega_c^{\text{cl}} \tau_{tr})^2} + \frac{E_Z}{\mu^2 \tau_{sj}} \zeta \Omega_c^{\text{cl}} \tau_{tr} \right], \quad (51a)$$

$$\begin{aligned} \sigma_{xy} = & -\frac{e^2}{2h} \left[\text{sgn}(E_Z) \theta(E_Z^2 - \mu^2) + \frac{E_Z}{|\mu|} \theta(\mu^2 - E_Z^2) \right] \\ & + \frac{\sigma_{xx}^{(B)}}{1 + (\Omega_c^{\text{cl}} \tau_{tr})^2} \left[\zeta \Omega_c^{\text{cl}} \tau_{tr} \left(1 + \frac{2\zeta \Omega_c^{\text{cl}} \tau_{tr}}{1 + (\Omega_c^{\text{cl}} \tau_{tr})^2} \frac{\tau_{tr}}{\tau_a} \right) \right. \\ & \left. - \frac{\tau_{tr}}{\tau_a} - \frac{E_Z}{\mu^2 \tau_{sj}} \right]. \end{aligned} \quad (51b)$$

Here $\zeta = -\text{sgn}(\mu B)$ and we have introduced the notations $v(\mu) = |\mu| / (2\pi v_0^2) \theta(\mu^2 - E_Z^2)$ and $v(\mu) = v_0 \sqrt{1 - E_Z^2 / \mu^2}$ for the density of states and velocity at the Fermi level. The classical conductance at zero magnetic field is

$$\sigma_{xx}^{(B)}(\mu) = 2\pi \frac{e^2}{h} v(\mu) \frac{v^2(\mu) \tau_{tr}(\mu)}{D(\mu)}. \quad (52)$$

At zero magnetic field, Eqs. (51) reproduce the results of Ref. [124].

The first term in the transverse conductivity in Eq. (51b) represents the so-called intrinsic Hall conductivity [125] related to the modification of the classical equations of motion for a wave packet caused by the Berry curvature of the Dirac band. Equations (51) contain also terms characterized by times τ_a and τ_{sj} . These are the scattering times associated to the skew-scattering and the side-jump processes, respectively [73,74,125]. Assuming short-range impurities, one can express them, as well as the transport scattering time τ_{tr} , in terms of disorder amplitude V_0 (see Ref. [124] and Appendix C8) [126]:

$$\frac{1}{\tau_a} = \frac{\pi v(\mu) (n_i V_0^2)^2 [3E_Z(\mu^2 - E_Z^2)]}{8v_0^2 \mu^3}, \quad (53a)$$

$$\frac{1}{\tau_{sj}} = 2\pi n_i V_0^2 v(\mu), \quad (53b)$$

$$\frac{1}{\tau_{tr}} = 2\pi n_i V_0^2 v(\mu) \frac{1 + 3\left(\frac{E_Z}{\mu}\right)^2}{4}. \quad (53c)$$

Here n_i is the concentration of impurities. The behavior of the Drude conductivity tensor as a function of the chemical potential and the magnetic field is illustrated in Figs. 9 and 10.

C. Levitation of critical states

Equating the Drude value of the Hall conductance, Eq. (51b), with the transition lines of the RG flow (i.e., integer g_{xy}), one obtains the phase boundaries of QH phases in the B - μ plane.

At small $E_Z \ll 1/\tau_q$ we can neglect all the contributions of the anomalous Hall effect in Eqs. (51). Assuming further that the dominant source of disorder is Coulomb impurities, we can deduce the dependence of the transport scattering time on the chemical potential: $\tau_{tr} \propto \mu$. Accordingly, the combination

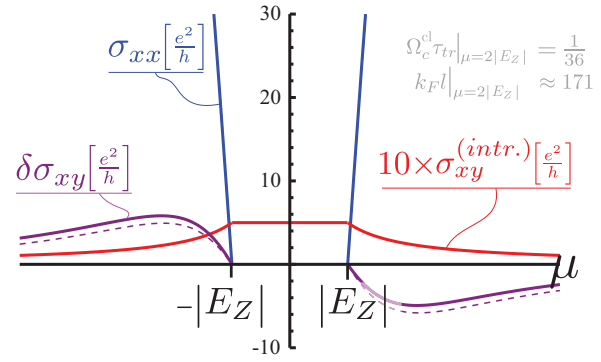


FIG. 9. (Color online) Dependence of the classical conductivities on chemical potential. The transverse conductivity was split into intrinsic (red, $\sigma_{xy}^{(\text{intr.})}$) and Fermi-surface (violet, $\delta\sigma_{xy}$) contributions. The dashed curves are obtained by reflection with respect to the origin and visualize the magnitude of the AHE contributions.

$\Omega_c^{\text{cl}} \tau_{tr} \propto B$ is independent of μ , and the energies of critical states are given by

$$\mu_{\text{deloc}} = \pm \sqrt{\Omega_c^2 |n| \frac{1 + (\Omega_c^{\text{cl}} \tau_{tr})^2}{(\Omega_c^{\text{cl}} \tau_{tr})^2} + E_Z^2}, \quad n \in \mathbb{Z}, \quad (54)$$

where Ω_c is the quantum cyclotron frequency defined in Eq. (17). For nonzero n , Eq. (54) describes the “floating up” or, equivalently, “levitation” of delocalized critical states separating QH phases. In the limit $\Omega_c^{\text{cl}} \tau_{tr} \gg 1$ the usual LL spectrum of gapped Dirac fermions is recovered. For $n = 0$ the solutions to be retained are $\mu_{\text{deloc}} = -\text{sgn}(B)E_Z$. This is a consequence of the AS index theorem, according to which the zeroth LL is fully spin polarized. The definite spin

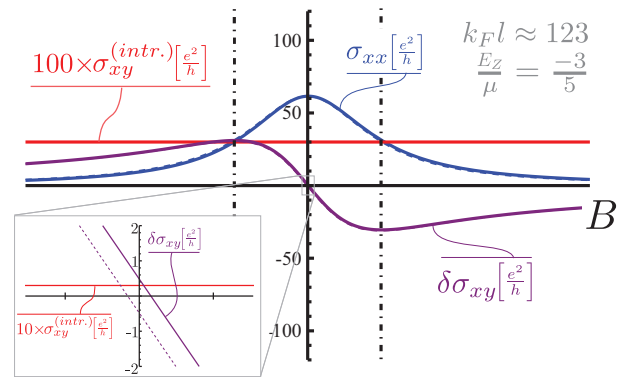


FIG. 10. (Color online) Dependence of the classical conductivity tensor on magnetic field. The transverse conductivity was split into intrinsic (red, $\sigma_{xy}^{(\text{intr.})}$) and Fermi-surface (violet, $\delta\sigma_{xy}$) contributions. The dot-dashed vertical lines denote the position where $\Omega_c^{\text{cl}} \tau_{tr} = 1$. In the inset, the contributions to the transverse conductance are plotted in the limit of vanishing B field. The ticks on the abscissa denote $\Omega_c^{\text{cl}} \tau_{tr} = 1/20$. The dashed curves are obtained by reflection $B \rightarrow -B$ and visualize the magnitude of the AHE contributions. In this plot, the Zeeman energy is assumed to be B -field independent (which could result from an exchange coupling to a nearby ferromagnetic layer).

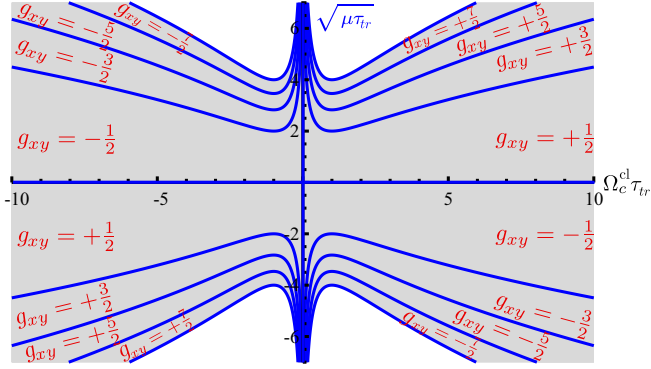


FIG. 11. (Color online) Levitation of delocalized states of gapless Dirac fermions for Coulomb impurities (μ/τ_{tr} and $\Omega_c^{\text{cl}}\tau_{tr} \propto B$ are μ -independent).

polarization predicts the sign of the Zeeman energy and thus of the energy level. It is worth emphasizing that, according to this result, the zeroth LL is immune against strong scattering. As a result, in the limit of strong scattering, $\Omega_c^{\text{cl}}\tau_{tr} \ll 1$, the phases with $\sigma_{xy} = \pm e^2/2h$ extend all the way from $\mu = 0$ up to large values of μ ; see Figs. 11 and 12. The robustness of the $\sigma_{xy} = \pm e^2/2h$ state against disorder was indeed observed numerically [59,127].

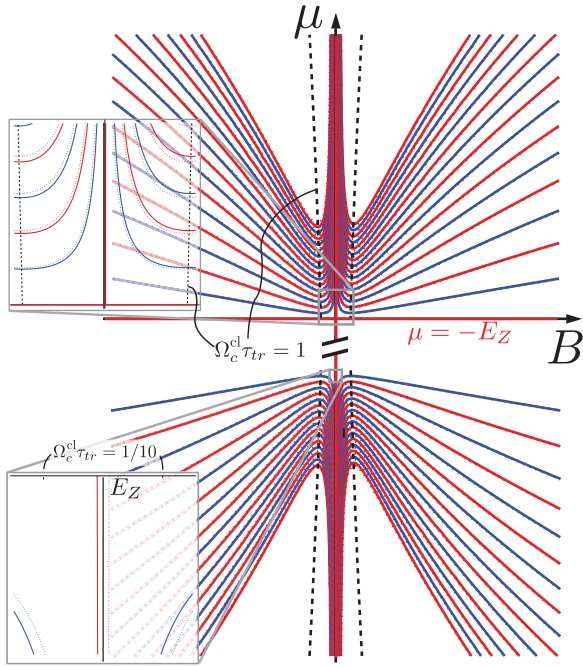


FIG. 12. (Color online) Phase diagram of QH phases in the B - μ plane (“levitation scenario”) for the case of short-range impurities. Here, as in Fig. 10, $E_Z < 0$ is assumed to be B -field independent. The floating up of delocalized states with odd (even) number is depicted by solid blue (red) curves. The dashed lines correspond to $\Omega_c^{\text{cl}}\tau_{tr} = 1$. The insets magnify the region of weak magnetic fields. The asymmetry under $B \rightarrow -B$ (dotted blue/red curves) is a consequence of the AHE. Disorder strength is determined by $|\mu|\tau_{sj} = 100$.

TABLE I. Typical experimental energy scales of 3D TI in kelvins [43,128,129]: The bulk band gap M , the cyclotron frequency $\Omega_c = \sqrt{2}|e|Bv_0^2/\hbar$, the Zeeman energy $|E_Z| = g\mu_B B$, and the inelastic scattering rate $1/\tau_{tr}$. Bulk g factors [130,131] entering E_Z were typically determined outside the TI regime. The presented values of E_Z correspond to the maximal Zeeman energy, with perfect alignment of pseudospin σ and electron spin s (see main text). Here we disregard Zeeman energy due to exchange coupling.

Quantity	Bi ₂ Se ₃	Strained HgTe
Bulk band gap M/k_B	3480 K	255 K
Cyclotron freq. $\hbar\Omega_c/k_B$	210 K $\times \sqrt{B}$ [T]	210 K $\times \sqrt{B}$ [T]
Zeeman energy $ E_Z /k_B$	21 K $\times B$ [T]	15 K $\times B$ [T]
Scattering rate $\hbar/(\tau_{tr}k_B)$	127 K	10 K

Our findings about the levitation of critical states in the absence of the anomalous Hall effect are summarized in Fig. 11. In this plot we assumed that $E_Z = 0$ and also took into account that for Coulomb impurities $\sqrt{\mu\tau_{tr}} \propto \mu$. A generalization of this plot to the case of a fully developed anomalous QHE, $E_Z \gg 1/\tau_q$, is shown in Fig. 12.

VII. EXPERIMENTAL REALIZATION

After having derived the effective electrodynamic theory, Eq. (49), via the two-step integration of matter fields, we return to the possibility of experimental observation of the half-integer Hall conductivity.

A. Typical experimental scales

In Table I, typical energy scales of experimental setups are presented. In the exemplary 3D TI experiments the Zeeman contribution appears to be negligible [43,132]. This observation is consistent with the calculated values of $|E_Z| = g\mu_B B$; see Table I. As a side remark, we note that the spin σ appearing in Eq. (21) in general does not coincide with the physical electron spin s [133,134]. The mixing angle ϕ depends on how the crystal is cut and in general $E_Z \sim g\mu_B B \cos \phi$. In this section we neglect the possible B -independent Zeeman energy due to exchange coupling and proximity to a ferromagnet.

B. Image magnetic monopole effect

1. Magnitude of the effect

It is useful to estimate the typical magnetic field strength associated with the mirror monopole effect. The charge $Q_0 = U z_0$ at distance z_0 of the QH system of “filling factor” ν is bound by the scale of “magnetic breakdown” $|e|U \lesssim \Omega_c(\eta_{\nu+1}\sqrt{|\nu+1|} - \eta_\nu\sqrt{|\nu|})$. Using this bound and Eq. (11), the ratio of image magnetic field and quantizing external field can be estimated:

$$\frac{B_{\text{image}}}{B} = \frac{g}{|\mathbf{r} + z_0\hat{e}_z|^2 B} \lesssim \frac{\alpha\Omega_c}{z_0|e|B} \sim \alpha \frac{v_0 l_B}{c z_0}. \quad (55)$$

This ratio is of the order of $B_{\text{image}}/B \sim 10^{-7}$ for the typical magnetic field strength $B \sim 1$ T and the distance $z_0 \sim 1 \mu\text{m}$.

While in an idealized system at the QH plateau, the longitudinal conductivity σ_{xx} is exactly zero, in a realistic

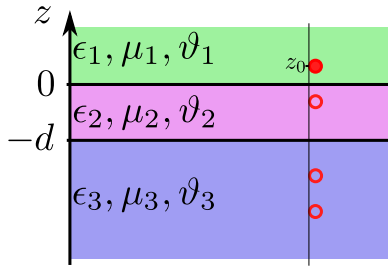


FIG. 13. (Color online) Sketch of the setup discussed in the main text. An electric test charge (solid dot) is placed above a double QH structure (e.g., a thin 3D TI slab) and creates a series of magnetic and electric mirror charges (circles).

situation it always takes a small but nonzero value due to a finite temperature. This allows a rearrangement of charges in the QH system, which leads to screening of the test charge and, as a result, destroys the driving force of ring currents and thus the image monopole effect. In Ref. [90] the decay rate of the image monopole effect after sudden appearance of a test charge was found to be

$$\frac{1}{\tau} = \frac{2\pi\sigma_{xx}}{z_0} = \frac{\alpha c g_{xx}}{z_0} \sim 10^{12} \text{ s}^{-1} \times g_{xx}. \quad (56)$$

The decay of the magnetic monopole effect enforces one to perform finite frequency measurements (or optical measurements; see below). We note, however, that already in the early days of the QH effect the longitudinal conductance on the QH plateau was demonstrated [8] to be $g_{xx} \lesssim 10^{-6}$. Thus, the decay of the monopole effect does not seem to constitute an insuperable difficulty.

2. Topological magnetoelectric effect in thin 3D TI films

In this section we consider the image magnetic monopole effect for a double QH structure (i.e., a double domain wall of the theta angle multiplying the $\mathbf{E} \cdot \mathbf{B}$ term). This problem is relevant for realistic 3D TI experiments: As was stated above, the electric test charge should be placed at macroscopic distance from the QH systems. On the other hand, typical 3D TI samples are only a few hundred angstroms thick. Thus, the test charge simultaneously probes both TI surfaces, a double QH structure.

A realistic experimental setup is shown in Fig. 13, where the electric test charge Q_0 (solid dot) is placed above a double QH structure at position $(0,0,z_0)$. The upper QH system, in the plane $z=0$, has Hall conductance $\sigma_{xy}^{\text{top}} = (\vartheta_1 - \vartheta_2)e^2/2\pi h$, while the lower one is characterized by $\sigma_{xy}^{\text{bottom}} = (\vartheta_2 - \vartheta_3)e^2/2\pi h$. In addition, in the three bulk regions denoted by $a=1$ ($0 < z$), $a=2$ ($-d < z < 0$), and $a=3$ ($z < -d$), localized charges might induce nontrivial electric permittivity ϵ_a and magnetic permeability $\mu_a = 1/\epsilon_a c_a^2$.

Following Ref. [88], we use the unified description in terms of the vector $(\mathbf{D}_a, 2\alpha \mathbf{B}_a)^T$ which is connected to \mathbf{E}_a and \mathbf{H}_a via

$$\begin{pmatrix} \mathbf{D}_a \\ 2\alpha \mathbf{B}_a \end{pmatrix} = \mathcal{M}_a \begin{pmatrix} 2\alpha \mathbf{E}_a \\ \mathbf{H}_a \end{pmatrix} \quad (57a)$$

with the matrix

$$\mathcal{M}_a = \frac{2\alpha}{c_a^2 \epsilon_a} \begin{pmatrix} \frac{\vartheta_a^2}{4\pi^2} + \left(\frac{c_a \epsilon_a}{2\alpha}\right)^2 & -\frac{\vartheta_a}{2\pi} \\ -\frac{\vartheta_a}{2\pi} & 1 \end{pmatrix}. \quad (57b)$$

The electromagnetic field above the plane $z=0$ can be expressed in terms of the two-component potential $\underline{\Phi}_1 = (\Phi_{1,E}, 2\alpha \Phi_{1,M})^T$,

$$(\mathbf{D}_1, 2\alpha \mathbf{B}_1)^T = -\nabla \underline{\Phi}_1. \quad (58)$$

To present the potential $\underline{\Phi}_1$, it is convenient to perform the Fourier transformation with respect to coordinates in the plane, $(x, y) \rightarrow (q_x, q_y)$,

$$\underline{\Phi}_1(x, y, z, z_0) = \int_0^\infty dq \frac{q}{2\pi} \underline{\Phi}_1(q, z, z_0) J_0(q\rho). \quad (59)$$

Here $J_0(q\rho)$ is the zeroth Bessel function, $\rho = \sqrt{x^2 + y^2}$ is the modulus of the 2D component of the position vector, and $q = \sqrt{q_x^2 + q_y^2}$ is the norm of the 2D component of momentum. As shown in Appendix D, the Fourier transform of the two-component potential $\underline{\Phi}_1$ is given by

$$\underline{\Phi}_1(q, z, z_0) = \frac{2\pi}{q} \{e^{-|z-z_0|q} + e^{-(z+z_0)q} T_{\text{eff}}\} \begin{pmatrix} Q_0 \\ 0 \end{pmatrix}. \quad (60)$$

Here we introduced the matrices

$$T_{\text{eff}} = (R_{32}^+ R_{21}^+ e^{dq} + R_{32}^- R_{21}^- e^{-dq})^{-1} \times (R_{32}^+ R_{21}^- e^{dq} + R_{32}^- R_{21}^+ e^{-dq}) \quad (61)$$

and $R_{ab}^\pm = 1 \pm \mathcal{M}_a \mathcal{M}_b^{-1}$. Each of the limits $d \rightarrow \infty$, $d \rightarrow 0$, $(\epsilon_2, \mu_2, \vartheta_2) = (\epsilon_3, \mu_3, \vartheta_3)$, and $(\epsilon_2, \mu_2, \vartheta_2) = (\epsilon_1, \mu_1, \vartheta_1)$ reproduces the result for a single domain wall; see Appendix D.

The two-component potential, Eq. (59), can also be represented as an infinite sum of mirror charges; see Appendix D [135]. In the limit $z_0 \ll d$ the dominant contribution arises from the mirror charge, which is located in $-d < z < 0$ and solely determined by σ_{xy}^{top} . In contrast, for $z_0 \gg d$ the double QH system behaves effectively as a single QH system with the Hall conductivity $\sigma_{xy}^{\text{tot}} = \sigma_{xy}^{\text{top}} + \sigma_{xy}^{\text{bottom}}$. Again the field configuration displays the mirror monopole, but this time its strength is determined by σ_{xy}^{tot} . This is illustrated in Fig. 14 where we plot the magnetic field corresponding to the potential, Eq. (59), for two otherwise identical 3D TI slabs of different thickness, $d = 10 \mu\text{m}$ and $d = 20 \text{nm}$ [136]. In these plots, we have assumed that the distance of a charge from the top surface is $z_0 = 2 \mu\text{m}$ and the Hall conductivities are $\sigma_{xy}^{\text{top}} = e^2/2h$ and $\sigma_{xy}^{\text{bottom}} = -7e^2/2h$. Thus, for a thick slab the condition $z_0 \ll d$ is well satisfied and the magnetic field is mainly determined by the mirror monopole corresponding to the upper surface with $\sigma_{xy}^{\text{top}} = e^2/2h$. On the other hand, the thickness d of a thin slab is much smaller than z_0 , so that the monopole corresponding to the total Hall conductivity $\sigma_{xy}^{\text{tot}} = -3e^2/h$ is observed.

It is worth emphasizing that the magnetic field plotted in Fig. 14 only includes the field induced by the image monopole and not the magnetic field generating the QH state. As noted before, typical magnetic field strengths in 3D TI QH experiments are of the order of a few teslas [43]. The induced monopole field per test charge Q_0 is of the order of $10 \text{ nT}/|e|$. We can estimate the voltage associated

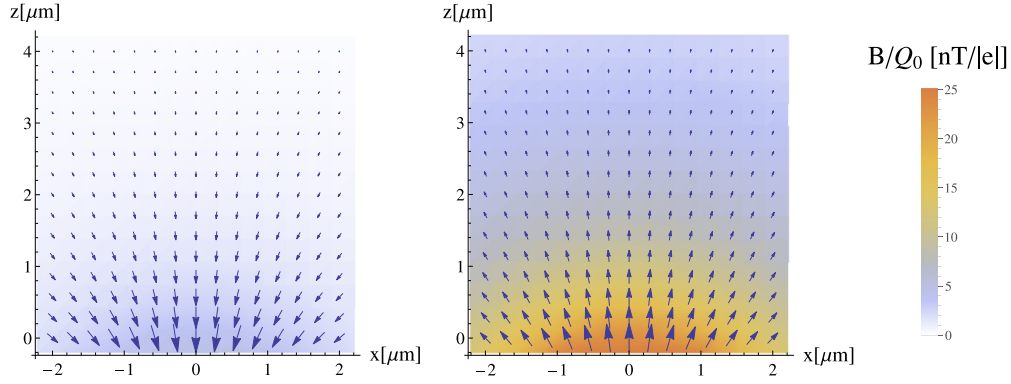


FIG. 14. (Color online) The magnetic field configuration for 3D TI in the QH state in a setup as depicted in Fig. 13. Left: slab of thickness $10 \mu\text{m}$. Right: slab of thickness 20 nm . In both figures $z_0 = 2 \mu\text{m}$, $\sigma_{xy}^{\text{top}} = e^2/2h$, $\sigma_{xy}^{\text{bottom}} = -7e^2/2h$, and, for simplicity, $\epsilon_1 = \epsilon_2 = \epsilon_3$ and $\mu_1 = \mu_2 = \mu_3$.

with magnetic breakdown to be $U \sim 0.01 \dots 0.1 \text{ V}$, which at a distance of $2 \mu\text{m}$ corresponds to $Q_0 \sim 14 \dots 140|e|$. Therefore, the induced magnetic field can be expected to be of the order of $0.1 \dots 1 \mu\text{T}$. Measurement of such a variation of the magnetic field is quite challenging from the experimental point of view.

C. Spectroscopic measurement: Topological Faraday and Kerr rotation

As discussed above, a measurement of the half-integer Hall conductivity should be local and contactless. The magnetic monopole effect satisfies these requirements but its magnitude is very small and might pose a serious experimental obstacle. This motivates us to think about possible alternatives.

A possible experimental probe of the QH effect is based on the topological Faraday and Kerr rotation in spectroscopic setups [2,51,137,138]. In these experiments the frequency of light is typically of the order of THz, with a wavelength $\lambda \sim 300 \mu\text{m}$. For a sufficiently disordered realistic system the condition

$$\omega\tau \equiv \frac{c}{v_0} \frac{l}{\lambda} \lesssim 1 \quad (62)$$

can be well satisfied. The system is then in the diffusive regime, opening a possibility for approaching the regime of quantized Hall conductivity.

Faraday and Kerr rotation induced by surface states of 3D TI were studied in recent spectroscopic experiments [128,139] (see also earlier works Ref. [140,141]), and magneto-oscillations of conductivities were indeed observed. In these experiments, the systems were in the diffusive regime, $\omega\tau \sim 0.1 \dots 1$. This implies that the RG flow of conductivities, Fig. 5, should be directly observable in the frequency dependence of optical conductivity $\sigma_{ij}(\omega)$ measured in THz spectroscopy.

There exists, however, a problem related to a small thickness d of realistic TI samples. Indeed, in order to probe separately each of the surfaces in a spectroscopic experiment, d should be larger than the wavelength λ . On the other hand, for state-of-art structures the opposite condition is satisfied, $d \ll \lambda$. This appears to be a serious obstacle for a measurement of conductivities of individual surfaces by spectroscopic means.

VIII. CONCLUSIONS AND OUTLOOK

In this paper, we studied the quantum Hall effect of a single-species (2+1)-dimensional Dirac fermion. We focused on the case of 3D topological insulator surface states, where the half-integer QHE is a manifestation of fermion number fractionalization; see Sec. II. Our key results are as follows:

(1) We explained in Sec. II why a naive attempt to measure the half-integer Hall conductivity of a surface of a 3D TI fails.

(2) We have further reviewed in Sec. II the topological magnetoelectric effect and demonstrated that it can be used for measurement of the half-quantized Hall conductivity in topological insulator surfaces with locally broken time-reversal invariance.

(3) Subsequently, in Sec. III we have shown that the half-quantized value is not in contradiction to Laughlin's flux insertion argument (which predicts, in its conventional form, an integer value of g_{xy} as a consequence of gauge invariance). Specifically, we have modified Laughlin's argument to the case of a 3D TI and demonstrated that it leads to half-quantized values of conductivities of each of the surfaces.

(4) Next, in Sec. IV, we employed the vortex state basis to calculate the conductivity tensor and explicitly uncovered the half-integer contribution of the zeroth LL. This calculation also allowed us to extend the topological magnetoelectric effect beyond the linear response.

(5) In Sec. V we derived the unified field theory treating both diffusive matter fields and EM gauge potentials. In contrast to the case of the integer quantum Hall effect, two different theta angles appear. One of them is associated with the Hall conductivity σ_{xy} , while the other one (reminiscent of chiral anomaly) provides a shift of the renormalization flow diagram.

(6) We discussed the RG flow and the phase diagram in great detail. To this end, the semiclassical conductivity tensor of Dirac fermions in magnetic field was derived in Sec. VI.

(7) Finally, in Sec. VII we carried out an analysis of conditions for experimental observation of the half-integer QHE. We have paid particular attention to implications of the slab geometry characteristic for currently manufactured TI samples.

We conclude the paper with a few remarks of a more general character:

(i) First, we would like to comment on the issue of a physically observable topological \mathbb{Z}_2 invariant of 3D TIs that has been discussed in the literature. It has been argued that the theta angle ϑ of the bulk $\mathbf{E} \cdot \mathbf{B}$ term plays this role. We have shown that in the presence of a boundary, this angle gives rise to a topological angle $\theta = \pm\pi$ of the boundary NL σ M theory. While this angle is indeed a \mathbb{Z}_2 invariant, it does not couple to gauge potentials and thus does not directly represent a measurable quantity. The situation should be contrasted to the paradigmatic case of the QH effect where the Hall conductivity which is the topological invariant directly corresponds to the theta angle of the theory. In the present case, the role of the angle θ is in shifting the RG flow diagram (and thus the fixed-point values of the Hall conductivity). Such an indirect physical meaning of topological invariants might be applicable also to other symmetry classes.

(ii) We hope that our work will motivate further experimental efforts for the observation of half-integer QHE in surfaces of 3D TIs. It is also worth emphasizing that the TME is not specific to 3D TI surfaces but should also take place in conventional QH systems. There, the parameter regime might be more favorable (allowing in particular a higher number of charges on the probing tip). Corresponding experimental studies would be certainly of great interest.

(iii) Some of our results on transport properties of 2D Dirac fermions may be relevant also in a context more general than TI surfaces. In particular, the peculiar critical behavior of the $\mathbf{B} = 0$ QH transition (Sec. V D 2) could also be observable in doped graphene. Further, the calculation of the semiclassical transport coefficients (that served as starting values for the RG) in Sec. VI and Appendix C is generic and applies to any 2D material with a nonvanishing Berry curvature.

(iv) Finally, it is worth emphasizing that even though topological insulators avoid the fermion doubling theorem [92] by spatially separating two single Dirac or Majorana modes, the gauge invariance still implies strong constraints. Specifically, the anomalous contributions of the two surfaces mutually cancel, both in the analysis of Laughlin's argument, Sec. III, and of the parity anomaly, Sec. V A. Such an additive cancellation of anomalies from opposite boundary states also occurs, e.g., in the context of topological Josephson junctions [142,143]. In this reasoning, the fermion doubling plays a crucial role (even though the two species are spatially separated). On the other hand, one could also regard the Dirac (or Majorana) fermions on the whole boundary of TIs in dimensions larger than one as a single mode. In the context of 3D TIs, it is instructive to imagine a sample of, e.g., spherical form. Then the notion of fermion doubling loses its meaning, as there is just a single species of Dirac fermions on the whole closed boundary of the sample. Nevertheless, as we discussed in Sec. V A, the theory is internally consistent and the parity anomaly is avoided. Local response properties are controlled by a theory of a single species of Dirac fermions, and the theory is unambiguously defined due to the fact that surface is a closed manifold. We therefore conclude that the reason for single-species Dirac fermions to appear only on boundaries of higher-dimensional bulk systems (which themselves have no boundary) is very deep and ultimately follows from gauge invariance. We expect similar arguments to hold also for

other dimensions and classes of topological insulators and superconductors.

ACKNOWLEDGMENTS

We acknowledge useful discussions with J. T. Chalker, T. Champel, S. Florens, Y. Gefen, T. Giamarchi, D. Hernangomez-Perez, P. Kotetes, D. G. Polyakov, M. Titov, and P. Wölfle. This work was supported by DFGSPP 1666 "Topological Insulators," the German-Israeli Foundation, BMBF, the Council for Grants of the President of the Russian Federation (Grant No. MK-4337.2013.2), the Dynasty Foundation, RAS programs, Ministry of Education and Science of the Russian Federation, and RFBR Grant No. 14-02-00333.

APPENDIX A: SEMICLASSICAL CALCULATION OF CURRENT DENSITY

In this Appendix we present the semiclassical calculation of current density induced by external potential in QH sample with smooth disorder.

1. Notation

We consider the model of a single Dirac cone, specified by Eqs. (15) and (21). Further, we use the notation

$$H_0 = v_0(\Pi_x \sigma_y - \Pi_y \sigma_x) = \begin{pmatrix} 0 & -i v_0 \Pi_- \\ i v_0 \Pi_+ & 0 \end{pmatrix} \quad (\text{A1})$$

with

$$-i \Pi_- = -i(\Pi_x - i \Pi_y), \quad i \Pi_+ = i(\Pi_x + i \Pi_y). \quad (\text{A2})$$

These objects have the following commutation relation:

$$[-i \Pi_-, i \Pi_+] = 2i[\Pi_x, \Pi_y] = 2|e|\epsilon_{ij}\partial_i A_j = 2/l_B^2, \quad (\text{A3})$$

where $l_B = (|e|B)^{-1/2}$ is the magnetic length. Under the assumption of $B > 0$ we define creation and annihilation operators

$$b = -\frac{l_B}{\sqrt{2}}(-i \Pi_-), \quad b^+ = -\frac{l_B}{\sqrt{2}}i \Pi_+. \quad (\text{A4})$$

Then, using the cyclotron frequency $\Omega_c = \frac{\sqrt{2}v_0}{l_B}$, we can rewrite Eq. (15) as

$$H_0 = -\Omega_c \begin{pmatrix} 0 & b \\ b^+ & 0 \end{pmatrix}. \quad (\text{A5})$$

Independently of the gauge, this Hamiltonian has eigenstates

$$|n, k\rangle_D = \frac{1}{\sqrt{1 + \eta_n^2}} \begin{pmatrix} -\eta_n |n| - 1, k \\ |n|, k \end{pmatrix}, \quad (\text{A6})$$

with eigenenergies $E_n = \Omega_c \eta_n \sqrt{|n|}$ [$\eta_n = \text{sgn}(n)$ for $n \neq 0$ and $\eta_0 = 0$]. The quantum number $n \in \mathbb{Z}$ labels the Landau level (LL) while $k = 1, 2, \dots, \frac{\Phi_{\text{tot}}}{\Phi_0}$ accounts for the degeneracy. The eigenstates $||N|, k\rangle$ constituting the spinor in Eq. (A6) are the conventional eigenstates of the $|N|$ th LL for electrons with parabolic dispersion.

2. Gradient expansion

The central assumption for the semiclassical calculation is that the potential $V(\mathbf{r})$ is smooth on the scale of the magnetic length. In the vortex state basis [see Eq. (22) on p. 8] we expand its matrix elements in gradients:

$$(V)_{12} = (V)_{12}^{(0)} + (V)_{12}^{(1)} + \mathcal{O}(l_B^2 \partial^2 V). \quad (\text{A7})$$

[For any operator O we use the shorthand notation $(O)_{12} \equiv \langle 1|O|2\rangle$ and $|1\rangle = |n_1, \mathbf{R}_1\rangle_D$.] The zeroth order is $[(V)_{12} = (\mathbf{R}_2 + \mathbf{R}_1)/2]$

$$(V)_{12}^{(0)} = V(\mathbf{c}_{12}) \langle 1|2\rangle. \quad (\text{A8})$$

The first order is $[\mathbf{d}_{12} = (\mathbf{R}_2 - \mathbf{R}_1)/2]$

$$(V)_{12}^{(1)} = (V)_{12}^{(1,0)} + (V)_{12}^{(1,+)} + (V)_{12}^{(1,-)} \quad (\text{A9})$$

with

$$(V)_{12}^{(1,0)} = i\hat{z} \cdot [\nabla V(\mathbf{c}_{12}) \times \mathbf{d}_{12}] \langle 1|2\rangle, \quad (\text{A10a})$$

$$(V)_{12}^{(1,+)} = -i \frac{E_{n_1} + E_{n_2}}{2|e|\Omega_c^2} (j_+)_{12} \partial_- V(\mathbf{c}_{12}), \quad (\text{A10b})$$

$$(V)_{12}^{(1,-)} = i \frac{E_{n_1} + E_{n_2}}{2|e|\Omega_c^2} (j_-)_{12} \partial_+ V(\mathbf{c}_{12}). \quad (\text{A10c})$$

The solution of the Dyson equation for the retarded/advanced single-electron Green's functions within the same approximation leads to

$$G_{12}^{R/A}(\omega) \approx G_{12}^{(0),R/A}(\omega) + G_{12}^{(1),R/A}(\omega) \quad (\text{A11})$$

with

$$G_{12}^{(0),R/A} = \frac{\langle 1|2\rangle}{\omega^\pm - E_{n_2} - V(\mathbf{R}_2)}, \quad (\text{A12})$$

$$G_{12}^{(1),R/A} = \frac{(V)_{12}^{(1)}}{[\omega^\pm - E_{n_1} - V(\mathbf{R}_1)][\omega^\pm - E_{n_2} - V(\mathbf{R}_2)]}. \quad (\text{A13})$$

Here we use the shorthand notation $\omega^\pm = \omega \pm i0$.

3. Current density

We base our calculation of the current density in arbitrary potential configuration on general results on vortex states and the semiclassical expansion reported in Ref. [70].

The current density [see Eq. (27)] is the $\mathbf{x}_1 \rightarrow \mathbf{x}_2$ limit of

$$\begin{aligned} \langle \hat{j}_\pm(\mathbf{x}_1, \mathbf{x}_2) \rangle &= \sum_{1,2} \int \frac{d\omega}{2\pi} i n_F(\omega) [G_{21}^R(\omega) - G_{21}^A(\omega)] \\ &\times {}_D \langle n_1, \mathbf{R}_1 | \mathbf{x}_1 \rangle j_\pm \langle \mathbf{x}_2 | n_2, \mathbf{R}_2 \rangle_D. \end{aligned} \quad (\text{A14})$$

Here we introduced shorthand notation

$$\sum_1 = \int \frac{d^2 R_1}{2\pi l_B^2} \sum_{|n_1|=0}^{\infty} \sum_{\eta_{n_1}}. \quad (\text{A15})$$

The matrix elements of the first quantized current operators, Eq. (28), will be useful. They can be expressed via spinor

components of $|n, \mathbf{R}\rangle_D$ in the following way:

$$(j_+)_{12} = -2iev_0 \langle n_1, \mathbf{R}_1, \uparrow | n_2, \mathbf{R}_2, \downarrow \rangle, \quad (\text{A16})$$

$$(j_-)_{12} = 2iev_0 \langle n_1, \mathbf{R}_1, \downarrow | n_2, \mathbf{R}_2, \uparrow \rangle. \quad (\text{A17})$$

To proceed further we use the gradient expansion of the Green's functions (A11). The important simplification comes from the fact that we are interested in the slow (on the scale of magnetic length) part of the current density (cf. discussion in Sec. IV). We will see shortly that most of the terms of gradient expansion (A11) do not contribute in this approximation. To demonstrate this fact we will need the Fourier representation of the vortex states

$$\begin{aligned} \langle \mathbf{p} | n, \mathbf{R} \rangle &= \frac{4l_B \pi e^{-i\mathbf{p}\mathbf{R}}}{\sqrt{2\pi n!}} \left[i\sqrt{2}l_B \left(p_+ + \frac{iR_+}{2l_B^2} \right) \right]^n \\ &\times \exp \left[\left(p_- - \frac{iR_-}{2l_B^2} \right) \left(p_+ + \frac{iR_+}{2l_B^2} \right) l_B^2 \right]. \end{aligned} \quad (\text{A18})$$

Here, $p_\pm = p_x \pm ip_y$ and R_\pm is defined analogously.

a. Contributions of $V_{12}^{(0)}$ and $V_{12}^{(1,0)}$

The simplest terms of the gradient expansion are those involving $V_{12}^{(0)}$ and $V_{12}^{(1,0)}$. Writing down the corresponding current densities $J_\pm(\mathbf{q})$ in momentum representation we find [see Eq. (27) and the $\mathbf{x}_1 \rightarrow \mathbf{x}_2$ limit of Eq. (A14)]

$$\begin{aligned} J_\pm(\mathbf{q})|_{V_{12}^{(0)}, V_{12}^{(1,0)}} &\propto \int (d\mathbf{p}) \langle 2|1\rangle \langle 1|\mathbf{p}-\mathbf{q}\rangle j_\pm \langle \mathbf{p}|2\rangle \\ &\approx e^{-i\mathbf{q}\mathbf{R}_1} \int (d\mathbf{p}) \langle 2|1\rangle \langle 1|\mathbf{p}\rangle j_\pm \langle \mathbf{p}|2\rangle \\ &= e^{-i\mathbf{q}\mathbf{R}_1} \langle 2|1\rangle (j_\pm)_{12} = 0. \end{aligned} \quad (\text{A19})$$

In this expression \mathbf{q} is the slow momentum associated with the macroscopic vector potential $A_\mp(-\mathbf{q})$ and $\langle 1|\mathbf{p}-\mathbf{q}\rangle \approx e^{-i\mathbf{q}\mathbf{R}_1} \langle 1|\mathbf{p}\rangle$ to zeroth order in $ql_B \ll 1$ [see Eq. (A18)]. Similar analysis shows that only $V_{12}^{(1,\mp)}$ and not $V_{12}^{(1,\pm)}$ contribute to J_\pm .

b. Leading contribution

The leading contribution to the current densities can now be presented as

$$\begin{aligned} \langle \hat{j}_\pm(\mathbf{x}_1, \mathbf{x}_2) \rangle &= \sum_{1,2} \frac{\pm i n_F [E_{n_1} + V(\mathbf{R}_1)]}{2|e|\Omega_c^2} \frac{E_{n_1} + E_{n_2}}{E_{n_1} - E_{n_2}} \\ &\times [\partial_\pm V(\mathbf{c}_{12})(j_\mp)_{21} \langle 1|\mathbf{x}_1\rangle j_\pm \langle \mathbf{x}_2|2\rangle \\ &+ \partial_\pm V(\mathbf{c}_{12})(j_\mp)_{12} \langle 2|\mathbf{x}_1\rangle j_\pm \langle \mathbf{x}_2|1\rangle]. \end{aligned} \quad (\text{A20})$$

This expression can be further simplified by employing the relation

$$\sum_2 \frac{E_{n_1} + E_{n_2}}{E_{n_1} - E_{n_2}} \langle \mathbf{x}_2|2\rangle (j_+)_{21} = -(2|n_1| + 1) j_+ \langle \mathbf{x}_2|1\rangle. \quad (\text{A21})$$

Here we used $(j_+)_{21} \propto \delta_{|n_2|-1, |n_1|}$ and the following identities:

$$\sum_2 \left\{ \begin{matrix} 1 \\ \eta_{n_2} \end{matrix} \right\} \langle \mathbf{x}|2\rangle \langle 2|\mathbf{x}'\rangle = \left\{ \begin{matrix} 1 \\ 0 \end{matrix} \right\} \delta(\mathbf{x} - \mathbf{x}') \mathbf{1}_\sigma. \quad (\text{A22})$$

As a result, we obtain

$$\begin{aligned} \langle \hat{j}_{\pm}(\mathbf{x}_1, \mathbf{x}_2) \rangle &= \pm i |e| l_B^2 \sum_1 n_F [E_{n_1} + V(\mathbf{R}_1)] \partial_{\pm} V(\mathbf{R}_1) \\ &\times [\langle 1|\mathbf{x}_1 \rangle \langle \mathbf{x}_2|1 \rangle - 2|n_1 \rangle \langle 1|\mathbf{x}_1 \rangle \sigma_z \langle \mathbf{x}_2|1 \rangle]. \end{aligned} \quad (\text{A23})$$

The term proportional to $|n_1 \rangle$ does not contribute to the slow part of the current. Indeed, consideration similar to that of Eq. (A19) leads to

$$\int (d\mathbf{p}) |n_1 \rangle \langle 1|\mathbf{p} - \mathbf{q} \rangle \sigma_z \langle \mathbf{p}|1 \rangle \stackrel{q l_B \ll 1}{\approx} |n_1 \rangle \langle 1|\sigma_z|1 \rangle = 0. \quad (\text{A24})$$

c. Regularizing the divergence

The expression (A20) is singular in the limit $\mathbf{x}_1 \rightarrow \mathbf{x}_2$. The singularity can be regularized by adding and subtracting the following term (corresponding to the linear-response current at zero temperature and chemical potential $\mu = 0^+$):

$$\begin{aligned} X_{\pm}(\mathbf{x}) &= \frac{\pm i |e| \partial_{\pm} V(\mathbf{x})}{2\pi} \lim_{\mathbf{x}' \rightarrow \mathbf{x}} \int d^2 R \sum_{n \leq 0} \langle n, \mathbf{R} | \mathbf{x} \rangle \langle \mathbf{x}' | n, \mathbf{R} \rangle_D \\ &= \frac{\pm i |e| \partial_{\pm} V(\mathbf{x})}{2\pi} \\ &\times \lim_{\mathbf{x}' \rightarrow \mathbf{x}} \int d^2 R \sum_{n \leq 0} \left\{ \frac{\langle \mathbf{x}' | |n, \mathbf{R} \rangle \langle |n, \mathbf{R} | \mathbf{x} \rangle}{1 + |\eta_n|} \right. \\ &\quad \left. + \frac{\eta_n^2 \langle \mathbf{x}' | |n-1, \mathbf{R} \rangle \langle |n-1, \mathbf{R} | \mathbf{x} \rangle}{1 + |\eta_n|} \right\} \\ &= \pm i |e| \partial_{\pm} V(\mathbf{x}) \\ &\times \lim_{\mathbf{x}' \rightarrow \mathbf{x}} \left[l_B^2 \delta(\mathbf{x} - \mathbf{x}') + \frac{\langle 0, \mathbf{x}' | 0, \mathbf{x} \rangle}{4\pi} \right]. \end{aligned} \quad (\text{A25})$$

To get the δ -function contribution we have used the resolution of identity, Eq. (24), for up and down components separately. However, the double weight of down component of the zeroth LL generates the second contribution in the angular brackets: this is where half-integer g_{xy} comes from.

APPENDIX B: DERIVATION OF THE NL σ M DESCRIBING THE HALF-INTEGER QHE

1. No net B field: Non-Abelian bosonization

The first step of the derivation of NL σ M for the QH problem is to apply non-Abelian bosonization to the system of disordered Dirac fermions which is TR invariant on average but contains a random Zeeman term.

The model under consideration is Eq. (34), with the following white-noise scalar disorder potential,

$$\langle V(\mathbf{x}) V(\mathbf{x}') \rangle = \frac{1}{\pi \nu \tau_{sc}} \delta(\mathbf{x} - \mathbf{x}'), \quad (\text{B1})$$

and a random Zeeman term $H_Z = m \sigma_z$,

$$\langle m(\mathbf{x}) m(\mathbf{x}') \rangle = \frac{1}{\pi \nu \tau_Z} \delta(\mathbf{x} - \mathbf{x}'). \quad (\text{B2})$$

After disorder averaging, the Matsubara action of our system receives an additional contribution:

$$\begin{aligned} S^{\text{dis}} &= -\frac{1}{2\pi \nu} \int_{\mathbf{x}} \left\{ \frac{1}{\tau_{sc}} [\bar{\psi}(\mathbf{x}) \psi(\mathbf{x})] [\bar{\psi}(\mathbf{x}) \psi(\mathbf{x})] \right. \\ &\quad \left. + \frac{1}{\tau_Z} [\bar{\psi}(\mathbf{x}) \sigma_z \psi(\mathbf{x})] [\bar{\psi}(\mathbf{x}) \sigma_z \psi(\mathbf{x})] \right\}. \end{aligned} \quad (\text{B3})$$

a. SCBA

On the mean-field level the fermionic Green's functions are given by the self-consistent Born approximation (SCBA). The SCBA equation for the self-energy reads

$$\Sigma_n = -\frac{1}{\pi \nu \tau} \mathcal{G}_n(\mathbf{x}, \mathbf{x}). \quad (\text{B4})$$

Here the scattering rate $1/\tau = 1/\tau_{sc} + 1/\tau_Z$. The solution of Eq. (B4) is (in the limit $k_F l \gg 1$)

$$\Sigma_n = \frac{i}{2\tau} \text{sgn}(n). \quad (\text{B5})$$

b. Non-Abelian bosonization

In order to go beyond the mean-field treatment, we derive the NL σ M from the fermionic action. We will employ the double cutoff truncation scheme in Matsubara space [26] and use non-Abelian bosonization [144], with the dictionary for the $\mathbf{U}(2N'_M N_R) \times \mathbf{U}(2N'_M N_R)$ invariant model being [145,146]

$$\psi^{\uparrow} \otimes \bar{\psi}^{\downarrow} \leftrightarrow \frac{1}{4\pi \nu_0} U^{\dagger} \partial_{+} U, \quad (\text{B6a})$$

$$\psi^{\downarrow} \otimes \bar{\psi}^{\uparrow} \leftrightarrow \frac{1}{4\pi \nu_0} U \partial_{-} U^{\dagger}, \quad (\text{B6b})$$

$$\psi^{\uparrow} \otimes \bar{\psi}^{\uparrow} \leftrightarrow -\lambda U^{\dagger}, \quad (\text{B6c})$$

$$\psi^{\downarrow} \otimes \bar{\psi}^{\downarrow} \leftrightarrow \lambda U. \quad (\text{B6d})$$

Here $U \in \mathbf{U}(2N'_M N_R)$ is a unitary matrix field. Typically it is decomposed in a phase (Abelian bosonization) and a special unitary part,

$$U = e^{i \sqrt{\frac{4\pi}{2N'_M N_R}} \Phi} \tilde{U}.$$

The dimensionful constant λ is of the order of the UV cutoff. In the presence of disorder and a finite chemical potential it turns out to be of the order of the density of states; see below, Appendix B1 c.

The kinetic part of the action can now be rewritten as [147–150]

$$\begin{aligned} S &= \int_{\mathbf{x}} \frac{1}{2} (D_i \Phi)^2 + \int_{\mathbf{x}} \frac{1}{8\pi} \text{Tr} D_i \tilde{U}^{\dagger} D_i \tilde{U} \\ &\quad + \int_{\mathbf{x}, w} \frac{-i}{12\pi} \epsilon_{ijk} \text{Tr} (\tilde{U}^{\dagger} D_i \tilde{U}) (\tilde{U}^{\dagger} D_j \tilde{U}) (\tilde{U}^{\dagger} D_k \tilde{U}) \\ &\quad + \int_{\mathbf{x}, w} \frac{i}{8\pi} \epsilon_{ijk} \text{Tr} F_{ij} (\tilde{U}^{\dagger} D_k \tilde{U} + D_k \tilde{U} \tilde{U}^{\dagger}) \\ &\doteq \int_{\mathbf{x}} \frac{1}{2} (D_i \Phi)^2 + \int_{\mathbf{x}} \frac{1}{8\pi} \text{Tr} \partial_i \tilde{U}^{\dagger} \partial_i \tilde{U} \end{aligned} \quad (\text{B7})$$

$$\begin{aligned}
& + \int_{x,w} \frac{-i}{12\pi} \epsilon_{ijk} \text{Tr}(\tilde{U}^\dagger \partial_i \tilde{U})(\tilde{U}^\dagger \partial_j \tilde{U})(\tilde{U}^\dagger \partial_k \tilde{U}) \\
& + \int_x \frac{-ie}{4\pi} \text{Tr}[A_- \tilde{U}^\dagger \partial_+ \tilde{U} + A_+ \tilde{U} \partial_- \tilde{U}^\dagger] \\
& + \int_x \frac{-e^2}{4\pi} \text{Tr}[A_- \tilde{U}^\dagger A_+ \tilde{U} - A_+ A_-]. \quad (\text{B8})
\end{aligned}$$

Here the symbols D_i denote long derivatives, $D_i = \partial_i - ieA_i^{(0)}$ when acting on a scalar field and $D_i = \partial_i - ie[A_i, \cdot]$ when acting on a matrix field. The gauge potentials are arbitrary $\mathbf{U}(2N'_M N_R)$ gauge potentials [split in traceless (traceful) components A_i ($A_i^{(0)}$); F_{ij} is the corresponding field strength tensor. For the problem of disordered Dirac fermions coupled to $\mathbf{U}(1)$ gauge potentials, we will set $A_i = \hat{A}_i$ in the end [see Eq. (39)]. The symbol \doteq here denotes equality for all cases when gauge fields are nontopological (recall that we are interested in situations without net magnetic flux through the spatial plane).

The expressions containing integrals over the variable w involve the extension of the base manifold $[(x, w) \in (\mathbb{R}^2 \cup \{\infty\}, [0, 1])]$. In these terms \tilde{U} implicitly denotes a different function $\tilde{U}(x, w)$ which coincides with the physical field on the physical space $\tilde{U}(x, 0) = \tilde{U}(x)$ while taking a uniform fixed value at $w = 1$; e.g., $\tilde{U}(x, 1) = \mathbf{1}$.

c. Bosonized SCBA

The SCBA equation (B4) can be rederived in the bosonic language:

$$\begin{aligned}
\Sigma &= \frac{1}{\pi v \tau} \langle \psi \otimes \bar{\psi} \rangle_{SCBA} \\
&\Leftrightarrow \frac{1}{\pi v \tau} \left\langle \left(\begin{array}{cc} -\lambda U^\dagger & \frac{1}{4\pi v_0} U^\dagger \partial_+ U \\ \frac{1}{4\pi v_0} U \partial_- U^\dagger & \lambda U \end{array} \right)_\sigma \right\rangle_{SCBA}. \quad (\text{B9})
\end{aligned}$$

The symbol $(\dots)_{SCBA}$ denotes self-consistent SCBA average. Equations (B9) are consistent with the previous solution provided $U = i\Lambda$ and $\lambda = v\pi/2$ [$\Lambda_{nn'} = \delta_{nn'} \text{sgn}(n)$].

d. Bosonized effective action

We now return to Eq. (B3). We bosonize both channels of possible soft modes

$$\begin{aligned}
S^{\text{dis}} &\Leftrightarrow \frac{-1}{2\pi v \tau_{sc}} \int_x \left[\left\{ \text{tr} \left(\begin{array}{cc} -\lambda U^\dagger & \frac{U^\dagger \partial_+ U}{4\pi v_0} \\ \frac{U \partial_- U^\dagger}{4\pi v_0} & \lambda U \end{array} \right)_\sigma \right\}^2 \right. \\
&\quad \left. - \text{tr} \left\{ \left(\begin{array}{cc} -\lambda U^\dagger & \frac{U^\dagger \partial_+ U}{4\pi v_0} \\ \frac{U \partial_- U^\dagger}{4\pi v_0} & \lambda U \end{array} \right)_\sigma \right\} \right] \\
&\quad + \frac{-1}{2\pi v \tau_Z} \int_x \left[\left\{ \text{tr} \left(\begin{array}{cc} -\lambda U^\dagger & \frac{U^\dagger \partial_+ U}{4\pi v_0} \\ \frac{-U \partial_- U^\dagger}{4\pi v_0} & -\lambda U \end{array} \right)_\sigma \right\}^2 \right. \\
&\quad \left. - \text{tr} \left\{ \left(\begin{array}{cc} -\lambda U^\dagger & \frac{U^\dagger \partial_+ U}{4\pi v_0} \\ \frac{-U \partial_- U^\dagger}{4\pi v_0} & -\lambda U \end{array} \right)_\sigma \right\} \right] \\
&\doteq \frac{\lambda^2}{2\pi v} \int_x \left[\frac{\text{tr}([U^\dagger + U]^2)}{\tau} \right.
\end{aligned}$$

$$\left. - \frac{(\text{tr}[U^\dagger - U]^2)}{\tau_{sc}} - \frac{(\text{tr}[U^\dagger + U]^2)}{\tau_Z} \right]. \quad (\text{B10})$$

Here, the sign \doteq indicates that in this formula we omitted the gradient terms which renormalize the kinetic part of the action as well as a constant.

e. Saddle-point equations

By infinitesimal left rotation of spatially constant U we determine the saddle-point equations for the disorder-induced potential

$$\begin{aligned}
0 &= \frac{i\lambda^2}{\pi v} \left[\frac{(U^2 - [U^\dagger]^2)}{\tau} + \frac{(U^\dagger - U)\text{tr}[U^\dagger + U]}{\tau_{sc}} \right. \\
&\quad \left. + \frac{(U^\dagger - U)\text{tr}[U^\dagger + U]}{\tau_Z} \right]. \quad (\text{B11})
\end{aligned}$$

We see that the SCBA solution $U = i\Lambda$ solves the saddle-point equation.

f. Goldstone manifold and field theory

We will now rotate the bosonic fields by slow, small, unitary rotations: $U \rightarrow U_{\text{soft}}^\dagger U U_{\text{soft}}$. For the saddle-point solution $U = i\Lambda$ these fields equally annihilate the disorder-induced mass terms of Eq. (B10). Thus the effective field theory will be constructed on a saddle-point manifold, namely the coset space formed by the $Q = U_{\text{soft}}^\dagger \Lambda U_{\text{soft}}$ which is $\mathbf{U}(2N_M N_R)/\mathbf{U}(N_M N_R) \times \mathbf{U}(N_M N_R)$. To derive the effective field theory, Eq. (41) of the main text, the following steps are in order: (i) The prefactor of the gradient term is renormalized by integration of the U fields in SCBA approximation [33]. (ii) Upon restriction to the coset space, the Wess-Zumino-Novikov-Witten term in third line from the bottom of Eq. (B8) becomes the theta term with short derivatives and angle $\theta = \pi \pmod{2\pi}$ [39,151]. (iii) The last two lines of the same Eq. (B8) provide the gauge potentials entering the long derivatives of the gradient term. It is an important observation that terms containing $Q^\dagger \partial_\pm Q$ and $\epsilon_{ij} \text{tr} A_i Q^\dagger A_j Q$ drop out in view of the hermiticity and unitarity of Q . Therefore the theta term has short derivatives. (iv) Frequency and interaction terms were not discussed in this Appendix, but can be equally included following Ref. [33]. (v) The subscript soft is omitted in all other parts of this paper.

2. Finite net magnetic field: Gradient expansion

We now turn to the derivation of the NL σ M describing disordered Dirac fermions in strong magnetic field ($\Omega_c \tau \gg 1$). The fermionic action on saddle-point level is

$$\begin{aligned}
S[\bar{\psi}, \psi] &= \int_x \bar{\psi} [-i\hat{\epsilon} - ie\hat{\Phi} + H_0(\mathbf{p} - e[\mathcal{A} + \hat{\mathbf{A}}]) \\
&\quad - \mu - i(\Sigma^R)'' Q] \psi. \quad (\text{B12})
\end{aligned}$$

The SCBA is justified in the center of LLs with large index $|n| \gg 1$. For the present case of Dirac fermions, the imaginary part of retarded self-energy $(\Sigma^R)'' = 1/2\tau$ is energy dependent and nontrivial (trivial) in spin space for the zeroth (all other) LLs; see, e.g., Ref. [40] for more details.

Just as in the previous section, we set $Q = U^\dagger \Lambda U$ with slow unitary $(2N_M N_R) \times (2N_M N_R)$ matrix field U . Note that at this stage, all sums and traces over Matsubara indices go from negative to positive infinity. Thus Λ is an infinite matrix with only diagonal entries $\Lambda_{nn'} = \delta_{nn'} \text{sgn}(n)$. In order to obtain finite-dimensional Λ (and thus Q), a second cutoff will be introduced at the end of this section [26].

In order to perform an accurate gradient expansion of the action, it is convenient to reexpress the partition function as

$$\begin{aligned} \mathcal{Z} &= \int \mathcal{D}Q \int \mathcal{D}[\bar{\psi}, \psi] e^{-S[\bar{\psi}, \psi]} \\ &= \int \mathcal{D}Q \mathcal{J}[U, \hat{\Phi}, \hat{A}_i] \int \mathcal{D}[\bar{\psi}', \psi'] e^{-S[\bar{\psi}', \psi']}. \end{aligned} \quad (\text{B13})$$

Here the rotated fields $\psi' = U\psi$ and $\bar{\psi}' = \bar{\psi}U^\dagger$ were introduced at the expense of the Jacobian $\mathcal{J}[U, \hat{\Phi}, \hat{A}_i]$. The action for the rotated fermions reads

$$S[\bar{\psi}', \psi'] = \int_x \bar{\psi}' [-\mathcal{G}^{-1} - ie\Phi + \mathbf{J} \cdot \mathbb{A}] \psi', \quad (\text{B14})$$

where we use the notation $J_i = \delta H_0 / \delta A_i$ and the rotated gauge potentials are

$$\begin{aligned} \Phi &= \frac{1}{e} U [\hat{\epsilon}, U^\dagger] + U \hat{\Phi} U^\dagger, \\ \mathbb{A}_i &= -\frac{1}{e} U [-i\partial_i, U^\dagger] + U \hat{A}_i U^\dagger. \end{aligned} \quad (\text{B15})$$

We denote the SCBA Green's function by

$$\begin{aligned} \mathcal{G}_{mm'}^{\alpha\alpha'}(\mathbf{x}, \mathbf{x}') &= ([i\epsilon_m - H_0(\mathbf{p} - e\mathcal{A}) + \mu \\ &\quad + i(\Sigma^R)'' \text{sgn}(\epsilon_m)]^{-1})_{\mathbf{x}, \mathbf{x}'} \delta_{mm'}^{\alpha\alpha'}. \end{aligned} \quad (\text{B16})$$

As we are working in the limit $\epsilon_n \ll (\Sigma^R)''$, we will partly drop the frequency dependence below.

We will further use the notation

$$-\mathbf{G}^{-1} = -\mathcal{G}^{-1} - ie\Phi + \mathbf{J} \cdot \mathbb{A}.$$

Since we are interested in the topological theta term involving spatial derivatives only, we omit Φ in what follows. Integrating fermions out, we get

$$\mathcal{Z} = \int \mathcal{D}Q \mathcal{J}[U, \hat{\Phi}, \hat{A}_i] e^{-S_{\text{eff}}}, \quad (\text{B17})$$

with

$$S_{\text{eff}} = -\text{Tr} \ln[-\mathbf{G}^{-1}]. \quad (\text{B18})$$

Here and below Tr includes also the spatial integration. The expansion of S_{eff} in \mathbb{A} (omitting Φ and the constant term) yields

$$S_{\text{eff}} \approx \text{Tr}[\mathcal{G}_0 J_i \mathbb{A}_i] + \frac{1}{2} \text{Tr}[\mathcal{G}_0 J_i \mathbb{A}_i \mathcal{G}_0 J_j \mathbb{A}_j]. \quad (\text{B19})$$

a. The RR and AA correlators in the term $\mathcal{O}(\mathbb{A}^2)$

First, we will disregard the diffusive fields and set $\mathbb{A} = \hat{\mathbb{A}}$. Recall that we are working with infinite Matsubara sums. The expansion contains the standard conductivity term

$$\frac{1}{2} \text{Tr}[\mathcal{G} J_i \hat{A}_i \mathcal{G} J_j \hat{A}_j] = e^2 \sum_{m>0, \alpha} \int_x m(A_i)_{-m}^\alpha g_{ij}(m) (A_j)_m^\alpha, \quad (\text{B20})$$

with

$$g_{ij}(m) = \frac{1}{e^2 A m} \sum_k \text{Sp}[J_i \mathcal{G}_{k+m} J_j \mathcal{G}_k]. \quad (\text{B21})$$

Here A denotes the sample area. The symbol Sp involves trace in spin and real space only. The $RR + AA$ contribution to g_{xx} for Dirac fermions is nonzero but negligible as compared to the RA contribution. In contrast, for the transverse dc conductivity we find the standard g_{xy}^{II} contribution:

$$\begin{aligned} &\frac{1}{2} \text{Tr}[\mathcal{G} J_{[i} \hat{A}_i \mathcal{G} J_{j]} \hat{A}_j] \\ &\stackrel{RR+AA}{=} e^2 g_{xy}^{II} \epsilon_{ij} \sum_{m>0, \alpha} \int_x m(A_i)_{-m}^\alpha (A_j)_m^\alpha. \end{aligned} \quad (\text{B22})$$

(Square brackets in the indices denote antisymmetrization.) Now we return to the full \mathbb{A} which we write as $\mathbb{A} = \Delta\mathbb{A} + \hat{\mathbb{A}}$. Clearly, $\Delta\mathbb{A} = \mathbb{A} - \hat{\mathbb{A}}$ is a finite $(2N_M N_R) \times (2N_M N_R)$ matrix. We will show that also for the full \mathbb{A} we have

$$\begin{aligned} &\frac{1}{2} \text{Tr}[\mathcal{G} J_{[i} \mathbb{A}_i \mathcal{G} J_{j]} \mathbb{A}_j] \\ &\stackrel{RR+AA}{=} e^2 g_{xy}^{II} \epsilon_{ij} \sum_{m>0, \alpha} \int_x m(A_i)_{-m}^\alpha (A_j)_m^\alpha. \end{aligned} \quad (\text{B23})$$

Indeed, all terms linear or quadratic in $\Delta\mathbb{A}_i$ involve traces over the finite $(2N_M N_R) \times (2N_M N_R)$ space. All of these finite traces vanish by symmetry; for example,

$$\begin{aligned} &\frac{1}{2} \text{Tr}[\mathcal{G} J_{[i} \Delta\mathbb{A}_i \mathcal{G} J_{j]} \Delta\mathbb{A}_j] \\ &\stackrel{RR}{=} \frac{1}{2A} \text{Sp}[\mathcal{G}^R J_{[i} \mathcal{G}^R J_{j]}] \text{Tr} \left[\Delta\mathbb{A}_i \frac{1+\Lambda}{2} \Delta\mathbb{A}_j \frac{1+\Lambda}{2} \right] = 0. \end{aligned} \quad (\text{B24})$$

b. The RA correlator in the term $\mathcal{O}(\mathbb{A}^2)$

For the RA correlator we obtain the standard result:

$$\begin{aligned} &\frac{1}{2} \text{Tr}[\mathcal{G} J_i \mathbb{A}_i \mathcal{G} J_j \mathbb{A}_j] \stackrel{RA}{=} \sum_i \text{Tr}[\mathbb{A}_i \mathbb{A}_i - \mathbb{A}_i \Lambda \mathbb{A}_i \Lambda] \\ &\quad \times \frac{1}{8A} \text{Sp}[\mathcal{G}^A J_x \mathcal{G}^R J_x + \mathcal{G}^R J_x \mathcal{G}^A J_x] \\ &\quad + 2\text{Tr}[\Lambda(\mathbb{A}_x \mathbb{A}_y - \mathbb{A}_y \mathbb{A}_x)] \\ &\quad \times \frac{1}{8A} \text{Sp}[\mathcal{G}^R J_x \mathcal{G}^A J_y - \mathcal{G}^A J_x \mathcal{G}^R J_y]. \end{aligned} \quad (\text{B25})$$

In what follows we use the notation

$$\begin{aligned} g_{xx} &= \frac{1}{e^2 A} \text{Sp}[\mathcal{G}^R J_x \mathcal{G}^A J_x], \\ g_{xy}^I &= \frac{-1}{2e^2 A} \text{Sp}[\mathcal{G}^R J_x \mathcal{G}^A J_y - \mathcal{G}^A J_x \mathcal{G}^R J_y]. \end{aligned} \quad (\text{B26})$$

c. Term of $\mathcal{O}(\mathbb{A}^4)$

We follow the steps presented in Ref. [20] and use

$$\frac{\partial}{\partial \mu} \mathcal{G}(\mathbf{x}, \mathbf{x}') = - \int d^2 x'' \mathcal{G}(\mathbf{x}, \mathbf{x}'') \mathcal{G}(\mathbf{x}'', \mathbf{x}') \quad (\text{B27})$$

to rewrite the $\mathcal{O}(\mathbb{A}^1)$ part of the action as

$$\begin{aligned} \text{Tr} \mathcal{G} \mathbf{J} \cdot \mathbb{A} &= - \int_{-\infty}^{\mu} d\tilde{\mu} \int_{\mathbf{x}, \mathbf{x}'} \text{tr}[\mathcal{G}(\mathbf{x}, \mathbf{x}') \mathcal{G}(\mathbf{x}', \mathbf{x}) J_i \mathbb{A}_i(\mathbf{x})] \\ &= - \frac{1}{2} \frac{\partial}{\partial B} \int_{-\infty}^{\mu} d\tilde{\mu} \text{tr}^{\sigma} \mathcal{G}^{R-A}(0,0) \text{Tr}[\epsilon_{ij} \partial_i \mathbb{A}_j \Lambda] \\ &\quad - \frac{1}{2} \frac{\partial}{\partial B} \int_{-\infty}^{\mu} d\tilde{\mu} \text{tr}^{\sigma} \mathcal{G}^{R+A}(0,0) \text{Tr}[\epsilon_{ij} \partial_i \mathbb{A}_j]. \end{aligned} \quad (\text{B28})$$

The term $\text{Tr}[\epsilon_{ij} \partial_i \mathbb{A}_j] = 0$ vanishes, since it contains commutators of small matrices and the only noncommuting term is $\text{Tr} \hat{A} = 0$ by assumption of purely dynamic gauge fields. In contrast, the $\text{Tr}[\epsilon_{ij} \partial_i \mathbb{A}_j \Lambda]$ term plays an important role: its prefactor $\partial n / \partial B$ is related to g_{xy}^{II} by the Smrcka-Streda formula [78].

d. Collecting all terms

We are now in position to present the full gradient expansion of S_{eff} :

$$\begin{aligned} S_{\text{eff}} &= \frac{g_{xx} e^2}{4} \text{Tr}[\mathbb{A}_i \mathbb{A}_i - \mathbb{A}_i \Lambda \mathbb{A}_i \Lambda] \\ &\quad - \frac{g_{xy}^I e^2}{2} \epsilon_{ij} \text{Tr}[\Lambda (\mathbb{A}_i \mathbb{A}_j)] \\ &\quad - \frac{g_{xy}^{II} e^2}{2} \epsilon_{ij} \left[\frac{-i}{e} \text{Tr}[\partial_i \mathbb{A}_j \Lambda] + \sum_{m, \alpha} \int_{\mathbf{x}} m (A_i)_{\alpha}^m (A_j)_{-m}^{\alpha} \right]. \end{aligned} \quad (\text{B29})$$

In order to rewrite S_{eff} in a more compact way we will introduce a second cutoff N'_M in Matsubara space [26]. In particular, now also \hat{A} and Λ are *finite* matrices of size $(2N'_M N_R) \times (2N'_M N_R)$. We assume $N'_M / N_M \rightarrow \infty$. Then we can use the notation (from now on Tr denotes finite traces)

$$D_i Q \equiv \partial_i Q - ie[\hat{A}_i, Q] = -ieU^\dagger [\mathbb{A}_i, \Lambda] U \quad (\text{B30})$$

to express

$$\begin{aligned} \text{Tr} D_i Q D_i Q &= 2e^2 \text{Tr}[\mathbb{A}_i^2 - (\mathbb{A}_i \Lambda)^2], \\ \epsilon_{ij} \text{Tr} Q D_i Q D_j Q &= 4e^2 \epsilon_{ij} \text{Tr}[\Lambda \mathbb{A}_i \mathbb{A}_j] \\ &= 4e \epsilon_{ij} \left[-i \text{Tr}(\partial_i \mathbb{A}_j \Lambda) \right. \\ &\quad \left. + e \int_{\mathbf{x}} \sum_{n, \alpha} n (A_i)_{\alpha}^n (A_j)_{-n}^{\alpha} \right]. \end{aligned} \quad (\text{B31})$$

Including now the contribution of the Jacobian of the transformation from initial to rotated fermions we find the

sigma model action

$$S = \frac{1}{8} (g_{xx} \text{Tr}[D_i Q]^2 - g_{xy} \epsilon_{ij} \text{Tr} Q D_i Q D_j Q) - \ln \mathcal{J}(U, \hat{A}). \quad (\text{B32})$$

Finally, we will discuss the Jacobian $\mathcal{J}(U, \hat{A})$ in more detail. Generally speaking, its precise value depends on the regularization of the functional integral measure of the initial fermionic field theory. The same ambiguity is generally present in the microscopic calculation of g_{xy} due to the unbounded spectrum of Dirac fermions. The final result should however be independent of the regularization. We have learned in Sec. V A that one can regularize the fermionic theory in such a manner that the parity symmetry is preserved. In our present problem this does not contradict gauge invariance or any other fundamental principle. Choosing such a regularization, we see that g_{xy} vanishes for $B \rightarrow 0$. On the other hand, in the $B \rightarrow 0$ limit, the action should reproduce the result (41). We therefore conclude that, at least in this limit, the Jacobian $-\ln \mathcal{J}(U, \hat{A})$ equals the theta term with short derivatives.

Recall that the derivation of the theta term with short derivatives assumed nontopological gauge potentials. Differently said, the *total* flux through the surface should vanish.

Now consider a single Dirac cone in an infinite 2D plane with locally homogeneous magnetic field but zero total flux. (This implies the existence of at least one contour with $B = 0$ in this plane; it is necessary to keep zero total flux.) The equality of Eqs. (B7) and (B8) is still ensured. We further follow the strategy exposed in Appendix B1f. (i) The integration of U fields in the presence of locally homogeneous magnetic field is the bosonic equivalent to the integration of fermions performed in this section. In particular, it leads to Eq. (B29) with local values of g_{ij} . (ii) Upon restriction to the coset space, the Wess-Zumino-Novikov-Witten term becomes the theta term with short derivatives [33] which we identify with the Jacobian in the fermionic treatment (also for a nonvanishing magnetic field).

In the setup for real QH experiments on TI slabs, the Dirac states reside on a surface with locally homogenous B field and vanishing total flux. (We assume that no physical magnetic monopoles are located inside the TI bulk.) This setup is equivalent to the case of the 2D plane analyzed in the preceding paragraph. Note that typically, i.e., when the magnetic field is perpendicular to the two major surfaces of the slab, the sidewalls of the system form a contour of vanishing magnetic field. This concludes the derivation of Eq. (43) of the main text.

APPENDIX C: CLASSICAL CONDUCTIVITY TENSOR

In this Appendix we present the semiclassical Boltzmann calculation of the conductivity tensor in the presence of both orbital magnetic field and a Zeeman term $H_Z = m v_0^2 \sigma_z$.

1. Semiclassical theory of anomalous Hall effect

The basic concepts of anomalous Hall effect (AHE) are reviewed in Refs. [73, 74]. The contributions to the AHE are threefold [we denote the two bands by $\xi = \pm$ with dispersion relation $\epsilon_{\xi}(\mathbf{p}) = \xi \sqrt{v_0^2 \mathbf{p}^2 + (m v_0^2)^2}$]:

(i) intrinsic AHE, which is the contribution of integral over Berry connection $\Omega_\xi = -\frac{mv_0^4}{2\epsilon_\xi^3}$;

(ii) skew scattering $\omega_{ll'} \neq \omega_{l'l}$ contribution, which splits into (a) conventional ($\omega_{ll'} \propto V^3$) and (b) intrinsic ($\omega_{ll'} \propto V^4$). [Here $\omega_{l'l}$ is the squared scattering amplitude from state $l = (\mathbf{p}, \xi)$ to $l' = (\mathbf{p}', \xi')$.]

(iii) Side-jump contributions, which again are twofold, including (a) side-jump accumulation and (b) modification of collision integral in view of work performed due to the side jump at a single scattering event.

These contributions are reflected in the equations of motion [152–154]

$$\dot{r}_i = \overbrace{\frac{\partial \epsilon_\xi(\mathbf{p})}{\partial p_i}}^{\equiv v_i^{(\xi)}} - \epsilon_{ij} \dot{p}_j \Omega_\xi + \sum_{l'} \omega_{ll'} (\delta \mathbf{r}_{l'l})_i, \quad (\text{C1})$$

$$\dot{p}_i = F_i = q(E_i + \epsilon_{ij} \dot{r}_j B/c), \quad (\text{C2})$$

as well as in the collision integral of the Boltzmann equation

$$\partial_t f + \dot{\mathbf{r}} \cdot \partial_x f + \dot{\mathbf{p}} \cdot \partial_p f = \text{St}[f], \quad (\text{C3})$$

where

$$\text{St}[f] = - \sum_{l'} [\omega_{l'l} f_l - \omega_{ll'} f_{l'}]. \quad (\text{C4})$$

The precise modification of the collision integral, which will involve the work $W_{l \rightarrow 2} = \mathbf{F} \delta \mathbf{r}_{l_2 l_1}$, will be presented below, Sec. C 2.

It is worth noting that the collision integral for elastic scattering does not contain Pauli blocking terms (which would change the results in view of skew scattering). The reason [73] is that, in contrast to the case of inelastic scattering, the incoming and outgoing states l and l' should be considered as a single scattering state, and thus Pauli blocking factors [e.g., $f_l(1 - f_{l'})$] are superfluous. This can also be understood in the derivation of the Boltzmann equation from Schwinger-Keldysh quantum field theory. Since elastic scattering is evoked by a static disorder potential (it only couples to γ_{cl} in Keldysh space), the collision integral in the quantum kinetic equation $\Sigma^K - (\Sigma^R \circ F - F \circ \Sigma^A)$ contains only a single Keldysh Green's function/self-energy and thus only a single distribution function.

The side-jump shift of the trajectory is expressed as

$$\delta \mathbf{r}_{l_2 l_1} = \langle u_{\xi_2, \mathbf{p}_2} | i \partial_{\mathbf{p}_2} u_{\xi_2, \mathbf{p}_2} \rangle - \langle u_{\xi_1, \mathbf{p}_1} | i \partial_{\mathbf{p}_1} u_{\xi_1, \mathbf{p}_1} \rangle - (\partial_{\mathbf{p}_1} + \partial_{\mathbf{p}_2}) \arg(V_{l_2, l_1}) \quad (\text{C5})$$

even in the presence of smooth electromagnetic fields [we denote by $e^{i\mathbf{p}\mathbf{r}} |u_{\xi, \mathbf{p}}\rangle$ the eigenstates to the $B = 0$ limit of Hamiltonian (15)]. We will use the notation

$$\sum_{l'} \omega_{ll'} (\delta \mathbf{r}_{l'l}) = \left(1 - \frac{qB\Omega_\xi}{c}\right) \frac{\Omega_\xi \epsilon_\xi \mathbf{p}}{\tau^{sj}}, \quad (\text{C6})$$

with the mean side-jump time $\tau^{sj}(\epsilon_\xi)$. Here we introduced the matrix representation of the 2D Levi-Civita symbol

$(\epsilon)_{ij} = \epsilon_{ij}$. We can diagonalize the equations of motion as follows [122,123,155,156]:

$$\begin{pmatrix} \dot{r}_i \\ \dot{p}_i \end{pmatrix} = \frac{\begin{pmatrix} v_i^{(\xi)} + \sum_{l'} \omega_{ll'} (\delta \mathbf{r}_{l'l})_i - \epsilon_{ij} \Omega_\xi q E_j \\ \epsilon_{ij} [v^{(\xi)} + \sum_{l'} \omega_{ll'} (\delta \mathbf{r}_{l'l})]_j \frac{qB}{c} + q E_i \end{pmatrix}}{1 - \frac{\Omega_\xi q B}{c}}. \quad (\text{C7})$$

At

$$1 = \frac{\Omega_\xi q B}{c} = -\zeta \Omega_c^{\text{cl}} \frac{m v_0^2}{2\epsilon_\xi^2} \quad (\text{C8})$$

the clean classical equations of motion correspond to pure Hall response [156]. However, in parameter space this point lies outside the region of validity of the Boltzmann equation.

[We introduced $\zeta \Omega_c^{\text{cl}} = \frac{v_0^2 q B}{\epsilon_\xi c}$, $\zeta = \text{sgn}(qB\epsilon_\xi)$.]

It is worth noting that equations of motion (C7), which contain the disorder-induced side jump terms, do not correspond to a Hamiltonian flow. Without the side-jump terms, these equations are perfectly Hamiltonian, but with a modified Poisson bracket (we are not using canonical coordinates) [156]. Therefore, the invariant phase space volume element acquires an additional term [155]

$$dV = \left(1 - \frac{q\Omega_\xi B}{c}\right) d^2 p d^2 x. \quad (\text{C9})$$

We hence deduce that in the Boltzmann equation and in the equations determining current we need to use

$$\sum_{l'} \dot{} \int_{\xi'} (dp') \left(1 - \frac{qB\Omega_\xi}{c}\right). \quad (\text{C10})$$

In the following, we employ polar coordinates determining each momentum \mathbf{p} by modulus of kinetic energy and angle (ϵ, ϕ) with $\epsilon = \sqrt{v_0^2 p^2 + (m v_0^2)^2}$. In this notation we write

$$\hat{p} = (\cos \phi, \sin \phi), \hat{e}_\phi = (-\sin \phi, \cos \phi) = -\underline{\epsilon} \hat{p} \quad (\text{C11})$$

and

$$\nabla_{\mathbf{p}} f_l = \hat{p} \frac{\partial \epsilon}{\partial p} \partial_\epsilon f_l + \frac{\hat{e}_\phi}{p} \partial_\phi f_l = v^{(\xi)} \partial_{\epsilon_\xi} f_l + \frac{\hat{e}_\phi}{p} \partial_\phi f_l. \quad (\text{C12})$$

2. The collision kernel and side step

As explained above, upon a scattering event $l_1 \rightarrow l_2$ the final state corresponds to a trajectory that is shifted as compared to the initial state by

$$\delta \mathbf{r}_{l_2 l_1} \simeq \mathbf{r}_{l_2}(t=0) - \mathbf{r}_{l_1}(t=0). \quad (\text{C13})$$

If the scattering event takes place in an external electric (but not magnetic) field, the kinetic energy is not conserved, as the potential energy changes at the scattering event [73,74]

$$\Delta \epsilon^{\delta \mathbf{r}_{l_2 l_1}} \simeq U(\mathbf{r}_{l_2}) - U(\mathbf{r}_{l_1}) = \nabla U \delta \mathbf{r}_{l_2 l_1} = -q \mathbf{E} \delta \mathbf{r}_{l_2 l_1}. \quad (\text{C14})$$

More generally (in the presence of both \mathbf{E} and \mathbf{B} fields), we can say that there is a work to be performed at a scattering event $l_1 \rightarrow l_2$ with side jump. Energy conservation $\epsilon_{\text{initial}} = \epsilon_{\text{final}}$ implies

$$\xi_1 \epsilon(\mathbf{p}_1) = \xi_2 \epsilon(\mathbf{p}_2) - W_{l_1 \rightarrow 2}, \quad (\text{C15})$$

where $W_{1 \rightarrow 2} = \mathbf{F} \delta \mathbf{r}_{l_2 l_1}$. *A priori* it is not clear whether one should use $\mathbf{F} = \dot{\mathbf{p}}_1$ or $\mathbf{F} = \dot{\mathbf{p}}_2$. We will fix this question below, Appendix C 4.

The contribution of out-processes ($l \rightarrow l'$) to the collision integral is not altered. Contrary, for in-processes ($l' \rightarrow l$), energy conservation implies

$$f_{l'} = f(\xi, \epsilon - \xi W_{l' \rightarrow l}, \phi') \approx f_{l'} - \partial_{\epsilon_\xi} f_{l'} W_{l' \rightarrow l}. \quad (\text{C16})$$

Here we expanded the distribution function under the assumption of small work $W = W_{l' \rightarrow l} = \mathbf{F} \delta \mathbf{r}_{l'}$ as compared to the chemical potential. We will find below that this assumption is justified; see Eq. (C57).

3. Full Boltzmann equation

Let us return to the Boltzmann equation presented above (C3). It is worth splitting the contribution of $\dot{\mathbf{p}} \nabla_{\mathbf{p}} f$ into two terms, as follows:

$$\dot{\mathbf{p}} \partial_{\mathbf{p}} f = \dot{\mathbf{p}}_{\text{clean}} \partial_{\mathbf{p}} f + \frac{qB/c}{1 - qB\Omega/c} (\partial_{\mathbf{p}} f)_{\xi} \left[\sum_{l'} \omega_{l'} \delta \mathbf{r}_{l'} \right]. \quad (\text{C17})$$

Bringing the last term to the right-hand side of the Boltzmann equation leads to

$$\partial_t f + \dot{\mathbf{r}} \partial_{\mathbf{r}} f + \dot{\mathbf{p}}_{\text{clean}} \partial_{\mathbf{p}} f = St[f]_{\text{full}} \quad (\text{C18})$$

with

$$St[f]_{\text{full}} = St[f]_{(s)} + St[f]_{(a)} + St[f]_{W_E} + St[f]_{W_B}, \quad (\text{C19})$$

where

$$St[f]_{(s)} = - \sum_{l'} \omega_{l'}^{(s)} (f_l - f_{l'}), \quad (\text{C20})$$

$$St[f]_{(a)} = - \sum_{l'} \omega_{l'}^{(a)} (f_l + f_{l'}), \quad (\text{C21})$$

$$St[f]_{W_E} = - \sum_{l'} \omega_{l'} \partial_{\epsilon_\xi} f_{l'} \delta \mathbf{r}_{l'} \frac{q\mathbf{E}}{1 - \frac{qB\Omega}{c}}, \quad (\text{C22})$$

$$\begin{aligned} St[f]_{W_B} &= - \sum_{l'} \omega_{l'} \partial_{\epsilon_\xi} f_{l'} \delta \mathbf{r}_{l'} \frac{\underline{\epsilon} \tilde{\mathbf{v}} \frac{qB}{c}}{1 - \frac{qB\Omega}{c}} - \dot{\mathbf{p}}_{sj} \partial_{\mathbf{p}} f \\ &= - \sum_{l'} \omega_{l'} \partial_{\epsilon_\xi} f_{l'} \delta \mathbf{r}_{l'} \frac{\underline{\epsilon} \tilde{\mathbf{v}} \frac{qB}{c}}{1 - \frac{qB\Omega}{c}} \\ &\quad - \sum_{l'} \omega_{l'} \partial_{\epsilon_\xi} f_{l'} \delta \mathbf{r}_{l'} \frac{\underline{\epsilon}^T \mathbf{v}^{(\xi)} \frac{qB}{c}}{1 - \frac{qB\Omega}{c}}. \end{aligned} \quad (\text{C23})$$

Here we have introduced the notation $\omega_{l'}^{(s)} = (\omega_{l'} + \omega_{l'})/2$ and $\omega_{l'}^{(a)} = (\omega_{l'} - \omega_{l'})/2$ and neglected accumulation of side-jump and skew-scattering effects (higher orders in mv_0^2/μ). In the last line we used $\sum_{l'} \omega_{l'} \delta \mathbf{r}_{l'} \propto \underline{\epsilon} \mathbf{v}$ and dropped terms $\mathcal{O}(\omega_{l'}^2)$. The velocity $\tilde{\mathbf{v}}$ is a placeholder for $\mathbf{v}^{(\xi)}$ or $\mathbf{v}^{(\xi)'}$, because at this point, it is unclear whether $W = \dot{\mathbf{p}} \delta \mathbf{r}_{l'}$ or $W = \dot{\mathbf{p}}' \delta \mathbf{r}_{l'}$ should be chosen.

4. Conservation laws at $E = 0$

Clearly, for $E = 0$

$$\sum_l St[f]_{\text{full}} = 0 \text{ and } \sum_l \epsilon(\mathbf{p}) St[f]_{\text{full}} = 0 \quad (\text{C24})$$

provided

$$\delta \mathbf{r}_{l'} \underline{\epsilon} (\tilde{\mathbf{v}} - \mathbf{v}^{(\xi)'}) = 0. \quad (\text{C25})$$

Under the assumption that the side jump $\mathbf{r}_{l'}$ contains only terms proportional to $\mathbf{p} - \mathbf{p}'$ and $(\mathbf{p} + \mathbf{p}') \mathbf{p} \in \mathbf{p}'$ [see Eqs. (C5) and (C54) below] we find that the two solutions $\tilde{\mathbf{v}} = -\mathbf{v}^{(\xi)}$ and $\tilde{\mathbf{v}} = \mathbf{v}^{(\xi)'}$ are legitimate. Both possible solutions lead to the same collision integral $St[f]_{\text{full}}$ [see again Eq. (C25) for the solution $\tilde{\mathbf{v}} = -\mathbf{v}^{(\xi)}$]. We will use $\tilde{\mathbf{v}} = -\mathbf{v}^{(\xi)}$; then

$$St[f]_{W_B} = - \sum_{l'} \omega_{l'}^{(s)} \delta \mathbf{r}_{l'} \frac{\underline{\epsilon} \mathbf{v}^{(\xi)} \frac{qB}{c}}{1 - \frac{qB\Omega_\xi}{c}} (\partial_{\epsilon_\xi} f_l - \partial_{\epsilon_\xi} f_{l'}). \quad (\text{C26})$$

5. Back to the Boltzmann equation

The Boltzmann equation (C18) at zero E field is solved by any isotropic function $f_l = f_0$. The physical solution is the Fermi-Dirac distribution function. To access the static, homogeneous nonequilibrium distribution function we restrict ourselves to linear response and use the expansion in harmonics:

$$f_l = \sum_n f_n e^{in\phi} \leftrightarrow f_n = \int \frac{d\phi}{2\pi} f_l e^{-in\phi}. \quad (\text{C27})$$

The left-hand side of Eq. (C18) becomes (using $E_\pm = E_x \pm iE_y$)

$$\begin{aligned} \dot{\mathbf{p}}_{\text{clean}} \partial_{\mathbf{p}} f &= \sum_n \left\{ e^{i(n+1)\phi} \left[(\xi v \partial_{\epsilon_\xi} f_n - n f_n / p) \frac{qE_-}{2} \right] \right. \\ &\quad \left. + e^{i(n-1)\phi} \left[(\xi v \partial_{\epsilon_\xi} f_n + n f_n / p) \frac{qE_+}{2} \right] \right. \\ &\quad \left. + e^{in\phi} (-\zeta \Omega_c^{\text{cl}} i n f_n) \right\} \frac{1}{1 - \frac{qB\Omega_\xi}{c}}. \end{aligned} \quad (\text{C28})$$

The right-hand side becomes

$$St[f]_{(s)} = - \left(1 - \frac{qB\Omega_\xi}{c} \right) \sum_n \frac{f_n}{\tau_n^{(s)}} e^{in\phi} \quad (\text{C29})$$

with

$$\frac{1}{\tau_n^{(s)}} = \int (dp') \omega_{l'}^{(s)} (1 - e^{in(\phi' - \phi)}). \quad (\text{C30})$$

The first symmetric scattering rate $\frac{1}{\tau_1^{(s)}}$ is the transport rate

$$\frac{1}{\tau_1^{(s)}} = \frac{1}{\tau_{tr}}.$$

The skew scattering contribution to the collision term is

$$St[f]_{(a)} = - \left(1 - \frac{qB\Omega_\xi}{c} \right) \sum_n i \frac{f_n}{\tau_n^{(a)}} e^{in\phi}. \quad (\text{C31})$$

It contains the skew-scattering rates

$$\frac{1}{\tau_n^{(a)}} = -i \int (d\mathbf{p}') \omega_{l'l}^{(a)} [e^{in(\phi' - \phi)} + 1]. \quad (\text{C32})$$

The last term “+1” in the square bracket drops out in view of the definition of $\omega_{l'l}^{(a)}$.

The contribution of work by electrical field is (no accumulation of skew scattering and side jump)

$$\begin{aligned} \text{St}[f]|_{W_E} = & - \sum_n \partial_{\epsilon_\xi} f_n \frac{\Omega_\xi p i q}{\tau_{sj}^{(n)} 2} \\ & \times (e^{i(n+1)\phi} E_- - e^{i(n-1)\phi} E_+). \end{aligned} \quad (\text{C33})$$

Higher harmonics of the mean side-jump time $\tau_{sj}^{(n)}$ are defined analogously to (C6):

$$\sum_{l'} \omega_{l'l} (\delta \mathbf{r}_{l'l}) e^{in(\phi' - \phi)} = \left(1 - \frac{qB\Omega_\xi}{c}\right) \frac{\Omega_\xi \underline{\epsilon} \mathbf{p}}{\tau_{sj}^{(n)}}, \quad (\text{C34})$$

and thus $\tau_{sj}^{(0)} = \tau^{sj}$ from Eq. (C6).

The last contribution is the side-jump work by the B field. It reads

$$\text{St}[f]|_{W_B} = \sum_n \partial_{\epsilon_\xi} f_n e^{in\phi} \left(1 - \frac{qB\Omega_\xi}{c}\right) \frac{\langle W_{l' \rightarrow l}^{(B)} \rangle}{\tau_n^{(W)}}. \quad (\text{C35})$$

We introduced the averaged power

$$\frac{\langle W_{l' \rightarrow l}^{(B)} \rangle}{\tau_n^{(W)}} = \int (d\mathbf{p}') \omega_{l'l} \delta \mathbf{r}_{l'l} \frac{\underline{\epsilon} (-\mathbf{v}^{(\xi)}) \frac{qB}{c}}{1 - \frac{qB\Omega_\xi}{c}} (1 - e^{in(\phi' - \phi)}). \quad (\text{C36})$$

The subscript $l' \rightarrow l$ will be mostly omitted in the following.

In the linear response approximation, the Boltzmann equation involves only the 0th and (± 1)st harmonics:

$$\frac{\tau_{tr} \xi v m_1}{(1 - \frac{qB\Omega_\xi}{c})^2} (-\partial_{\epsilon_\xi} f_0) \frac{qE_-}{2} = m_2^{-1} f_1 - \partial_{\epsilon_\xi} f_1 \frac{\langle W^{(B)} \rangle \tau_{tr}}{\tau^{(W)}}. \quad (\text{C37})$$

In this equation, we introduced the complex functions $m_{1,2} = m_{1,2}(\epsilon_\xi)$ with

$$m_1 = \left[1 + i \left(1 - \frac{qB\Omega_\xi}{c}\right) \frac{\Omega_\xi k}{\tau_{sj} v \xi} \right], \quad (\text{C38a})$$

$$m_2 = \left\{ 1 + i \left[\frac{\tau_{tr}}{\tau_a} - \frac{\xi \Omega_c^{\text{cl}} \tau_{tr}}{(1 - \frac{qB\Omega_\xi}{c})^2} \right] \right\}^{-1}. \quad (\text{C38b})$$

For simplicity, we dropped the subscript 1 in all of the scattering rates, thus $\tau_1^{(W)} = \tau^{(W)}$, $\tau_1^{(a)} = \tau_a$, and we introduced the transport time $\tau_s^{(1)} = \tau_{tr}$.

6. Solution of the Boltzmann equation

a. A representation of the delta function

For the solution of the kinetic equation, the following broadened delta function will be needed:

$$\begin{aligned} \tilde{\delta}(\epsilon_\xi, \epsilon'') = & \text{sgn} \left(\text{Re} \left[\frac{\langle W^{(B)} \rangle}{\tau^{(W)}} \right] \right) \\ & \times \frac{e^{-\int_{\epsilon_\xi}^{\epsilon''} \frac{d\epsilon'}{[\langle W^{(B)} \rangle m_2 \tau_{tr} / \tau^{(W)}]_{\epsilon'}}}}{[\langle W^{(B)} \rangle m_2 \tau_{tr} / \tau^{(W)}]_{\epsilon''}} \\ & \times \theta \left(\text{sgn} \left(\text{Re} \left[\frac{\langle W^{(B)} \rangle}{\tau^{(W)}} \right] \right) (\epsilon'' - \epsilon_\xi) \right). \end{aligned} \quad (\text{C39})$$

As a function of ϵ_ξ it is peaked at ϵ'' and asymmetrically exponentially decaying into the direction prescribed by $\text{sgn}(\text{Re}[\langle W^{(B)} \rangle / \tau^{(W)}])$. It is assumed that this quantity is energy independent within a given band ξ ; see Eq. (C57) below for the case of Dirac electrons. Equation (C39) is applied to the AHE; in the regime of applicability, $\langle W^{(B)} \rangle / \tau^{(W)}$ is smooth on the scale on which $\tilde{\delta}$ decays; see Fig. 15.

The broadened delta function leads to the following approximate convolutions for functions $f(\epsilon)$ which are smooth on the scale of $\tau_{tr} \langle W^{(B)} \rangle / \tau^{(W)}$:

$$\int d\epsilon_\xi f(\epsilon_\xi) \tilde{\delta}(\epsilon_\xi, \epsilon'') \approx f(\epsilon'') - (f \langle W^{(B)} \rangle m_2 \tau_{tr} / \tau^{(W)})'_{\epsilon''}, \quad (\text{C40})$$

$$\int d\epsilon'' f(\epsilon'') \tilde{\delta}(\epsilon_\xi, \epsilon'') \approx f(\epsilon_\xi) + (f \langle W^{(B)} \rangle m_2 \tau_{tr} / \tau^{(W)})'_{\epsilon_\xi}. \quad (\text{C41})$$

b. General linear response solution

The general linear response solution for Eq. (C37) is

$$\begin{aligned} f_1(\epsilon_\xi) = & \int_{-\infty}^{\infty} d\epsilon'' \left\{ \left[\frac{\tau_{tr}}{(1 - \frac{qB\Omega_\xi}{c})^2} \xi v m_1 m_2 (-\partial_{\epsilon''} f_0) \right]_{\epsilon''} \right. \\ & \left. \times \tilde{\delta}(\epsilon_\xi, \epsilon'') \right\} \frac{qE_-}{2}. \end{aligned} \quad (\text{C42})$$

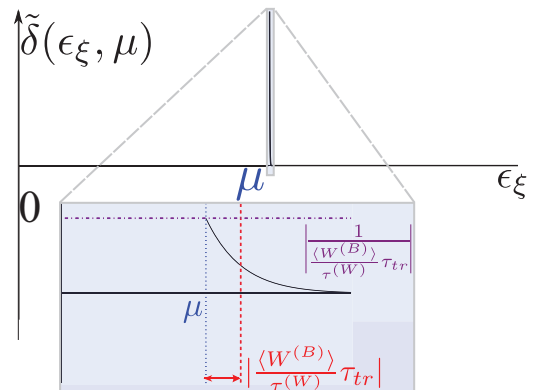


FIG. 15. (Color online) The broadened delta function entering the general solution of the kinetic equation. In the inset, the same function is shown in the vicinity of the chemical potential, where it takes the value $|\tau_{tr} \langle W^{(B)} \rangle / \tau^{(W)}|^{-1}$.

Formally, there is also an exponentially growing solution which has been dropped for obvious physical reasons. In the limit $T \gg |\langle W^{(B)} \rangle|$ the approximate solution is

$$f_1(\epsilon_\xi) = \left[\frac{\tau_{tr}}{\left(1 - \frac{qB\Omega_\xi}{c}\right)^2} \xi v m_1 m_2 (-\partial_{\epsilon_\xi} f_0) \right]_{\epsilon_\xi} \frac{qE_-}{2} + [\langle W^{(B)} \rangle m_2 \tau_{tr} / \tau^{(W)}]_{\epsilon_\xi} \times \partial_{\epsilon_\xi} \left[\frac{\tau_{tr}}{\left(1 - \frac{qB\Omega_\xi}{c}\right)^2} \xi v m_1 m_2 (-\partial_{\epsilon_\xi} f_0) \right]_{\epsilon_\xi} \frac{qE_-}{2}. \quad (\text{C43})$$

This solution can also be obtained by iteratively solving Eq. (C37). In the limit when temperature T is smaller than all other scales, we can use the zero-temperature solution

$$f_1(\epsilon_\xi) = \tilde{\delta}(\epsilon_\xi, \mu) \left[\frac{\tau_{tr}}{\left(1 - \frac{qB\Omega_\xi}{c}\right)^2} \xi v m_1 m_2 \right]_{\mu} \frac{qE_-}{2}. \quad (\text{C44})$$

When convoluted with a function $f(\epsilon_\xi)$ which is smooth on the scale of the magnetic work (for example the current), $f_1(\epsilon_\xi)$ will be approximated according to Eq. (C40). By comparison with Eq. (C43) we see that the results for the current in the limits $|\langle W^{(B)} \rangle| \ll T \ll \mu$ and $T \ll |\langle W^{(B)} \rangle| \ll \mu$ coincide.

7. Conductivity at $T = 0$ and $\mu \gg T \gg |\langle W^{(B)} \rangle|$

a. Intrinsic contribution

As explained, the total current density also has a contribution of the filled bands (intrinsic AHE):

$$\mathbf{j}^{\text{intr}} = \sum_l \frac{-\Omega_\xi q^2 \epsilon \mathbf{E}}{1 - \frac{\Omega_\xi q B}{c}} f_{0,l} = \sigma_{xy}^{\text{intr}} \epsilon \mathbf{E}, \quad (\text{C45})$$

where in the case of Dirac fermions [124,157]

$$\sigma_{xy}^{\text{intr}} = -\frac{q^2}{4\pi} \left[\text{sgn}(m) \theta(m^2 v_0^4 - \mu^2) + \frac{m v_0^2}{|\mu|} \theta(\mu^2 - m^2 v_0^4) \right]. \quad (\text{C46})$$

b. Nonequilibrium contribution

The longitudinal and transverse conductivity are

$$\sigma_{xx} = \text{Re } \sigma(\mu) \text{ and } \sigma_{xy} = \text{Im } \sigma(\mu), \quad (\text{C47})$$

where the complex function $\sigma(\mu)$ is

$$\sigma(\mu) = \left[\sigma_{xx}^{(\beta)} \frac{m_1^2 m_2}{\left(1 - \frac{qB\Omega_\xi}{c}\right)^2} - \partial_\mu \left(\sigma_{xx}^{(\beta)} \frac{\langle W^{(B)} \rangle}{\tau^{(W)} \xi v} m_1 m_2 \right) \frac{v \xi \tau_{tr} m_1 m_2}{\left(1 - \frac{qB\Omega_\xi}{c}\right)^2} \right]. \quad (\text{C48})$$

In this expression we used the expression for the conductivity in zero magnetic field:

$$\sigma_{xx}^{(\beta)}(\mu) = q^2 v(\mu) \underbrace{\frac{v^2(\mu) \tau_{tr}(\mu)}{2}}_{D(\mu)}, \quad (\text{C49})$$

where $v(\mu)$ is the density of states.

8. Evaluation for Dirac fermions

While the solution given in Eqs. (C45) and (C48) is *a priori* general (not restricted to the situation of Dirac fermions) we now return to the case of 3D TI surface states. The various Fermi surface contributions are

$$m_1 = 1 - i \left(1 + \frac{1}{2} \frac{m v_0^2}{\mu} \frac{\zeta \Omega_c^{\text{cl}}}{\mu} \right) \frac{1}{2} \frac{m v_0^2}{\mu} \frac{1}{\mu \tau_{sj}} \approx 1 - i \frac{1}{2} \frac{m v_0^2}{\mu} \frac{1}{\mu \tau_{sj}}. \quad (\text{C50})$$

The approximation \approx keeps only the leading order $\mathcal{O}\left(\frac{m v_0^2}{\mu}, \frac{\Omega_c^{\text{cl}}}{\mu}\right)$. Note that the imaginary part (the side-jump contribution) is small in $1/k_F l$. Next,

$$m_2 = \frac{1 - i \left[\frac{\tau_{tr}}{\tau_a} - \frac{\zeta \Omega_c^{\text{cl}} \tau_{tr}}{\left(1 - \frac{qB\Omega_\xi}{c}\right)^2} \right]}{1 + \left[\frac{\tau_{tr}}{\tau_a} - \frac{\zeta \Omega_c^{\text{cl}} \tau_{tr}}{\left(1 - \frac{qB\Omega_\xi}{c}\right)^2} \right]^2} \approx \frac{1 + i \zeta \Omega_c^{\text{cl}} \tau_{tr}}{1 + (\Omega_c^{\text{cl}} \tau_{tr})^2} \left[1 + 2 \frac{\zeta \Omega_c^{\text{cl}} \tau_{tr}}{1 + (\Omega_c^{\text{cl}} \tau_{tr})^2} \frac{\tau_{tr}}{\tau_a} \right] - i \frac{\frac{\tau_{tr}}{\tau_a}}{1 + (\Omega_c^{\text{cl}} \tau_{tr})^2}. \quad (\text{C51})$$

a. Scattering rates in leading approximation: Short-range impurities

The symmetric scattering matrix element is

$$\omega_{ll'}^{(s)} = 2\pi n_i V_0^2 \delta(\epsilon_\xi(\mathbf{p}) - \epsilon_\xi(\mathbf{p}')) \times \left[\cos^2 \left(\frac{\phi - \phi'}{2} \right) + \left(\frac{m v_0^2}{\epsilon_\xi} \right)^2 \sin^2 \left(\frac{\phi - \phi'}{2} \right) \right], \quad (\text{C52})$$

where n_i and V_0 are concentration respectively strength of short-ranged impurities. The transport rate evaluated at the chemical potential immediately follows,

$$\frac{1}{\tau_{tr}} = \int (dp') \omega_{ll'}^{(s)} [1 - \cos(\phi' - \phi)] = 2\pi n_i V_0^2 v \frac{1 + 3\left(\frac{m v_0^2}{\mu}\right)^2}{4}. \quad (\text{C53})$$

According to Ref. [124] the side jump is

$$\delta \mathbf{r}_{ll'} = \frac{\Omega_\xi \epsilon (\mathbf{p} - \mathbf{p}')}{|\langle u_{\xi, \mathbf{p}} | u_{\xi, \mathbf{p}'} \rangle|^2} \quad (\text{C54})$$

and thus the side-jump rate follows to be

$$\frac{1}{\tau_{sj}} = 2\pi n_i V_0^2 v. \quad (\text{C55})$$

This is the same as the quantum rate in a normal material (the quantum rate is different for the Dirac problem). We also refer to Ref. [124] for the skew scattering rate, which is

$$\frac{1}{\tau_a} = \frac{\pi v(\mu)}{2} \left[\frac{n_i V_1^3 m(\mu^2 - m^2 v_0^4)}{2\mu^2} + \frac{(n_i V_0^2)^2 (3m(\mu^2 - m^2 v_0^4))}{4\mu^3} \right]. \quad (\text{C56})$$

Both terms in the square bracket are manifestly beyond the Born approximation (the first term involves the third moment of the disorder potential V_1^3).

The power provided by the B field is

$$\begin{aligned} \frac{\langle W^{(B)} \rangle}{\tau^{(W)}} &= 2\pi n_i V_0^2 v \frac{\frac{qB\Omega_\xi}{c}}{1 - \frac{qB\Omega_\xi}{c}} \xi v p \frac{3}{2} \\ &= \frac{3v_0^2 p^2}{2\mu\tau_{sj}} \left(-\frac{\frac{1}{2} \frac{mv_0^2}{\mu} \frac{\zeta\Omega_c^{\text{cl}}}{\mu}}{1 + \frac{1}{2} \frac{mv_0^2}{\mu} \frac{\zeta\Omega_c^{\text{cl}}}{\mu}} \right). \end{aligned} \quad (\text{C57})$$

In the case of short-range impurities we can omit the contribution of $\langle W^{(B)} \rangle$ to the conductivity since

$$\frac{\langle W^{(B)} \rangle}{\tau^{(W)}} \frac{\tau_{tr}}{\mu} \sim \frac{v_0^2 p^2}{\mu^2} \frac{\tau_{tr}}{\tau_{sj}} \frac{mv_0^2}{\mu} \frac{\Omega_c^{\text{cl}}}{\mu} \approx 0 \quad (\text{C58})$$

is beyond leading order in $\mathcal{O}(\frac{mv_0^2}{\mu}, \frac{\Omega_c^{\text{cl}}}{\mu})$.

APPENDIX D: MAGNETIC MIRROR CHARGE FOR A DOUBLE QH STRUCTURE

In this Appendix we consider the image magnetic monopole effect for a double QH structure (a double domain wall of $\mathbf{E} \cdot \mathbf{B}$ states). We consider the setup as in Fig. 16 and define the following three regions in real space:

- ① = $\{\mathbf{r} \in \mathbb{R}^3 | 0 < z\}$,
- ② = $\{\mathbf{r} \in \mathbb{R}^3 | -d \leq z \leq 0\}$,
- ③ = $\{\mathbf{r} \in \mathmathbb{R}^3 | z < -d\}$.

Region ② might correspond to the 3D TI; its surfaces should be characterized by a QH state with $\sigma_{xx} = 0$ and definite

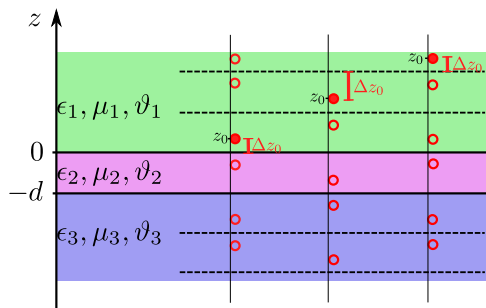


FIG. 16. (Color online) Sketch of three different scenarios for the setup discussed in Appendix D. The left and right scenarios correspond to case I, the middle one to case II.

σ_{xy} . Equivalently, one can describe the three regions $a \in \{\textcircled{1}, \textcircled{2}, \textcircled{3}\}$ by definite bulk ϑ_a . In addition, localized charges might contribute to nontrivial ϵ_a and μ_a .

1. Positions of the mirror charges

Let $z_0 > 0$ denote the position of the actual charge. We will need the quantity $\tilde{z}_0 = \{\frac{z_0}{2d}\} \times 2d$ (curly brackets denote the fractional part of a real number). We have to consider two separate cases:

(I) Let $z_0 \in [2kd, (2k+1)d]$ with $k \in \mathbb{N}_0$.

We define, according to Fig. 16, $\Delta z_0 \equiv \tilde{z}_0 < d$.

(II) Let $z_0 \in [(2k-1)d, 2kd]$ with $k \in \mathbb{N}$.

In this case, by definition and according to Fig. 16, $\Delta z_0 \equiv 2d - \tilde{z}_0 < d$.

In both cases, the position of (mirror) charges is thus given by (see again Fig. 16)

$$z_m^\pm \equiv 2md \pm \Delta z_0 \quad (m \in \mathbb{Z}). \quad (\text{D1})$$

By convention, the defining tuples (m, s) (with $m \in \mathbb{Z}$ and $s = \pm$) are ordered by the order implied of z_m^s [e.g., since $z_2^- < z_2^+$ the following inequality holds: $(2, -) < (2, +)$].

Clearly, depending on their (m, s) values, the charges reside in the following regions:

- ①: $(m, s) \geq (0, +)$,
- ②: $(m, s) = (0, -)$,
- ③: $(m, s) \leq (-1, +)$.

In case I, the actual charge sits at $z_0 = z_{\lfloor \frac{z_0}{2d} \rfloor}^+$ while for case

II $z_0 = z_{\lceil \frac{z_0}{2d} \rceil}^-$ follows. The symbols $\lfloor \dots \rfloor$ and $\lceil \dots \rceil$ denote floor and ceiling functions.

2. Solution of the image charge problem for the thin film

Following Karch [88], we use the unified description in terms of the vector $(\mathbf{D}, 2\alpha\mathbf{B})$ which is connected to \mathbf{E} and \mathbf{H} via

$$\begin{pmatrix} \mathbf{D} \\ 2\alpha\mathbf{B} \end{pmatrix} = \mathcal{M} \begin{pmatrix} 2\alpha\mathbf{E} \\ \mathbf{H} \end{pmatrix} \quad (\text{D2})$$

with the matrix

$$\mathcal{M} = \frac{2\alpha}{c^2\epsilon} \begin{pmatrix} \frac{\vartheta^2}{4\pi^2} + \left(\frac{c\epsilon}{2\alpha}\right)^2 & -\frac{\vartheta}{2\pi} \\ -\frac{\vartheta}{2\pi} & 1 \end{pmatrix}$$

in each of the three regions $a \in \{\textcircled{1}, \textcircled{2}, \textcircled{3}\}$. We make the following ansatz for the potential $\underline{\Phi} = (\Phi_E, 2\alpha\Phi_M)$ with $(\mathbf{D}, 2\alpha\mathbf{B}) = -\nabla\underline{\Phi}$:

$$\Phi_{\textcircled{1}} = \sum_{n=-\infty}^{\infty} \sum_{s=\pm} \frac{A_n^{(s)}}{|\mathbf{x} - z_n^{(s)} \hat{e}_z|}, \quad (\text{D3})$$

$$\Phi_{\textcircled{2}} = \sum_{n=-\infty}^{\infty} \sum_{s=\pm} \frac{B_n^{(s)}}{|\mathbf{x} - z_n^{(s)} \hat{e}_z|}, \quad (\text{D4})$$

$$\Phi_{\textcircled{3}} = \sum_{n=-\infty}^{\infty} \sum_{s=\pm} \frac{C_n^{(s)}}{|\mathbf{x} - z_n^{(s)} \hat{e}_z|}. \quad (\text{D5})$$

In order to fulfill the Poisson/Laplace equation the series of (mirror) charges [defined each as $\underline{A} = (A_E, 2\alpha A_M)$, etc.] has

the form

$$(\underline{B}_n^{(s)}) = (\dots, \underline{B}_{-1}^-, \underline{B}_{-1}^+; 0; \underline{B}_0^+, \underline{B}_1^-, \dots), \quad (\text{D6})$$

$$(\underline{C}_n^{(s)}) = (\dots, 0, 0; \underline{C}_0^-; \underline{C}_0^+, \underline{C}_1^-, \dots). \quad (\text{D7})$$

Further, in case I

$$(\underline{A}_n^{(s)}) = (\dots, \underline{A}_{-1}^-, \underline{A}_{-1}^+; \underline{A}_0^-; 0, \dots, 0, \underline{A}_{\lfloor \frac{z_0}{2d} \rfloor}^+, 0, \dots) \quad (\text{D8})$$

while in case II

$$(\underline{A}_n^{(s)}) = (\dots, \underline{A}_{-1}^-, \underline{A}_{-1}^+; \underline{A}_0^-; 0, \dots, 0, \underline{A}_{\lfloor \frac{z_0}{2d} \rfloor}^-, 0, \dots). \quad (\text{D9})$$

In these sequences, elements left of the first semicolon are associated with region ③, the element in between the two semicolons resides in region ②, while elements on its right are associated to charges in the positive half plane, region ①. Clearly $\underline{A}_{\lfloor \frac{z_0}{2d} \rfloor}^+$ and $\underline{A}_{\lfloor \frac{z_0}{2d} \rfloor}^-$ are given by the “bare” (actual) value of the charge \underline{Q} placed close to the interface.

a. Derivation of recursion relations

The position of mirror charges is constructed such that a reflection at the interface ①-② implies $z_m^{(s)} \rightarrow z_{-m}^{(-s)}$ and at a reflection at the interface ②-③ $z_m^{(s)} \rightarrow z_{-(m+1)}^{(-s)}$ ($-s = \mp$ for $s = \pm$). Then the continuity of perpendicular components of $(\underline{D}, 2\alpha \underline{B})$ and parallel components of $(2\alpha \underline{E}, \underline{H})$ yields the following infinite series of conditions:

$$\underline{A}_n^{(s)} - \underline{A}_{-n}^{(-s)} = \underline{B}_n^{(s)} - \underline{B}_{-n}^{(-s)}, \quad (\text{D10a})$$

$$\mathcal{M}_1^{-1}(\underline{A}_n^{(s)} + \underline{A}_{-n}^{(-s)}) = \mathcal{M}_2^{-1}(\underline{B}_n^{(s)} + \underline{B}_{-n}^{(-s)}), \quad (\text{D10b})$$

with $(n, s) \in \textcircled{1}$, and

$$\underline{B}_n^{(s)} - \underline{B}_{-(n+1)}^{(-s)} = \underline{C}_n^{(s)} - \underline{C}_{-(n+1)}^{(-s)}, \quad (\text{D11a})$$

$$\mathcal{M}_2^{-1}(\underline{B}_n^{(s)} + \underline{B}_{-(n+1)}^{(-s)}) = \mathcal{M}_3^{-1}(\underline{C}_n^{(s)} + \underline{C}_{-(n+1)}^{(-s)}), \quad (\text{D11b})$$

with $(n, s) \in \textcircled{1} \cup \textcircled{2}$. In this region $\underline{C}_{-(n+1)}^{(-s)} = 0$ and therefore (D11a) and (D11b) lead to

$$0 = (1 + \mathcal{M}_3 \mathcal{M}_2^{-1}) \underline{B}_{-1}^+, \quad (\text{D12a})$$

$$(1 - \mathcal{M}_3 \mathcal{M}_2^{-1}) \underline{B}_n^{(s)} = (1 + \mathcal{M}_3 \mathcal{M}_2^{-1}) \underline{B}_{-(n+1)}^{(-s)}, \quad (\text{D12b})$$

where $(n, s) \in \textcircled{1}$. We can plug this knowledge of \underline{B} 's back into (D10a) and (D10b) leading to the following final relations:

“Initial conditions”:

$$R_{21}^+ \underline{A}_0^- = R_{21}^- \underline{A}_0^+, \quad (\text{D13a})$$

$$R_{21}^+ \underline{A}_{-1}^+ = R_{21}^- \underline{A}_{-1}^-. \quad (\text{D13b})$$

“Recursive relations” $[(n, s) \in \textcircled{1}]$:

$$\begin{aligned} R_{32}^- R_{21}^- \underline{A}_{-n}^{(-s)} + R_{32}^+ R_{21}^+ \underline{A}_{-(n+1)}^{(-s)} \\ = R_{32}^- R_{21}^+ \underline{A}_n^{(s)} + R_{32}^+ R_{21}^- \underline{A}_{n+1}^{(s)}. \end{aligned} \quad (\text{D14})$$

Here we have defined $R_{ab}^\pm = 1 \pm \mathcal{M}_a \mathcal{M}_b^{-1}$.

b. Solution of recursion relations

The general solution of these relations for a charge sitting at $z_{n_0}^{(s_0)}$ is

$$\underline{A}_{n_0}^{(s_0)} = \underline{Q}, \quad (\text{D15a})$$

$$\underline{A}_n^{(s_0)} = 0 \quad \forall n \neq n_0, \quad (\text{D15b})$$

$$\underline{A}_n^{(-s_0)} = 0 \quad \forall n > -n_0, \quad (\text{D15c})$$

$$\underline{A}_{-n_0}^{(-s_0)} = (R_{21}^+)^{-1} (R_{21}^-) \underline{Q}, \quad (\text{D15d})$$

$$\begin{aligned} \underline{A}_{-(n_0+l)}^{(-s_0)} &= (-)^{l-1} [(R_{21}^+)^{-1} (R_{32}^+)^{-1} (R_{32}^-) (R_{21}^-)]^l \\ &\times [(R_{21}^-)^{-1} (R_{21}^+) - (R_{21}^+)^{-1} (R_{21}^-)] \underline{Q} \quad \forall l \geq 1. \end{aligned} \quad (\text{D15e})$$

c. Limits and checks

Two simple checks of the correctness of the result are in order.

(1) Let $(\epsilon_2, \mu_2, \vartheta_2) = (\epsilon_3, \mu_3, \vartheta_3)$. Then $R_{23}^- = 0$. It follows that the only nontrivial mirror charge is

$$\begin{aligned} \underline{A}_{-n_0}^{(-s_0)} &= (R_{21}^+)^{-1} (R_{21}^-) \underline{Q} \\ &= (\mathcal{M}_1 \mathcal{M}_2^{-1} + 1)^{-1} (\mathcal{M}_1 \mathcal{M}_2^{-1} - 1) \underline{Q}, \end{aligned} \quad (\text{D16})$$

in accordance with Ref. [88].

(2) Let $(\epsilon_1, \mu_1, \vartheta_1) = (\epsilon_2, \mu_2, \vartheta_2)$. Then $R_{21}^- = 0$ and $R_{21}^+ = 2$. It follows that the only nontrivial mirror-charge is

$$\underline{A}_{-(n_0-1)}^{(-s_0)} = (R_{32}^+)^{-1} (R_{32}^-) \underline{Q}, \quad (\text{D17})$$

in accordance with the previous limit and Ref. [88].

d. The potential and its Fourier transform

We can thus write

$$\begin{aligned} \underline{\Phi}_{\textcircled{1}}(\mathbf{x}, z_0) &= \frac{1}{|\mathbf{x} - z_0 \hat{e}_z|} \underline{Q} \\ &+ \frac{1}{|\mathbf{x} + z_0 \hat{e}_z|} (R_{21}^+)^{-1} (R_{21}^-) \underline{Q} \\ &- \sum_{l=1}^{\infty} \frac{[-(R_{21}^+)^{-1} (R_{32}^+)^{-1} (R_{32}^-) (R_{21}^-)]^l}{|\mathbf{x} + (z_0 + 2ld) \hat{e}_z|} \\ &\times [(R_{21}^-)^{-1} (R_{21}^+) - (R_{21}^+)^{-1} (R_{21}^-)] \underline{Q}. \end{aligned}$$

In Fourier space (Fourier transform only with respect to x and y coordinates) $\underline{\Phi}_{\textcircled{1}}$ simplifies:

$$\underline{\Phi}_{\textcircled{1}}(q, z, z_0) = \frac{2\pi}{q} \{e^{-|z-z_0|q} + e^{-(z+z_0)q} T_{\text{eff}}\} \underline{Q}.$$

We introduced the matrix

$$\begin{aligned} T_{\text{eff}} &= (R_{32}^+ R_{21}^+ e^{dq} + R_{32}^- R_{21}^- e^{-dq})^{-1} \\ &\times (R_{32}^+ R_{21}^- e^{dq} + R_{32}^- R_{21}^+ e^{-dq}). \end{aligned} \quad (\text{D18})$$

In view of 2D rotational invariance, the potential only depends on $q = |\vec{q}|$ (in this Appendix 2D vectors are denoted by arrows). One can exploit this formula and Fourier transform back to real space:

$$\Phi_{\oplus}(\mathbf{x}, z_0) = \int_0^{\infty} dq \frac{q}{2\pi} \Phi_{\oplus}(q, z, z_0) J_0(q\rho), \quad (\text{D19})$$

where $J_0(q\rho)$ is the zeroth Bessel function and $\rho = |\vec{x}|$ is the norm of the 2D component of \mathbf{x} perpendicular to \hat{e}_z .

This concludes the derivation of Eq. (60) of the main text.

e. Further limits and checks

With the help of Φ_{\oplus} in Fourier space and the matrix T_{eff} , one can easily check the $d \rightarrow \infty$ and $d \rightarrow 0$ limits. First consider $d \rightarrow \infty$. As expected, we obtain a single mirror charge at $z = -z_0$ with charge $(R_{21}^+)^{-1} R_{21}^- Q$. Now consider $d \rightarrow 0$. After a bit of algebra exploiting the definition of R_{ab}^{\pm} , we obtain the expected result: a single mirror charge at $z = -z_0$ with charge $(R_{31}^+)^{-1} R_{31}^- Q$ (the same result as if region $\textcircled{2}$ never existed).

-
- [1] M. Z. Hasan and C. L. Kane, *Rev. Mod. Phys.* **82**, 3045 (2010).
- [2] X.-L. Qi and S.-C. Zhang, *Rev. Mod. Phys.* **83**, 1057 (2011).
- [3] A. P. Schnyder, S. Ryu, A. Furusaki, and A. W. W. Ludwig, *Phys. Rev. B* **78**, 195125 (2008).
- [4] A. Kitaev, *AIP Conf. Proc.* **1134**, 22 (2009).
- [5] V. Gurarie, *Phys. Rev. B* **83**, 085426 (2011).
- [6] C. Callias, *Commun. Math. Phys.* **62**, 213 (1978).
- [7] R. Bott and R. Seeley, *Commun. Math. Phys.* **62**, 235 (1978).
- [8] K. v. Klitzing, G. Dorda, and M. Pepper, *Phys. Rev. Lett.* **45**, 494 (1980).
- [9] D. J. Thouless, M. Kohmoto, M. P. Nightingale, and M. den Nijs, *Phys. Rev. Lett.* **49**, 405 (1982).
- [10] B. A. Bernevig and S.-C. Zhang, *Phys. Rev. Lett.* **96**, 106802 (2006).
- [11] B. A. Bernevig, T. L. Hughes, and S.-C. Zhang, *Science* **314**, 1757 (2006).
- [12] L. Fu, C. L. Kane, and E. J. Mele, *Phys. Rev. Lett.* **98**, 106803 (2007).
- [13] J. E. Moore and L. Balents, *Phys. Rev. B* **75**, 121306 (2007).
- [14] R. Roy, *Phys. Rev. B* **79**, 195322 (2009).
- [15] M. König, S. Wiedmann, C. Brüne, A. Roth, H. Buhmann, L. W. Molenkamp, X.-L. Qi, and S.-C. Zhang, *Science* **318**, 766 (2007).
- [16] D. Hsieh, D. Qian, L. Wray, Y. Xia, Y. S. Hor, M. Z. Cava, and R. J. Hasan, *Nature (London)* **452**, 970 (2008).
- [17] S. C. Zhang, *Int. J. Mod. Phys. B* **6**, 25 (1992).
- [18] X.-G. Wen, *Int. J. Mod. Phys. B* **5**, 1641 (1991).
- [19] H. Levine, S. B. Libby, and A. M. M. Pruisken, *Phys. Rev. Lett.* **51**, 1915 (1983).
- [20] A. Pruisken, *Nucl. Phys. B* **235**, 277 (1984).
- [21] A. Pruisken, in *The Quantum Hall Effect*, edited by R. E. Prange and S. M. Girvin (Springer, New York, 1990), Graduate Texts in Contemporary Physics, Maryland Subseries.
- [22] B. Huckestein, *Rev. Mod. Phys.* **67**, 357 (1995).
- [23] B. Kramer, T. Ohtsuki, and S. Kettemann, *Phys. Rep.* **417**, 211 (2005).
- [24] F. Evers and A. D. Mirlin, *Rev. Mod. Phys.* **80**, 1355 (2008).
- [25] A. Altland and B. S. Simons, *Condensed Matter Field Theory* (Cambridge University Press, Cambridge, 2010), 2nd ed.
- [26] A. M. M. Pruisken, M. A. Baranov, and B. Skoric, *Phys. Rev. B* **60**, 16807 (1999).
- [27] A. M. Essin, J. E. Moore, and D. Vanderbilt, *Phys. Rev. Lett.* **102**, 146805 (2009).
- [28] A. M. Essin, A. M. Turner, J. E. Moore, and D. Vanderbilt, *Phys. Rev. B* **81**, 205104 (2010).
- [29] S. Ryu, J. E. Moore, and A. W. W. Ludwig, *Phys. Rev. B* **85**, 045104 (2012).
- [30] G. Y. Cho and J. E. Moore, *Ann. Phys.* **326**, 1515 (2011).
- [31] M. Mulligan and F. J. Burnell, *Phys. Rev. B* **88**, 085104 (2013).
- [32] H.-G. Zirnstein and B. Rosenow, *Phys. Rev. B* **88**, 085105 (2013).
- [33] E. J. König, P. M. Ostrovsky, I. V. Protopopov, I. V. Gornyi, I. S. Burmistrov, and A. D. Mirlin, *Phys. Rev. B* **88**, 035106 (2013).
- [34] For the notion of “local TR symmetry breaking,” see Eq. (3).
- [35] A. M. J. Schakel, *Phys. Rev. D* **43**, 1428 (1991).
- [36] K. S. Novoselov, A. K. Geim, S. V. Morozov, D. Jiang, M. I. Katsnelson, I. V. Grigorieva, S. V. Dubonos, and A. A. Firsov, *Nature (London)* **438**, 197 (2005).
- [37] Y. Zhang, Y.-W. Tan, H. L. Stormer, and P. Kim, *Nature (London)* **438**, 201 (2005).
- [38] V. P. Gusynin and S. G. Sharapov, *Phys. Rev. Lett.* **95**, 146801 (2005); *Phys. Rev. B* **73**, 245411 (2006).
- [39] A. Altland, *Phys. Rev. Lett.* **97**, 236802 (2006).
- [40] P. M. Ostrovsky, I. V. Gornyi, and A. D. Mirlin, *Phys. Rev. B* **77**, 195430 (2008).
- [41] A. H. Castro Neto, F. Guinea, N. M. R. Peres, K. S. Novoselov, and A. K. Geim, *Rev. Mod. Phys.* **81**, 109 (2009).
- [42] M. O. Goerbig, *Rev. Mod. Phys.* **83**, 1193 (2011).
- [43] C. Brüne, C. X. Liu, E. G. Novik, E. M. Hankiewicz, H. Buhmann, Y. L. Chen, X. L. Qi, Z. X. Shen, S. C. Zhang, and L. W. Molenkamp, *Phys. Rev. Lett.* **106**, 126803 (2011).
- [44] L. Fu and C. L. Kane, *Phys. Rev. B* **76**, 045302 (2007).
- [45] D.-H. Lee, *Phys. Rev. Lett.* **103**, 196804 (2009).
- [46] C.-X. Liu, X.-L. Qi, H. J. Zhang, X. Dai, Z. Fang, and S.-C. Zhang, *Phys. Rev. B* **82**, 045122 (2010).
- [47] G. Rosenberg, H.-M. Guo, and M. Franz, *Phys. Rev. B* **82**, 041104(R) (2010).
- [48] K. Nomura and N. Nagaosa, *Phys. Rev. Lett.* **106**, 166802 (2011).
- [49] A. A. Zyuzin and A. A. Burkov, *Phys. Rev. B* **83**, 195413 (2011).
- [50] O. Vafek, *Phys. Rev. B* **84**, 245417 (2011).
- [51] W.-K. Tse and A. H. MacDonald, *Phys. Rev. B* **84**, 205327 (2011).
- [52] H. Li, L. Sheng, and D. Y. Xing, *Phys. Rev. B* **84**, 035310 (2011).
- [53] R.-L. Chu, J. Shi, and S.-Q. Shen, *Phys. Rev. B* **84**, 085312 (2011).
- [54] Z. Yang and J. H. Han, *Phys. Rev. B* **83**, 045415 (2011).

- [116] S. Gattenlöhner, W. R. Hanne, P. M. Ostrovsky, I. V. Gornyi, A. D. Mirlin, and M. Titov, *Phys. Rev. Lett.* **112**, 026802 (2014).
- [117] J. Chalker and P. Coddington, *J. Phys. C: Solid State Phys.* **21**, 2665 (1988).
- [118] H. Fukuyama, *J. Phys. Soc. Jpn.* **52**, 18 (1983).
- [119] S. Kivelson, D.-H. Lee, and S.-C. Zhang, *Phys. Rev. B* **46**, 2223 (1992).
- [120] E. V. Gorbar, V. P. Gusynin, V. A. Miransky, and I. A. Shovkovy, *Phys. Rev. B* **78**, 085437 (2008).
- [121] R. B. Laughlin, *Phys. Rev. Lett.* **52**, 2304 (1984).
- [122] D. T. Son and B. Z. Spivak, *Phys. Rev. B* **88**, 104412 (2013).
- [123] K.-S. Kim, H.-J. Kim, and M. Sasaki, *Phys. Rev. B* **89**, 195137 (2014).
- [124] N. A. Sinitsyn, A. H. MacDonald, T. Jungwirth, V. K. Dugaev, and J. Sinova, *Phys. Rev. B* **75**, 045315 (2007).
- [125] D. Xiao, M.-C. Chang, and Q. Niu, *Rev. Mod. Phys.* **82**, 1959 (2010).
- [126] For simplicity we omit the contribution to the skew scattering time proportional to the third moment of the disorder potential; see Appendix C 8.
- [127] T. Morimoto, Y. Hatsugai, and H. Aoki, *Phys. Rev. Lett.* **103**, 116803 (2009).
- [128] A. M. Shuvaev, G. V. Astakhov, G. Tkachov, C. Brüne, H. Buhmann, L. W. Molenkamp, and A. Pimenov, *Phys. Rev. B* **87**, 121104 (2013).
- [129] C. J. Lin, X. Y. He, J. Liao, X. X. Wang, V. Sacksteder, IV, W. M. Yang, T. Guan, Q. M. Zhang, L. Gu, G. Y. Zhang *et al.*, *Phys. Rev. B* **88**, 041307 (2013).
- [130] H. Köhler and E. Wöchner, *Phys. Status Solidi (b)* **67**, 665 (1975).
- [131] Y. Guldner, C. Rigaux, M. Grynberg, and A. Mycielski, *Phys. Rev. B* **8**, 3875 (1973).
- [132] J. Chen, X. Y. He, K. H. Wu, Z. Q. Ji, L. Lu, J. R. Shi, J. H. Smet, and Y. Q. Li, *Phys. Rev. B* **83**, 241304 (2011).
- [133] F. Zhang, C. L. Kane, and E. J. Mele, *Phys. Rev. B* **86**, 081303 (2012).
- [134] F. Zhang, C. L. Kane, and E. J. Mele, *Phys. Rev. Lett.* **110**, 046404 (2013).
- [135] Clearly, the first of these charges corresponds to Eq. (11).
- [136] For the actual plotting of Fig. 14, the series of mirror charges was truncated. For the left (right) plot corresponding to $d = 10 \mu\text{m}$ ($d = 20 \text{ nm}$) the first 21 (201) mirror charges were taken into account.
- [137] J. Maciejko, X.-L. Qi, H. D. Drew, and S.-C. Zhang, *Phys. Rev. Lett.* **105**, 166803 (2010).
- [138] G. Tkachov and E. M. Hankiewicz, *Phys. Rev. B* **84**, 035405 (2011).
- [139] R. Valdés Aguilar, A. V. Stier, W. Liu, L. S. Bilbro, D. K. George, N. Bansal, L. Wu, J. Cerne, A. G. Markelz, S. Oh *et al.*, *Phys. Rev. Lett.* **108**, 087403 (2012).
- [140] G. S. Jenkins, A. B. Sushkov, D. C. Schmadel, N. P. Butch, P. Syers, J. Paglione, and H. D. Drew, *Phys. Rev. B* **82**, 125120 (2010).
- [141] J. N. Hancock, J. L. M. van Mechelen, A. B. Kuzmenko, D. van der Marel, C. Brüne, E. G. Novik, G. V. Astakhov, H. Buhmann, and L. W. Molenkamp, *Phys. Rev. Lett.* **107**, 136803 (2011).
- [142] L. Fu and C. L. Kane, *Phys. Rev. B* **79**, 161408 (2009).
- [143] F. Crépin and B. Trauzettel, *Phys. Rev. Lett.* **112**, 077002 (2014).
- [144] E. Witten, *Commun. Math. Phys.* **92**, 455 (1984).
- [145] V. Knizhnik and A. Zamolodchikov, *Nucl. Phys. B* **247**, 83 (1984).
- [146] A. Tsvetlik, *Quantum Field Theory in Condensed Matter Physics* (Cambridge University Press, Cambridge, 2007).
- [147] L. Faddeev, *Lett. Math. Phys.* **1**, 289 (1976).
- [148] A. Gerasimov, *arXiv:hep-th/9305090*.
- [149] A. Losev, G. Moore, N. Nekrasov, and S. Shatashvili, *arXiv:hep-th/9511185*.
- [150] A. V. Smilga, *Phys. Rev. D* **54**, 7757 (1996).
- [151] M. Bocquet, D. Serban, and M. Zirnbauer, *Nucl. Phys. B* **578**, 628 (2000).
- [152] M.-C. Chang and Q. Niu, *Phys. Rev. B* **53**, 7010 (1996).
- [153] G. Sundaram and Q. Niu, *Phys. Rev. B* **59**, 14915 (1999).
- [154] N. A. Sinitsyn, Q. Niu, and A. H. MacDonald, *Phys. Rev. B* **73**, 075318 (2006).
- [155] D. Xiao, J. Shi, and Q. Niu, *Phys. Rev. Lett.* **95**, 137204 (2005).
- [156] C. Duval, Z. Horvath, P. A. Horvathy, L. Martina, and P. Stichel, *Mod. Phys. Lett. B* **20**, 373 (2006).
- [157] A. W. W. Ludwig, M. P. A. Fisher, R. Shankar, and G. Grinstein, *Phys. Rev. B* **50**, 7526 (1994).